P-04-28

Oskarshamn site investigation

Interpretation of geophysical borehole data from KSH01A, KSH01B, KSH02 (0–100 m), HSH01, HSH02 and HSH03, and compilation of petrophysical data from KSH01A and KSH01B

Håkan Mattsson, Hans Thunehed
GeoVista AB

January 2004

Svensk Kärnbränslehantering AB
Swedish Nuclear Fuel
and Waste Management Co
Box 5864
SE-102 40 Stockholm Sweden
Tel 08-459 84 00
+46 8 459 84 00
Fax 08-661 57 19
+46 8 661 57 19

ISSN 1651-4416
SKB P-04-28

Oskarshamn site investigation

Interpretation of geophysical borehole data from KSH01A, KSH01B, KSH02 (0–100 m), HSH01, HSH02 and HSH03, and compilation of petrophysical data from KSH01A and KSH01B

Håkan Mattsson, Hans Thunehed
GeoVista AB

January 2004

Keywords: Borehole, Logging, Geophysics, Geology, Bedrock, Fractures, Salinity, Porosity, Temperature gradient, Pseudo geology, Pseudo bedrock, Pseudo fracture.

Abstract

This document reports the results gained from the interpretations of borehole geophysical logging data from the boreholes KSH01A, KSH01B, KSH02 (0–100 m), HSH01, HSH02 and HSH03 in Simpevarp. The major aim of the project is to create pseudogeology (lithology) loggings and pseudofracture loggings (position of large fractures and estimated fracture frequency) based on geophysical logging data. Analyses of petrophysical parameters measured on 42 core samples from KSH01A and KSH01B are also presented.

The results of the investigations indicate that the bedrock at 0–600 m depth, in the vicinity of KSH01A, KSH01B and KSH02 (0–100 m), is dominated by quartzmonzodiorite with some occurrence of fine-grained dioritoid and minor sections of fine-granite granite. Below 600 m depth (KSH01A) the physical properties of the rocks show large variations, which indicate a more heterogeneous lithology. This is displayed in the pseudo geological logging as a mixture of ca 5–20 m long sections of mainly granite (medium to coarse grained), Ävrö granite, fine-grained granite and quartz monzodiorite, with minor occurrence of fine-grained mafic rock (diorite to gabbro) and fine-grained dioritoid. The poor data quality of some of the loggings from the percussion drilled boreholes HSH01–03 unfortunately prevents a reliable calculation of pseudo geology loggings for these boreholes.

Comparing the results of the pseudogeology classification to the geological core logging (Boremap) shows a fair agreement regarding lithological boundaries and rock types. However, the petrophysical study shows that the fine-grained dioritoid and the quartz monzodiorite have almost identical physical properties. These two rock types can therefore not be separated in the statistical classification.

This investigation further indicates that it is possible to use geophysical data to detect sections where the rock is intensely altered (pseudo alteration logging). Increased fracturing and/or alteration is indicated along the sections ca 140–160 m, ca 200–290 m and ca 540–640 m of KSH01A; and at ca 50–65 m of KSH02 (0–100 m). AMS and electric resistivity data from core samples, independently from each other, indicate that the rocks of the lowermost ca 300 m of KSH01A (section 700–1000 m) may have suffered from plastic deformation.

Sammanfattning

Föreliggande rapport presenterar tolkning av borrhålsgeofysiska data från KSH01A, KSH01B, KSH02 (0–100 m), HSH01, HSH02 och HSH03 på Simpevarpshalvön. Huvudsyftet med projektet är att ta fram s k pseudogeologiska loggar (litologi, sprickor, sprickfrekvens och möjlig omvandling) baserade på geofysiska loggningsdata. En sammanställning av petrofysiska data mätta på 42 borrkärneprover från KSH01A och KSH01B presenteras också.

Undersökningen indikerar att de översta ca 600 m av berggrunden i närheten av borrhålen KSH01A, KSH01B och KSH02 (0–100 m) helt domineras av kvartsmonzodiorit, med smärre inslag av finkornig dioritoid och finkornig granit. Mellan 600 m och 1000 m djup (KSH01A) verkar berggrunden vara mycket mer heterogent sammansatt, vilket avspeglas i relativt stora variationer i fysikaliska egenskaper. Den pseudogeologiska klassificeringen indikerar här en blandning av ca 5–20 m långa sektioner av finkornig granit, medel- till grovkornig granit, Ävrögranit och kvartsmonzodiorit, samt mindre inslag av finkornig mafisk bergart (diorit till gabbro) och finkornig dioritoid. AMS-data och elektriska egenskaper mätta på borrkärneprover indikerar, oberoende av varandra, att de nedersta ca 300 m av KSH01A (sektion 700–1000 m) kan ha utsatts för plastisk deformation. Flera av de geofysiska loggarna från hammarborrhålen HSH01–HSH03 är av tveksam kvalitet. Pseudogeologiska loggar presenteras bara för HSH02, med denna tolkning bör behandlas med viss försiktighet.

En jämförelse mellan den pseudogeologiska bergartsklassificering och Boremap visar en relativt god överensstämmelse beträffande bergarter och läget på bergartsgränser. En möjlig svaghet hos den pseudogeologiska klassificeringen är dock att den inte klarar av att skilja mellan bergarterna kvartsmonzodiorit och finkornig dioritoid. Orsaken är att dessa två bergarter har nästan identiska fysikaliska egenskaper och således inte avviker från varandra i de geofysiska loggarna.

Vidare visar denna undersökning att det är möjligt att med godtagbar träffsäkerhet identifiera sektioner i borrhål där berggrunden påverkats av kraftig omvandling. Förhöjd sprickfrekvens och/eller omvandling indikeras längs sektionerna ca 140–160 m, ca 200–290 m och ca 540–640 m av KSH01A; och längs ca 50–65 m av KSH02 (0–100 m).

Contents

1 Introduction

SKB performs site investigations for localization of a deep repository for high level radioactive waste. The site investigations are performed at two sites, Forsmark and Simpevarp. This document reports the results gained from the interpretation of borehole geophysical logging data from the cored boreholes KSH01A, KSH01B and KSH02 (0–100 m), and from the percussion drilled boreholes HSH01, HSH02 and HSH03 in Simpevarp. A compilation of petrophysical data from measurements on core samples from KSH01A and KSH01B is also presented.

Pseudo bedrock loggings, pseudo alteration loggings and pseudo fracture loggings (including pseudo fracture frequency) are created by a combined statistically based interpretation of the different geophysical logging data. Porosity, silicate density, vertical temperature gradient and the salinity are also calculated.

The measurements in the cored boreholes were performed by Rambøll /1/ and in the percussion drilled holes by Malå Geoscience AB/Raycon /2/. The interpretation presented in this report is performed by GeoVista AB in accordance with the instructions and guidelines from SKB (activity plan AP PS 400-03-019 and method description MD 221.003, SKB internal controlling documents) and under supervision of Leif Stenberg, SKB.

A compilation of petrophysical data measured on 42 core samples from KSH01A and KSH01B is presented. Measurements of the magnetic susceptibility, remanent magnetization, anisotropy of magnetic susceptibility (AMS), density, porosity, electric resistivity and induced polarization were performed at the laboratory of the Division of Applied Geophysics, Luleå University of Technology.

An earlier geophysical logging interpretation of the percussion drilled part of KSH01A (0–100 m) performed on geophysical logging data logged by Malå Geoscience AB/ Raycon /2/ is reported separately /7/ because the presentation of pseudo geology and pseudo fracturing from geophysical logging data has been developed during the course of the project.

2 Objective and scope

The purpose of geophysical measurements in boreholes is to gain knowledge of the physical properties of the bedrock in the vicinity of the borehole. A combined interpretation of the different logging methods (in this case density, magnetic susceptibility and natural gamma radiation), together with petrophysical data and/or data from geological core logging, makes it possible to estimate the physical signature of different rock types. This allows a statistically based bedrock classification (pseudogeology logging) of the borehole. The location and frequency of fractures is estimated by interpretations of data from the short normal resistivity (N16), single point resistance (SPR), caliper, sonic and focused resistivity (300 cm) loggings in the cored boreholes. In the percussion drilled boreholes fractures are estimated from the short normal, SPR and caliper logging data (sonic and focused resistivity measurements were not performed in the percussion drilled boreholes). The results of the fracture calculations are presented as so called pseudo fracture loggings and pseudo fracture frequency loggings.

The main objective of these investigations is to use the results from interpretations of geophysical data as supportive information during the so called “single-hole interpretation”, which is a combined borehole interpretation of core logging (Boremap) data, geophysical data, radar data and FZI (fracture zone index).

The compilation and evaluation of petrophysical data from samples from the cores of KSH01A and KSH01B was performed in order to try to establish petrophysical signatures of certain rock types in order to investigate the possibilities of distinguishing different rock types based on their petrophysical properties. The petrophysical data is also used to perform quality controls of the logging data and constitutes supportive information to the rock type classification.

3 Equipment

3.1 Description of equipment for petrophysical measurements

The measurements of magnetic remanence were performed with a cryogenic DC-SQUID magnetometer from 2G Enterprises and the anisotropy of magnetic susceptibility (AMS), including the magnetic volume susceptibility, was measured with a KLY-3 Kappabridge from Geofyzika Brno. Masses for the density and porosity determinations were measured with a digital Mettler Toledo PG 5002. The electric resistivity and induced polarization measurements were performed by use of a two-electrode in-house equipment (Luleå University of Technology) /3/.

3.2 Description of equipment for analyses of logging data

The software used for the interpretation are WellCad v3.2 (ALT), which is mainly used for plotting, Grapher v4 (Golden Software), mainly used for plotting and some statistical analyses, and a number of in-house software developed by GeoVista AB on behalf of SKB.

4 Execution

4.1 Laboratory measurements

Preparations of the drill cores were performed by a technician at the laboratory of the Division of Applied Geophysics, Luleå University of Technology, according to the standard techniques used for example, in the preparation of samples for paleomagnetic analyses. The core samples are not oriented with reference to any co-ordinate system, there is only a mark indicating section up and section low. The remanence vectors and anisotropy orientations were therefore performed only with reference to the core. Declination data of these parameters are consequently meaningless but inclination variations may be possible to interpret if the borehole is sub-vertical. The dip of KSH01A is 80.6°, the dip of KSH01B is 87.9° and the dip of KSH02 is 85°, which probably is steep enough to allow a meaningful interpretation of inclination variations in all three holes, with an accuracy of ca ± 10°.

The general measuring technique of the borehole samples was as follows. Electric and induced polarization measurements were firstly performed. The sample was soaked in tap water according to MD 230.001 (SKB internal controlling document). The surface of the sample was gently dried with a piece of paper before the sample was mounted in the two-electrode sample holder. Measurements were performed with a saw-tooth current wave-form with the frequencies 0.1, 0.6 and 4 Hz. All measurements were done in direct sequence to avoid drying of the sample. Harmonics of the lower frequencies were used to correct for possible drift due to drying. The electric resistivity of the soaking water was measured at regular intervals and recorded. The procedure was repeated after soaking the samples in water where 125 g of NaCl had been dissolved in 5 kg of water.

Four 22 mm long specimens were then drilled perpendicularly of each core sample. AMS measurements were performed on all four specimens and a measurement of the remanent magnetization was performed on one specimen. All specimens plus, if possible, the remains of the core sample, were then assembled and the density (wet and dry) and porosity measurements were performed. The samples were soaked in water for 48 hours (or more) and the mass was measured in air and in water, which allows a calculation of the wet density. The samples were dried in an oven at 107°C for 48 hours and the mass was measured in air. The three mass measurements allow a calculation of the porosity. The sample volume was then calculated by the use of Archimedes principle, and the dry density was calculated by dividing the dry mass with the volume. The average sample volume for the density and porosity measurements is ca 100 cm^3.

Measurements of density and porosity were performed according to MD 160.002 (SKB internal controlling document). The instruction is written to conform to rock mechanical measurements on drill cores from deep drillings, where the density and porosity determinations are parts of other types of measurements, not directly relevant for the geological core logging. The time to dry and soak the samples (48 hours in this investigation) is e.g. shorter than what is recommended in MD 160.002.

Calibration of instruments for measurements of petrophysical parameters were performed in accordance to the manual for each instrument respectively.

4.2 Preparation of the logging data

The logging data were checked for spikes and/or other obvious incorrect data points. Such erroneous data points were when discovered replaced by values interpolated from surrounding data. According to information from the performance of the logging measurements the depth from the ground surface down to solid rock is ca 10 m. Logging data from the uppermost 10–12 m of the boreholes were therefore excluded to avoid erroneous results. Several loggings (for example sonic, gamma-gamma and focused resistivity) of KSH02 show deviating behaviors (probably erroneous readings) down to ca 20 m depth. The uppermost 20 m of this borehole were therefore excluded in the interpretations.

4.3 Interpretation of the logging data

The execution of the interpretation can be summarized in the following four steps:

1. Preparations of the logging data (calculations of noise levels, median filtering, error estimations, re-sampling, drift correction, length adjustment, correction of resistivity loggings for fluid resistivity and borehole diameter, calculation of apparent porosity, calculation of salinity, calculation of vertical temperature gradient).

The loggings are median filtered (generally 5 point filters for the resistivity loggings and 3 point filters for other loggings) and re-sampled to common depth co-ordinates (0.1 m point distance). The data of the resistivity loggings are corrected for the influence of the borehole diameter and the borehole fluid resistivity. The apparent porosity is calculated during the correction of the resistivity loggings. The calculation is based on Archie's law; $>\sigma = a\ \sigma_w\ \phi^m + \sigma_s$ where σ = bulk conductivity (S/m), σ_w = pore water conductivity (S/m), ϕ = volume fraction of pore space, σ_s = surface conductivity (S/m) and "a" and "m" are constants. A least squares curve fit on resistivity and porosity data measured on rock samples is required to determine the three unknown constants "a", "m" and "σ_s". Curve fits were performed on the petrophysical resistivity and porosity data presented in this report. Since "a" and "m" vary significantly with variations in the borehole fluid resistivity, different estimations of the constants had to be performed with reference to the actual fluid resistivity in each borehole respectively. The estimated constants are presented in Table 5-1, Section 5.1.3.

The vertical temperature gradient (in degrees/km) is calculated from the fluid temperature logging for 9 m sections according to the following equation /4/:

$$TempGrad = \frac{1000\left[9\sum zt - \sum z \sum t\right]\sin\varphi}{9\sum z^2 - \left(\sum z\right)^2}$$

where z = depth co-ordinate (m), t = fluid temperature (°C) and ϕ = borehole inclination (°).

The estimated water salinity is calculated as ppm NaCl in water following the simple relation from Crain's Petrophysical Handbook where:

$$WS = \frac{400000}{(1.8t + 32)^{0.88}\sqrt{\rho}}$$

WS = Water salinity (ppm NaCl), t = temperature (°C) and ρ = resistivity (Ωm).

2. Interpretation rock types (classification to pseudo bedrock logging and pseudo alteration logging based on analyses of the density, magnetic susceptibility and natural gamma radiation data. Calculation of silicate density)

The rock classification is performed by use of the maximum likelihood method. Co-variance matrices (rock type signature) are calculated for each rock type respectively. The calculations are performed by use of logging data from sections of a mapped borehole as reference. Petrophysical data are also used to support the calculations. The silicate density is calculated with reference to /5/.

Two sets of co-variance matrices were used, one matching the percussion drilled borehole HSH02 (previously derived for the percussion drilled part of KSH01A) and the other is applied to the cored boreholes. The two sets of co-variance matrices are listed below.

Percussion drilled borehole HSH02

Quartzmonzodiorite		
0.052486	0.196834	–0.241074
0.055284	0.024614	–0.034032
0.024614	0.233199	0.000391
–0.034032	0.000391	0.073852
Quartzmonzodiorite (low magnetic)		
–1.803361	–0.712372	0.136903
0.025008	0.018734	–0.033255
0.018734	0.175232	–0.041362
–0.033255	–0.041362	0.125991
Fine-grained granite		
–1.876511	–2.535494	4.316596
0.089125	0.189585	–0.388281
0.189585	0.449777	–0.739472
–0.388281	–0.739472	2.025803
Fine-grained mafic rock		
–1.277308	1.141177	0.135216
0.483601	0.024566	–0.046657
0.024566	0.30584	–0.157647
–0.046657	–0.157647	0.161276

Cored boreholes KSH01A, KSH01B and KSH02

Quartzmonzodiorite			Fine-grained granite 1		
5.132333	0.645883	–0.301259	–0.815914	–2.154941	3.619033
24.189366	1.290531	–0.725844	2.197124	0.343139	–0.279283
1.290531	0.742665	–0.051672	0.343139	0.572839	–0.447314
–0.725844	–0.051672	0.072645	–0.279283	–0.447314	1.144639
Ävrö granite			Fine-grained granite 2		
3.740628	0.004649	0.608303	3.827422	–0.855262	0.717202
21.36222	1.010979	0.442081	1.454918	0.030581	–0.169407
1.010979	0.560805	–0.260592	0.030581	0.397254	–0.082786
0.442081	–0.260592	0.338797	–0.169407	–0.082786	0.205961
Fine-grained dioritoid			Fine-grained granite 3		
–0.294939	–0.022813	–0.303534	–1.075339	–1.492746	3.578142
9.411136	0.528807	–0.241946	1.097794	0.163336	0.078261
0.528807	0.194547	0.014245	0.163336	0.030691	0.011929
–0.241946	0.014245	0.018461	0.078261	0.011929	0.887363
Fine-grained mafic rock			Granite medium to coarse grained		
–2.061346	1.873457	0.365742	2.324514	–0.859867	0.740258
0.002875	–0.022565	–0.0322	0.851112	0.149528	–0.316771
–0.022565	0.515094	0.286191	0.149528	0.037865	–0.052055
–0.0322	0.286191	0.966418	–0.316771	–0.052055	0.127605

A pseudo alteration logging is estimated by identifying sections along the boreholes where the density, natural gamma radiation and magnetic susceptibility simultaneously lay below certain threshold values. The threshold values were determined by analyzing logging data from KSH01A from sections where the geological core mapping indicates various degrees of alteration. The applied threshold values are:

density ≤ 2800 kg/m^3
natural gamma radiation ≤ 20 µR/h
magnetic susceptibility ≤ 0.003 SI

3. Interpretation of the position of fractures and pseudofracture frequency (classification to pseudo fracture logging and pseudo fracture frequency logging based on analyses of the short normal resistivity, caliper, single point resistance, sonic and focused resistivity (300 cm) loggings).

The position of large fractures is estimated by applying a second derivative filter to the logging data and then locating maxima (or minima depending on the logging method) in the filtered logging. Maxima (or minima) above (below) a certain threshold value (Table 4-1) are selected as probable fractures. The result is presented as a "mud logg" (column diagram) where column height 0 = no fracture, column height 1 = fracture indicated by one logging method, column height 2 = fracture indicated by two logging methods and so on. The estimated fracture frequency is calculated by applying a power function to the weighted sum (Table 4-1) of the maxima (minima) loggings. The power function is estimated by correlating the weighted sum to the mapped fracture frequency in one cored borehole (KSH01A Rambøll data) and in a percussion drilled hole (HSH02 Malå GeoScience AB/Raycon data).

The power functions used in this study are:

Cored borehole: Estimated fracture frequency = 1.15 (weighted sum)$^{0.88}$–1.
Percussion borehole: Estimated fracture frequency = 6 (weighted sum)$^{0.88}$–1.

Table 4-1. Threshold values and weights used for estimating position of fractures and calculate estimated fracture frequency, respectively.

	Borehole type	Sonic	Focused res. 300	Caliper	SPR	Normal res. 16
Threshold	Cored/percussion	0.4/no data	0.4/no data	0.15/0.7	1.0/1.3	2.5/0.23
Weight	Cored/percussion	2.5/no data	2.3/no data	3.3/1.0	1.8/1.3	0.55/1.0

4. Report evaluating the results (this report).

4.4 Data handling

The laboratory measurements produce raw-data files in ascii, binary or Microsoft Excel formats. All data files were delivered from the laboratory at the Luleå University of Technology to GeoVista AB. The data were then rearranged and placed in a Microsoft Excel file. Back-up files of all raw-data are stored both at GeoVista AB and at the laboratory.

The logging data of HSH01, HSH02 and HSH03 were downloaded from the SKB AB database SICADA via the internet. Data from KSH01A, KSH01B and KSH02 were delivered by SKB as Microsoft Excel files via email. Data from each method were stored on tab-separated ascii-files and the two columns containing section coordinate and the corresponding data values were then saved separately as standard ascii-files. The data processing was performed on the latter files. Core logging (Boremap) information was partly delivered via email and was also downloaded from the SKB AB database SICADA via the internet.

The delivered data have been inserted in the database (SICADA) of SKB. The SICADA reference to the present activity is field note no 264.

5 Results

5.1 Compilation of petrophysical data

The sampling covers 42 samples of 6 different groups of rock types. Each rock type group conforms to the SKB standard and the classification follows the core logging (Boremap) classification.

5.1.1 Density, magnetic susceptibility and remanence

The rock type classifications diagram in Figure 5-1 shows the distribution of the magnetic susceptibility versus density for each rock type group. This "geophysical" rock classification shows that both groups of granites fall at, or close to, the granite curve, slightly overlapping the granodiorite curve. The quartz monzodiorite rock has a very wide range of densities, varying from 2670 kg/m^3 to 2940 kg/m^3. This range almost covers the entire rock type spectrum of Figure 5-1 from granite to gabbro composition. The densities of the fine grained dioritoid rock samples completely overlap with the densities of the quartzmonzodiorite samples, but the susceptibility of the fine grained dioritoid is generally (but not statistically significant) lower. The single Ävrö granite sample constitutes an outlier with its high density of 2931 kg/m^3.

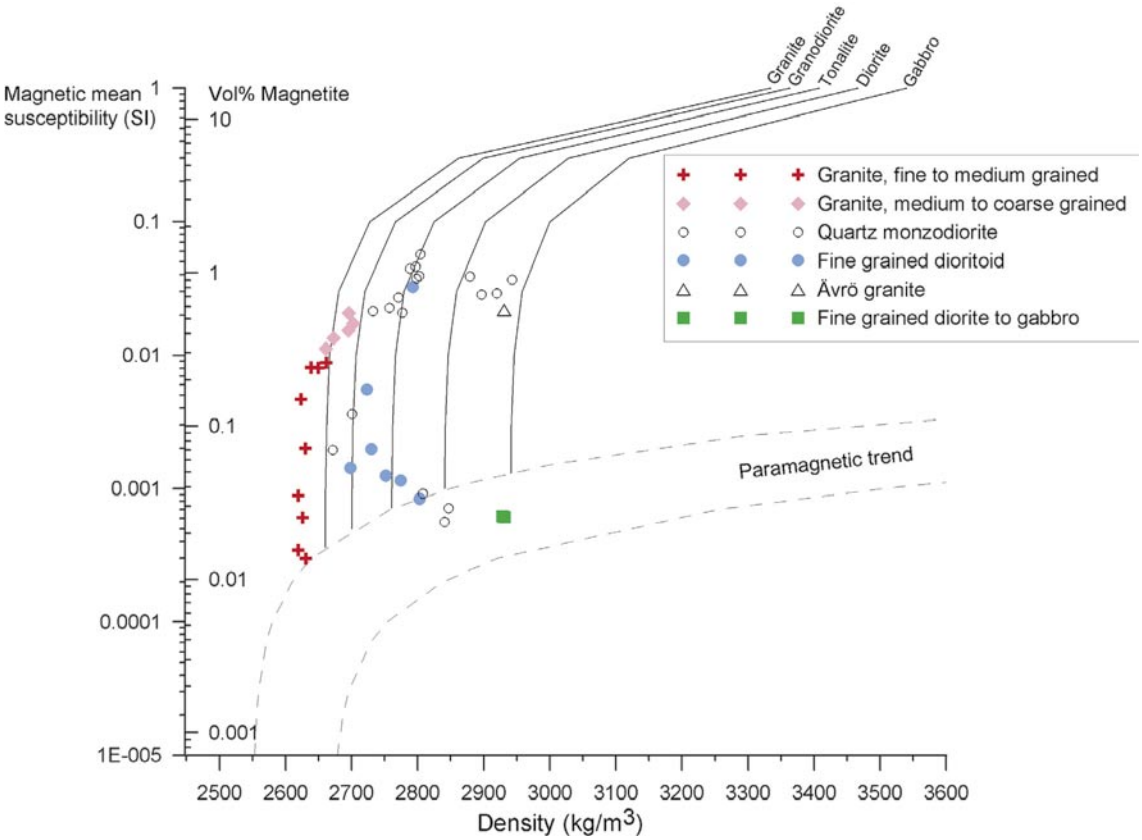

Figure 5-1. *Density-susceptibility rock classification diagram. See the text for explanation.*

It must be noted that the rock types used in the rock classification diagram do not conform perfectly to the geology of the Simpevarp area. There is for example no corresponding rock type curve for quartz monzodiorite, a rock type that occurs frequently in the area. This misfit is caused by the lack of high quality average density data and corresponding petrology data for these rock types. We therefore suggest that the data in rock classification diagram such as shown in Figure 5-1 should be used as indicators of the compositional variation between different rock types (or groups of rocks), and that these diagrams will be used to help identifying possible faulty rock classifications during the geological core logging and also to spot geographical variations in rock composition.

A histogram plot of the logarithm of the magnetic susceptibility of all samples clearly indicates a bimodal distribution, with one cluster at ca 0.001 SI and the other at ca 0.025 SI (Figure 5-2a). The fine grained granites and fine grained dioritoid samples dominate the low susceptibility group whereas the quartz monzodiorite mainly dominates the high susceptibility group (Figure 5-2b). Magnetite is most likely the dominant magnetic mineral in the high susceptibility rocks.

Q-values (Figure 5-3) average at Q = 0.30 and the distribution of the data is narrow, which is indicated by the low standard deviation of the mean of std = 0.18. The NRM intensity is higher for the quartz monzodiorite and the medium to coarse grained granite than for the other rock types. This indicates a higher content of ferromagnetic minerals (most likely magnetite) in the former rock types compared to the latter.

As stated in Section 4.1 it is possible to interpret the inclination of the remanence vector with an accuracy of ca ± 10°. In Figure 5-4 the NRM inclination is shown. A majority of the samples show inclinations of 30°–60°.

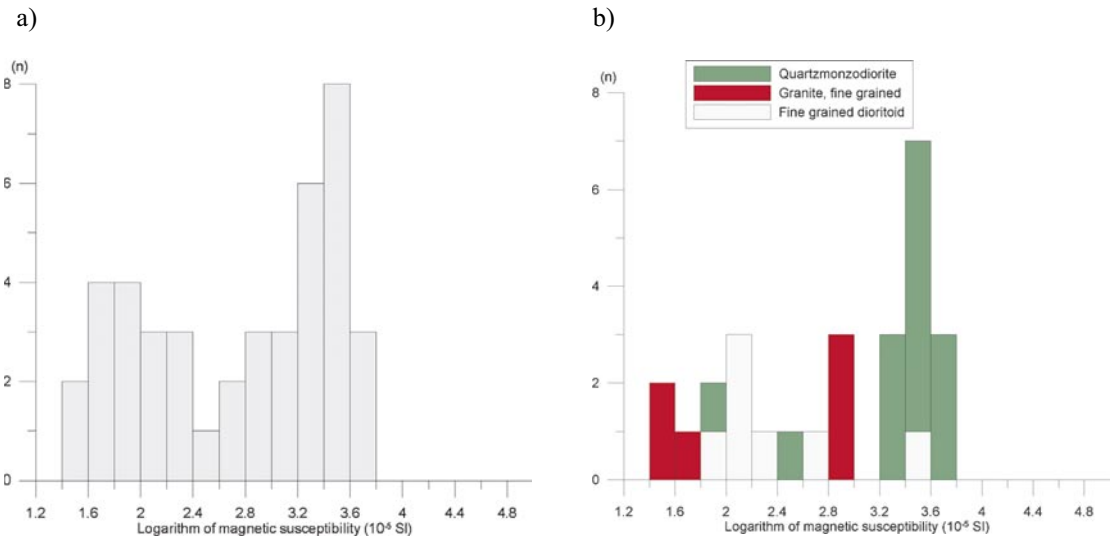

Figure 5-2. *Histogram of the mean susceptibility for a) all samples and b) the three most common rock types.*

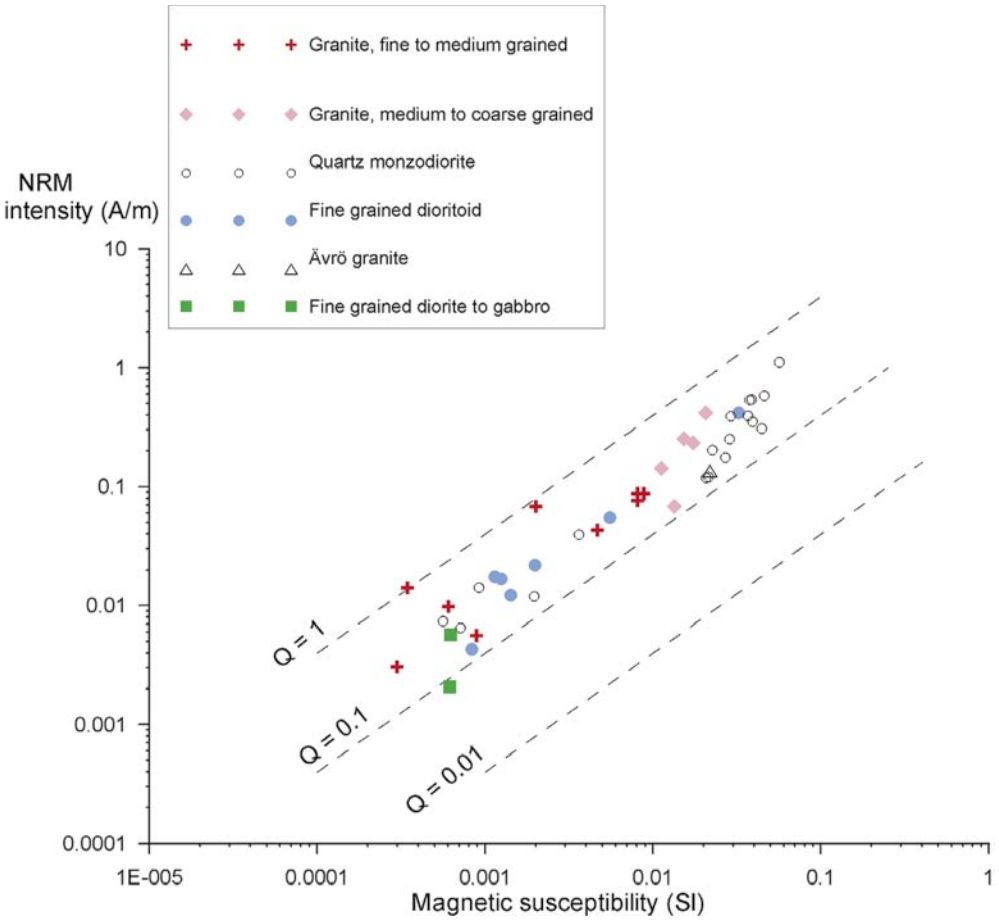

Figure 5-3. *NRM intensity versus magnetic susceptibility. Hatched lines indicate Q-values of 0.01, 0.1 and 1.*

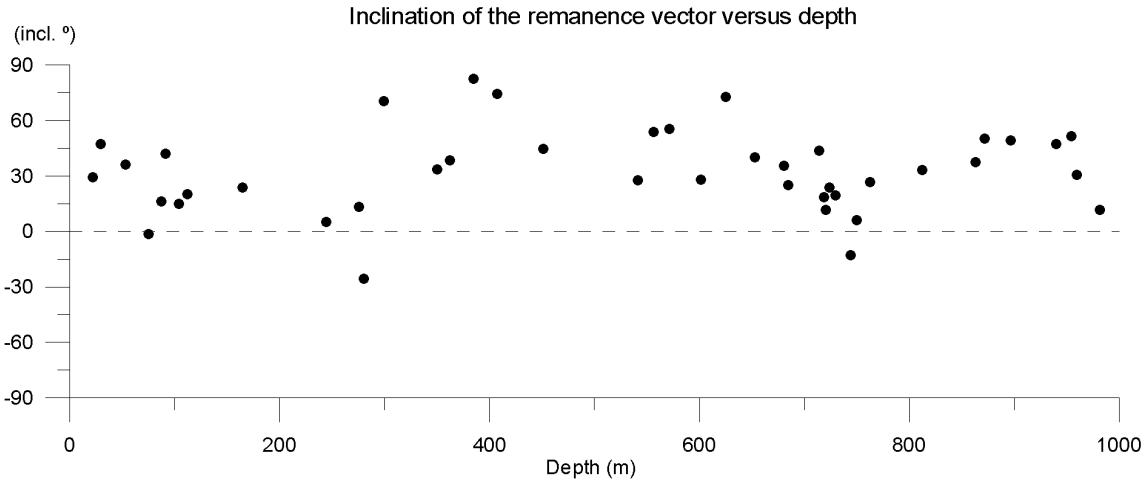

Figure 5-4. *Inclination of the remanence vector versus depth.*

5.1.2 Anisotropy of magnetic susceptibility

The anisotropy of magnetic susceptibility was measured on 4 specimens from each core sample. The resulting mean anisotropy parameters and inclinations of the magnetic foliation planes and lineations are shown in Figure 5-5.

The data of the degree of anisotropy (Figure 5-5a) is separated into a high and low susceptibility group. The magnetization of the rocks of the high susceptibility group is most likely governed by magnetite and for the low susceptibility group it is governed by paramagnetic minerals (e.g. micas and amphiboles). The P-parameters of the two groups can not be compared to each other sine they originate from different minerals. The degree of anisotropy, which indicates how well the magnetic minerals are aligned to each other and if they are deformed, clearly increases with depth for the high susceptibility group. Primary igneous rocks generally have a degree of anisotropy of less than ca P = 1.2. Under the assumption that magnetite is the dominant magnetic mineral of the high susceptibility rocks, these data indicate that the rocks below ca 700m depth have suffered from plastic deformation. That magnetite is the dominating magnetic mineral is supported by the Q-values and our interpretation is supported by the fact that the mean susceptibilities show no changes that correlate with those of the P-parameter. The deformation is also supported by the fact that the ellipsoid shape (Figure 5-5b) changes from prolate (elongated) to oblate (flattened) in a similar way as the degree of anisotropy. Primary magnetite has a prolate ellipsoid shape and compressive deformation may result in a flattening of the ellipsoid. In Figures 5-5c and 5-5d the inclination of the magnetic foliation plane and the magnetic lineation are plotted, respectively. Minor rocks (dykes) are denoted by open symbols and main rocks by filled symbols. There is a fairly well established increase in the inclination of the magnetic foliation with depth, for main as well as for minor rocks. This indicates that the possible deformation suggested by the increase in the degree of anisotropy with depth and the change in ellipsoid shape, had a dominant subhorizontal compressive component, since a subhorizontal compressive deformation would give rise to steepened foliation.

For the main rock group, the inclination of the magnetic lineations show a parabola-shaped trend of shallow dips close to surface, moderate to steep dips at ca 400–800 depth and mainly moderate dips from 800–1000 m depth.

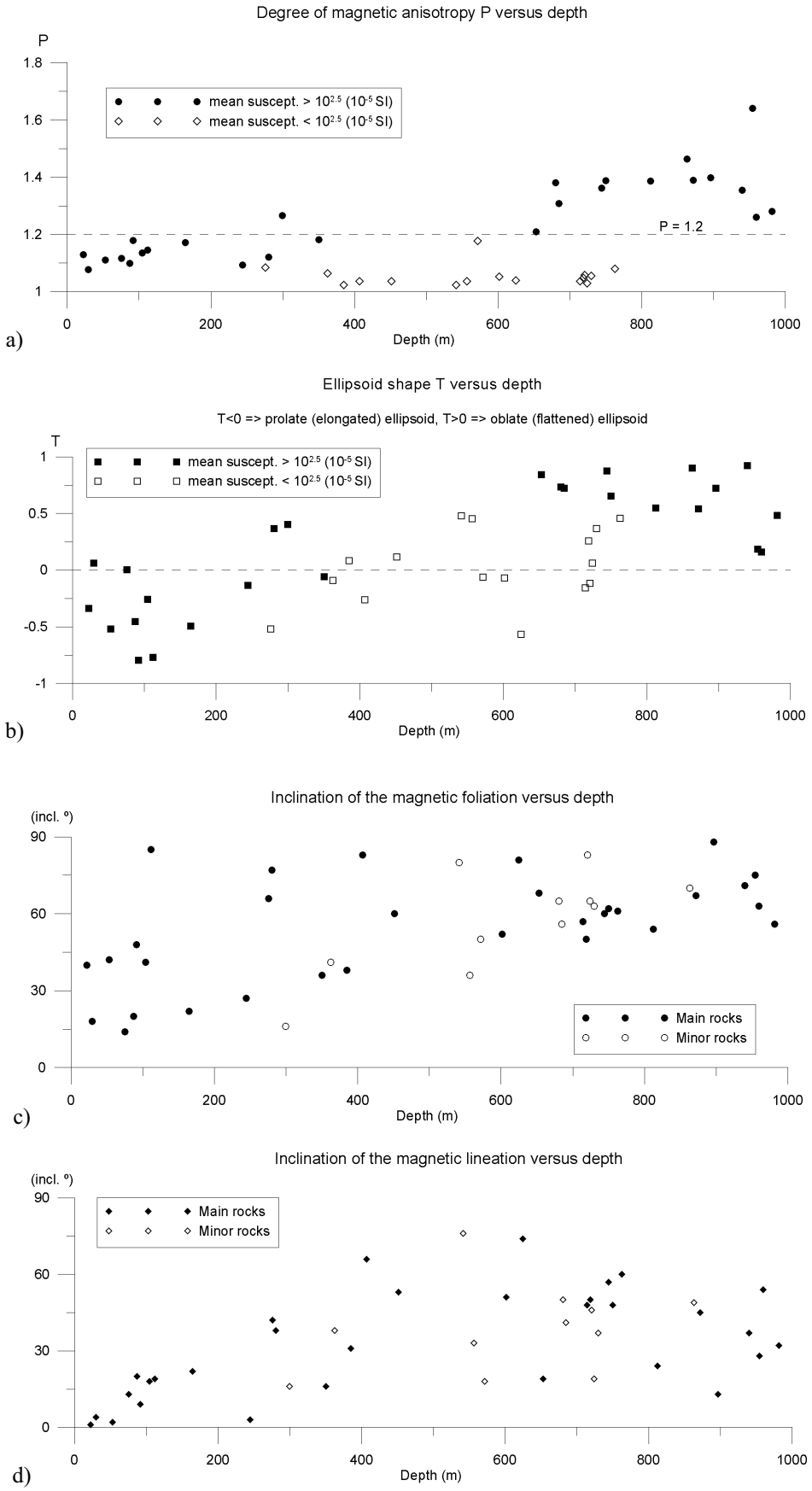

Figure 5-5. *Anisotropy parameters and AMS inclination directions for the rocks in KSH01A and KSH01B (see text for explanation).*

5.1.3 Electric resistivity and polarizability

The electric resistivity of the samples as measured in fresh water is plotted versus polarizability (IP) in Figure 5-6. The latter parameter is measured as the phase between applied current and measured potential difference over the sample. The IP phase values are generally low and show no correlation with resistivity. There are a number of resistivity values below 5000 Ωm which can be regarded as quite low. These low values appear for different rock types and thus has no relation to lithology. The samples of fine-grained granite all show very low IP values.

The resistivity and IP measured in saline water can be seen in Figure 5-7. The IP values have decreased to very low values for all the high resistivity samples, compared to above. This implies that the IP effect seen in the fresh water measurements are mainly due to effects related to surface conduction for these samples. Some of the low resistivity samples show an IP effect in saline water. This IP effect is probably not due to magnetite since most of the samples with high susceptibility also have high resistivity. The IP effect of these samples is more likely due to alteration minerals. The low resistivity samples with high IP are all red due to oxidation.

The relationship between IP in saline water and porosity is seen in Figure 5-8. There is a fairly clear correlation between high porosity and high IP. There are a number of samples with fairly high porosity values and these show IP effect that is suspected to be caused by alteration minerals. These high porosity samples of course correspond to the low resistivity samples in Figure 5-7.

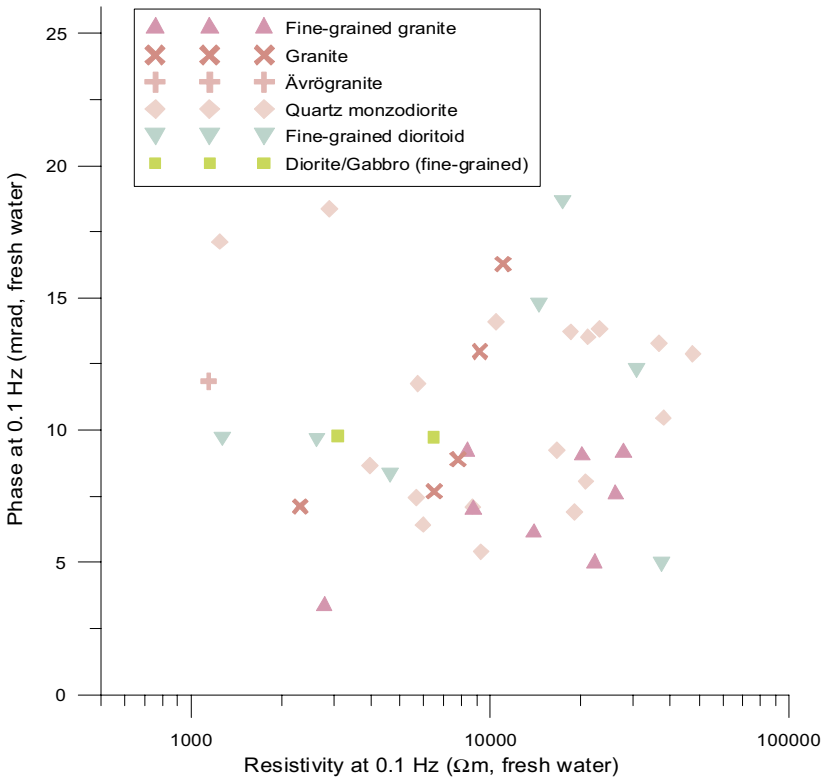

Figure 5-6. *IP effect as phase angle plotted against resistivity. Measurements in fresh water.*

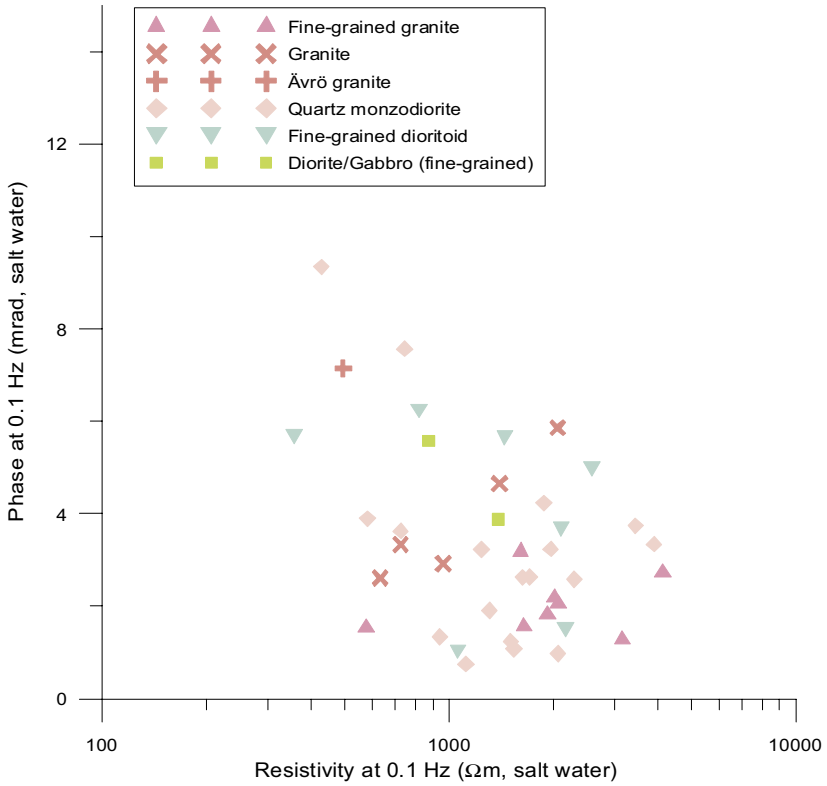

Figure 5-7. *IP effect as phase angle plotted against resistivity. Measurements in saline water.*

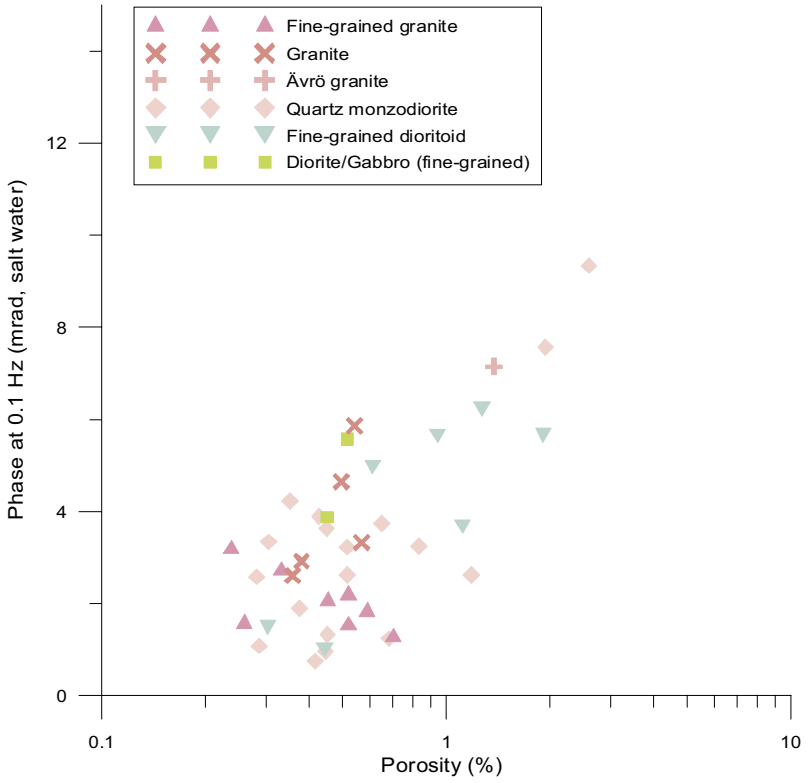

Figure 5-8. *IP effect as phase angle plotted against porosity. Measurements in saline water.*

The resistivity of the samples measured in fresh and saline water respectively can be seen in Figure 5-9. A straight solid line in the graph corresponds to equal resistivity for the two cases. All samples have a lower resistivity when soaked in saline water. However, the contrast is much lower than the contrast of the resistivity in the saline water compared to the fresh water, corresponding to the dashed line in Figure 5-9. The reason for this is that the electric conductivity of the samples is not just purely electrolytic in the pore space. There is an additional conductivity along the surface between the pores and the mineral grains called surface conductivity. This effect is reduced in saline water and hence the low contrast in resistivity seen for the samples in Figure 5-9. Surface conduction is expected to be high for samples containing large amounts of thin membrane pore spaces. For fresh, unaltered rocks the effect is therefore often strongest for high resistivity samples. However, in this case it is the low resistivity, high porosity samples that show the strongest effect of surface conduction in Figure 5-9. The presence of alteration minerals is probably the reason for this.

Figure 5-10 shows the relationship between the measured porosity and the resistivity measured in fresh water. A negative correlation is expected since high porosity should correspond to low resistivity and vice versa. Such a correlation can also be seen in Figure 5-10 but there is a fairly large scatter. The electric conductivity (reciprocal to resistivity) as a function of porosity can be modelled with Archie's law:

$$\sigma = a \cdot \sigma_w \cdot \phi^m \cdot s^n$$

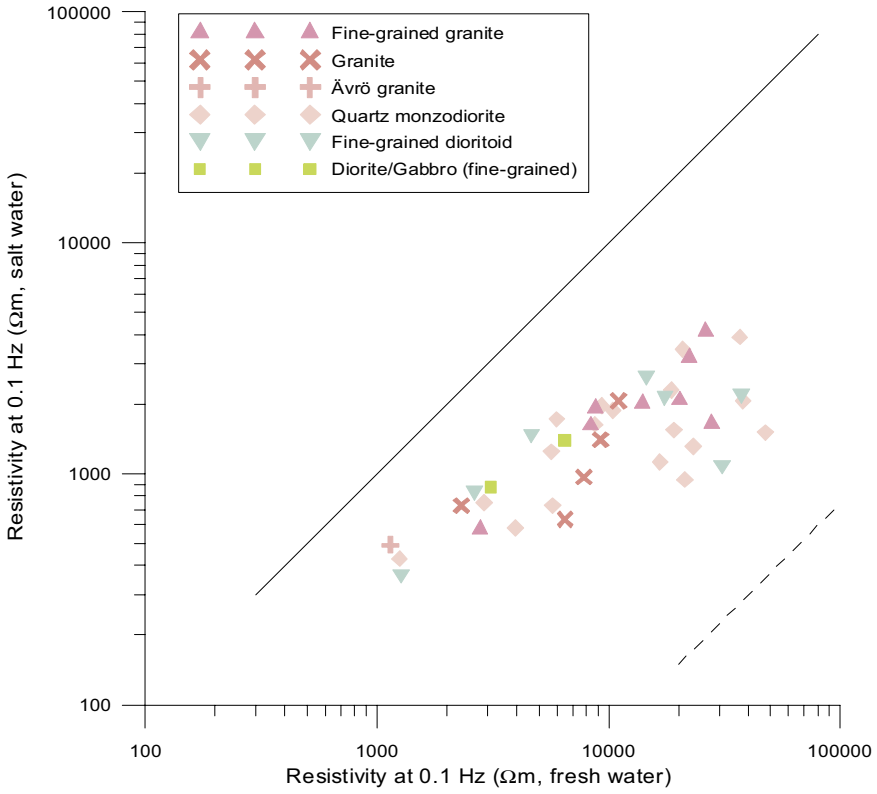

Figure 5-9. *Reisistivity measured in fresh and saline water. The solid line corresponds to equal values for the two cases. The dashed line corresponds to the contrast of the saturating waters.*

where

σ = bulk conductivity (=1/ρ, S/m)
σ_w = pore water conductivity (S/m)
ϕ = volume fraction of pore space
s = fraction of pore space that is water saturated
a, m, n = dimensionless numbers, m ≈ 1.5 to 2.2

Archie's law has been proven to work well for high-porosity sedimentary rocks. However, the contribution from surface conductivity is significant in crystalline rocks, especially when the pore water has low salinity. Since the surface conductivity depends upon pore space geometry, a scatter is often seen in plots like the one in Figure 5-10.

If a reasonable value of the parameter m in Archie's law is assumed (1.75 is in this case), it is possible to plot the resistivity for different values of the parameter a as straight lines in a double logarithmic graph as in Figure 5-10. The various samples will then get different apparent a-values. Large values will correspond to a large contribution of surface conductivity and vice versa. The samples in this study shows large variations in such apparent a-values ranging from less than 10 to over 100. No clear correlation between apparent a-values and lithology or porosity can be seen. The mafic fine-grained diorite/ gabbro seems to have high apparent a-values but there are on the other hand only two samples of this rock type.

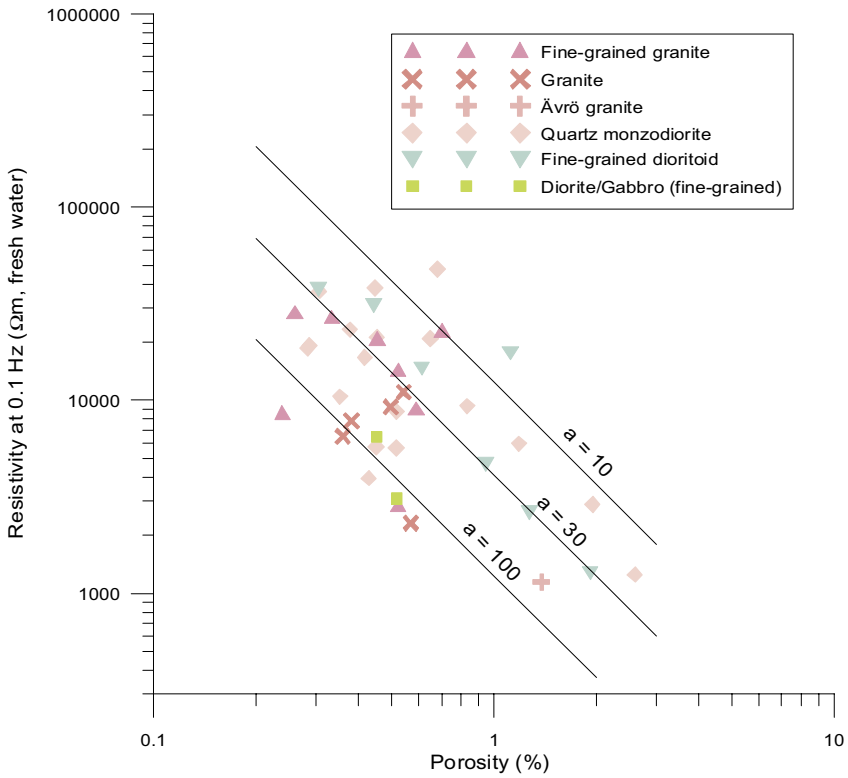

Figure 5-10. *Resistivity in fresh water as a function of porosity. The solid lines corresponds to resistivities calculated with Archie's law and m=1.75. High values for the parameter a indicates large contributions of surface conductivity.*

The relation between porosity and resistivity measured in saline water can be seen in Figure 5-11. Straight lines corresponding to resistivities calculated with Archie's law and m=1.75 are also shown. Two groups of samples can be identified. With a few exceptions all samples with a porosity of less than 0.7% have apparent a-values ranging from 1 to 10. This can be regarded as normal values. The surface conductivity effect should be reduced in saline water but the solution used was not saturated so some remaining effect is expected. The other group of samples have apparent a-values of less than 1. The porosity for these samples is above 0.6%. A value below 1 for the parameter a in Archie's law is unrealistic. We can therefore assume that the value of m (1.75) that has been assumed is not valid for these samples. They show a high resistivity in relation to their porosity. Still using Archie's law to model the behaviour of the samples, this corresponds to a higher value than 1.75 for the parameter m. This parameter models the texture of the pore space. High values will appear if the pore space consists of small cavities interconnected by joints and/or intergranular porosity.

Apparent a-values (according to Archie's law and m=1.75) for fresh and saline water measurements are plotted as a function of depth along the hole in Figures 5-12 and 5-13. Most samples show values around 10 to 30 in fresh water above 650 m depth. Below that depth there is a gradual increase in apparent a-values. High values are usually associated with foliated and/or mica-rich rocks and are expected in belts of ductile deformation.
A similar ascending trend can be seen for the deeper parts of the borehole for saline water measurements as well (Figure 5-13). In this case we can also see apparent a-values below 1.0. According to the discussion above these samples have fairly high porosity and are expected to have different pore space geometry than the other samples, possibly including small cavities.

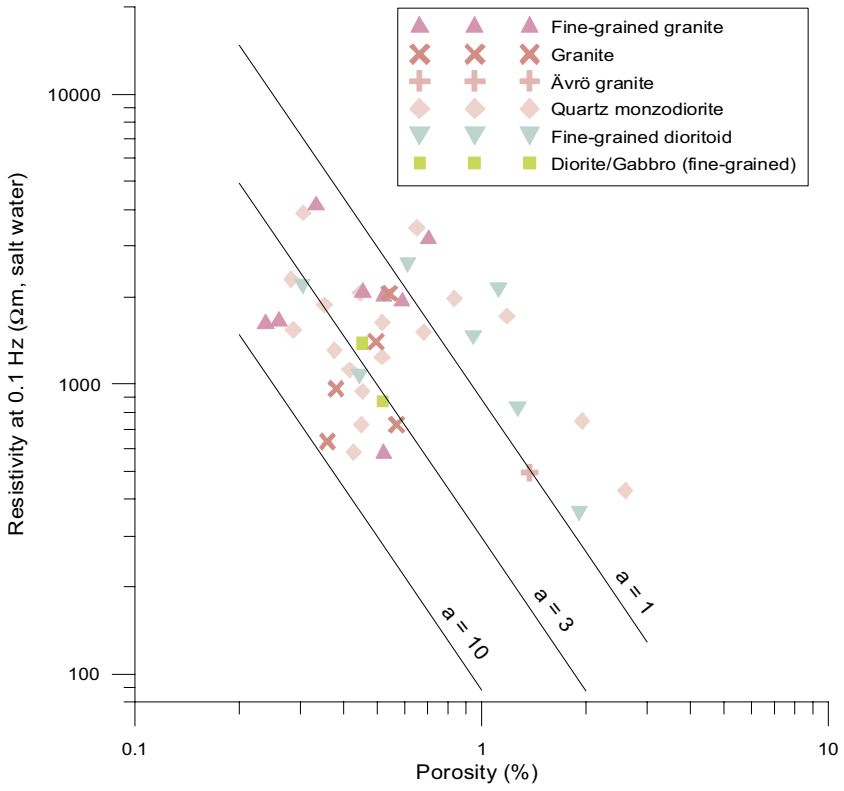

Figure 5-11. *Resistivity in saline water as a function of porosity. The solid lines corresponds to resistivities calculated with Archie's law and m=1.75. High values for the parameter a indicates large contributions of surface conductivity. Values below 1.0 are unrealistic indicating that the parameter m is underestimated for these samples.*

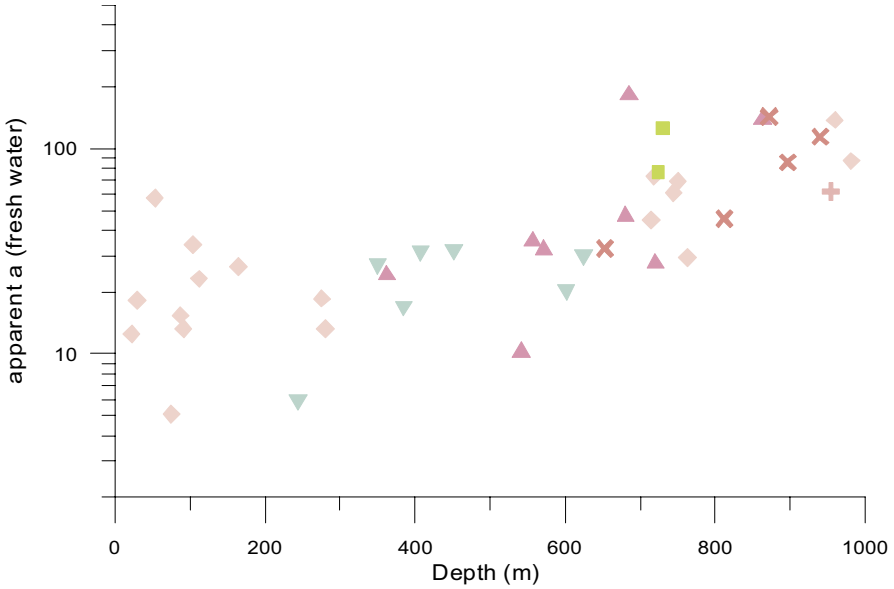

Figure 5-12. *Apparent a-values for resistivities calculated according to Archies law and m=1.75 in fresh water. The increase in the lower part of the hole might be an effect of ductile deformation. Rock types are according to the legends in Figures 5-6 to 5-11.*

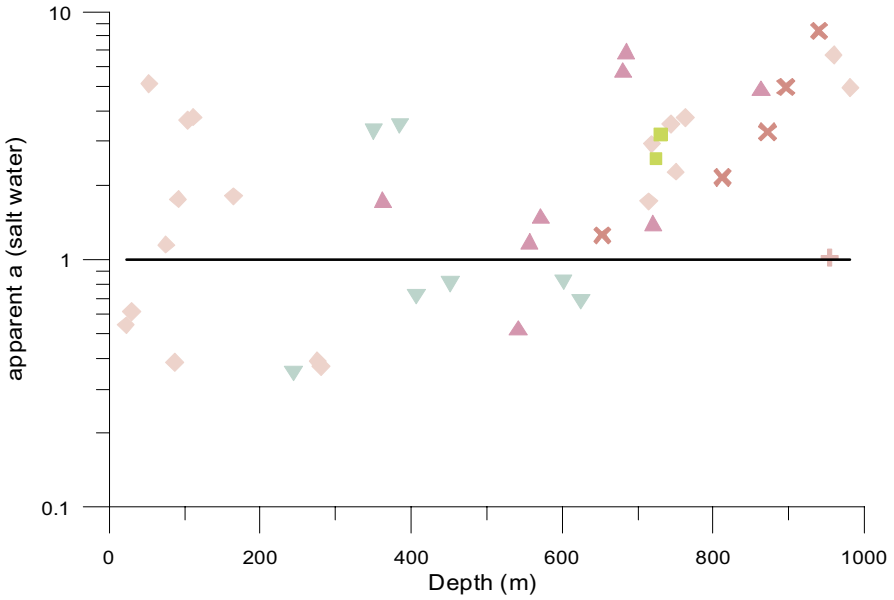

Figure 5-13. *Apparent a-values for resistivities calculated according to Archies law and m=1.75 in saline water. The increase in the lower part of the hole might be an effect of ductile deformation. Values below 1.0 indicates that the parameter m has been underestimated which indicates a different pore space texture. The samples with low values have high porosity. Rock types are according to the legends in Figures 5-6 to 5-11.*

When calculating the apparent porosity from the resistivity loggings the constants a and m are chosen in the way that they will conform to the average fluid resistivity of each specific borehole. In Table 5-1 below the different a- and m-values used in this investigation are presented.

Table 5-1. Values of the constants a and m in Archie's law used in the calculation of the apparent porosity.

Borehole	Average fluid resistivity (Ωm)	a	m
KSH01A (100–1000m)	1.3	1.35	0.889
KSH01B	7.3	6.68	1.073
KSH02	22.0	13.25	1.303
HSH01	8.2	8.19	1.126
HSH02	30.0	20.0	1.500
HSH03	9.6	6.68	1.073

5.2 Interpretation of logging data

A complete presentation of all processed loggings and the pseudo geology data is given in Appendices 1–7.

5.2.1 Controll of the logging data

Noise levels for all logging methods were calculated over the entire borehole length. The results are presented in Table 5-2. A majority of the loggings have noise levels below the recommended levels. However, all sonic and density loggings have noise levels clearly above. After median filtering of these loggings the noise levels decrease significantly, but still the noise is slightly above the recommended level. The noise after median filtering is, however, considered low enough not to exert a significant influence on the results of the interpretation of the data.

A qualitative inspection was performed on the loggings. The inspection indicates that the density and magnetic susceptibility logging of HSH01 and HSH03 were badly calibrated. Re-calibrated data were delivered by the logging firm but neither these data are considered showing reliable results. The loggings were therefore excluded in the interpretation and no pseudogeology is thus presented for HSH01 or HSH03. The inspection also shows that the long normal resistivity (N64) logging (only measured in the cored boreholes KSH01A, KSH01B and KSH02) indicates positive anomalies across fracture zones; a result that is physically unreliable. This logging is therefore excluded in all interpretations of fractures. The lateral resistivity logging of the cored boreholes is also excluded in all interpretations since this logging is not measured, but merely calculated on basis of data from the two normal resistivity loggings. The lateral resistivity logging is therefore just a function of the normal resistivity loggings and does not provide any new information.

Table 5-2. Noise levels in geophysical logging data (calculated over the entire borehole).

Logging method	KSH01A (100–1000m)	KSH01A (0–100m)	KSH01B	KSH02	HSH01	HSH02	HSH03	Recommended max noise level
Density (kg/m3)	18	No data	35	25	5	23	18	3–5
Magnetic susceptibility (SI)	$2*10^{-4}$	$4*10^{-4}$	$3*10^{-4}$	$0.8*10^{-4}$	$0.2*10^{-4}$	$0.4*10^{-4}$	$0.2*10^{-4}$	$1*10^{-4}$
Natural gamma radiation (µR/h)	0.5	No data	0.9	0.7	1.9	1.9	2.2	0.3
Lateral resistivity (%)	2.5	4.2	0.4	1.8	1.0	1.1	0.9	2.0
Short normal resistivity (%)	2.1	2.1	0.3	1.2	1.2	0.7	1.6	2.0
Long normal resistivity (N64) (%)	2.3	2.6	0.6	2.1	No data	No data	No data	2.0
Single point resistance (%)	2.4	No data	0.3	0.8	0.5	0.5	0.5	No data
Fluid resistivity (%)	0.08	0.07	0.01	0.02	0.1	0.1	0.2	2.0
Fluid temperature (°C)	0.0004	0.0002	0.0002	0.0005	0.01	0.004	0.004	0.01
Caliper (m)	0.000003	0.00001	0.000004	0.00001	0.00017	0.0004	0.0003	0.0005
Focused resistivity 300 (%)	19.2	6.9	18.1	15.7	No data	No data	No data	No data
Focused resistivity 140 (%)	No data	No data	17.2	17.0	No data	No data	No data	No data
Sonic (m/s)	46	70	45	65	No data	No data	No data	20

The single point resistance (SPR), lateral resistivity, short and long normal resistivity loggings of the percussion drilled part of KSH01A appear to be strongly influenced by the wide borehole diameter (ca 160 mm). The measured levels are significantly lower than in the cored part of the borehole and there is no correlation between anomalies in these loggings and the sonic logging. A correction of the short normal resistivity (N16) data made for the borehole diameter and the fluid resistivity does not improve these data in any significant way. All these loggings were excluded from the interpretation. The only loggings used for interpretation of fractures in the percussion drilled part of KSH01A are thus caliper, sonic and focused resistivity (300). The gamma-gamma (density) and natural gamma loggings were not measured by Rambøll in the percussion drilled part of KSH01A, thus no pseudogeology has been established for this part of KSH01A.

5.2.2 KSH01A (100–1000 m)

The result of the pseudogeology classification together with geophysical logging data, interpreted porosity, salinity and vertical temperature gradient logs for the borehole KSH01A is presented in Appendix 1.

Correction of loggings and apparent porosity

The geometric mean of the measured short normal resistivity (N16) is 2.0 kΩm (± 0.25 decades) and after correction it is 2.0 kΩm (± 0.26 decades). The geometric mean of the measured long normal resistivity (N64) is 1.25 kΩm (± 0.16 decades) and after correction it is 0.75 kΩm (± 0.16 decades).

The median porosity calculated on basis of the short normal resistivity (N16) data is 0.6% and it is 1.2% calculated on basis of the long normal resistivity (N64) data.

Vertical temperature gradient and salinity

The mean vertical temperature gradient is 13.6°C/km. Large anomalies in the temperature gradient, possibly related to large water bearing fractures, roughly appear along the sections 110–130 m, 260–330 m and 500–610 m (compare to fractures below).

The estimated salinity varies between 7000 and 10 000 ppm NaCl for the uppermost 600 m of the hole, and below 600 m the level decreases fairly linearly down to ca 2000 ppm NaCl.

Interpretation of rock types and fractures

The uppermost 500 m of the hole are completely dominated by quartz monzodiorite, with some occurrence of fine-grained dioritoid and fine-grained granite. In the lower 500–1000 m of the borehole there is more heterogenic distribution of rock types. Ävrö granite dominate the sections 550–700 m and 950–1000 m. Along section 550–700 m there is also a fairly large occurrence of fine-grained dioritoid as well as granite (both fine-grained and medium- to coarse-grained). From 700 m to 720 m there is a complete dominance of diorite to gabbro and from 720 m to 740 m there is a complete dominance of fine-grained granite. Along the section 860–940 m the natural gamma radiation level has increased, which results in the classification of mainly medium- to coarse-grained granite and fine-grained granite.

The pseudo fracture frequency indicates 5 sections of increased fracturing possibly related to deformation zones. These sections roughly are: 135–145 m, 197–214 m, 246–272 m, 555–562 m and 590–615 m.

5.2.3 KSH01A (0–100 m, percussion drilled, Rambøll data)

The result of the pseudofracture calculation together with geophysical logging data, interpreted salinity and vertical temperature gradient logs for the borehole KSH01A (0–100 m, percussion drilled part) is presented in Appendix 2.

An earlier geophysical logging interpretation of the percussion drilled part of KSH01A (0–100 m) performed on geophysical logging data logged by Malå Geoscience AB/Raycon /2/ is reported separately /7/ because the presentation of pseudo geology and pseudo fracturing from geophysical logging data has been developed during the course of the project.

Correction of loggings and apparent porosity

No results.

Vertical temperature gradient and salinity

The borehole fluid temperature data shows a continuous decrease down to ca 50 m depth. From ca 70 m to 100 m the temperature increases and for this section the mean vertical temperature gradient is ca 6.1°C/km. There are no large high frequency anomalies along the borehole.

At the top of the borehole the estimated salinity is ca 2000 ppm NaCl. A rapid increase in salinity occurs between 30 m and 70 m depth, and below this depth the level stabilizes at ca 7500 ppm NaCl.

Interpretation of rock types and fractures

No pseudogeology is calculated for this section of KSH01A due to the lack of data.

The pseudo fracture frequency does not indicate any major increased fracturing in the borehole. However, as noted earlier the data are only based on the sonic, caliper and focused resistivity loggings, which may result in an underestimation in relation to the true fracture frequency.

5.2.4 KSH01B

The result of the pseudogeology classification together with geophysical logging data, interpreted porosity, salinity and vertical temperature gradient logs for the borehole KSH01B is presented in Appendix 3.

Correction of loggings and apparent porosity

The geometric mean of the measured short normal resistivity (N16) is 6.8 kΩm (± 0.10 decades) and after correction it is 5.3 kΩm (± 0.10 decades). The geometric mean of the measured long normal resistivity (N64) is 2.6 kΩm (± 0.09 decades) and after correction it is 1.9 kΩm (± 0.08 decades).

The median porosity calculated on basis of the short normal resistivity (N16) data is 0.7% and it is 1.3% calculated on basis of the long normal resistivity (N64) data.

Vertical temperature gradient and salinity

The borehole fluid temperature data show a similar pattern a for the top 100 m of KSH01A. There is a continuous decrease down to ca 50 m depth. From ca 60 m to 90 m the temperature increases and for this section the mean vertical temperature gradient is ca 8.2°C/km. No major anomalies are seen in the temperature gradient.

Along the uppermost 10 m of the borehole the estimated salinity is ca 500 ppm NaCl. A rapid increase occurs between 25 m and 50 m depth, and below this depth the level stabilizes at ca 1100–1150 ppm NaCl. A minor positive jump occurs at ca 74 m depth.

Interpretation of rock types and fractures

The lithology is completely dominated by quartz monzodiorite with minor occurrence of fine-grained granite. No deformation zone is indicated in the pseudo alteration or pseudo fracture frequency loggings.

5.2.5 KSH02 (0–100 m)

The result of the pseudogeology classification together with geophysical logging data, interpreted porosity, salinity and vertical temperature gradient logs for the borehole KSH02 is presented in Appendix 4.

Correction of loggings and apparent porosity

The geometric mean of the measured short normal resistivity (N16) is 5.7 kΩm (± 0.15 decades) and after correction it is 3.9 kΩm (± 0.15 decades). The geometric mean of the measured long normal resistivity (N64) is 3.4 kΩm (± 0.13 decades) and after correction it is 2.9 kΩm (± 0.11 decades).

The median porosity calculated on basis of the short normal resistivity (N16) data is 1.1% and it is 1.3% calculated on basis of the long normal resistivity (N64) data.

Vertical temperature gradient and salinity

Apart from the uppermost ca 10 m of the borehole, where the fluid temperature increases step wise, there is an almost constant fluid temperature of ca 9°C in the entire borehole. The average temperature gradient is ca 4.3°C/km and there are three major anomalies at ca 20 m, ca 60 m and ca 90 m depth, of which those at 20 m and 90 m depth most likely are artificial.

The estimated salinity is fairly constant at a level of ca 250 ppm NaCl in the entire borehole.

Interpretation of rock types and fractures

The lithology is completely dominated by quartz monzodiorite, with some occurrence of Ävrö granite, fine-grained granite and fine-grained diorite to gabbro.

A possible deformation zone is indicated by increased pseudo fracture frequency and possible alteration along the section 50–66 m of the borehole.

5.2.6 HSH01

The result of the pseudofracture calculation together with geophysical logging data, interpreted salinity and vertical temperature gradient logs for the borehole HSH01 is presented in Appendix 5.

Correction of loggings and apparent porosity

The geometric mean of the measured lateral resistivity is 2.7 kΩm (± 0.27 decades) and after correction it is 1.7 kΩm (± 0.28 decades). The geometric mean of the measured short normal resistivity (N16) is 0.34 kΩm (± 0.43 decades) and after correction it is 0.28 kΩm (± 0.44 decades).

The median porosity calculated on basis of the lateral resistivity data is 1.2% and it is 3.7% calculated on basis of the short normal resistivity (N16) data.

Vertical temperature gradient and salinity

The fluid temperature data is rather noisy and the variation may indicate non-stable conditions. The average temperature gradient is close to zero (or ca 1.6°C/km), but there is a repeated anomaly pattern with a period length of ca 10 m. At ca 110–120 m depth there is a very large anomaly in the gradient data.

Along the uppermost 100 m of the borehole the salinity is estimated at ca 230–400 ppm NaCl. At 100 m depth there is a stepwise increase to ca 1330 ppm NaCl. This level is constant down to the bottom of the borehole, where there is an indication of a major increase in salinity.

Interpretation of rock types and fractures

No pseudogeology is calculated for the borehole. Two possible deformation zones are indicated by increased pseudofracture frequency along the sections 40–48 m and 161–168 m.

5.2.7 HSH02

The result of the pseudogeology classification together with geophysical logging data, interpreted porosity, salinity and vertical temperature gradient logs for the borehole HSH02 is presented in Appendix 6.

Correction of loggings and apparent porosity

The geometric mean of the measured lateral resistivity is 7.3 kΩm (± 0.23 decades) and after correction it is 4.7 kΩm (± 0.29 decades). The geometric mean of the measured short normal resistivity (N16) is 1.1 kΩm (± 0.22 decades) and after correction it is 0.92 kΩm (± 0.24 decades).

The median porosity calculated on basis of the lateral resistivity data is 0.8% and it is 2.4% calculated on basis of the short normal resistivity (N16) data.

Vertical temperature gradient and salinity

The fluid temperature data are noisy but show a rather well defined increase in temperature from top to bottom of the borehole. The average temperature gradient is ca 8.0°C/km. Between 120 m to 180 m depth there are a number of large anomalies in the temperature gradient.

The salinity is constant at ca 170 ppm NaCl from the top of the borehole down to 146 m depth, where there is a rapid increase to ca 285 ppm NaCl.

Interpretation of rock types and fractures

The pseudo geology indicates that the lithology in the vicinity of the borehole is dominated by Ävrö granite. Large sections of fine-grained diorite/gabbro are seen along the uppermost ca 70 m of the borehole. The large number of unclassified sections indicate that there is a poor fit of the logging data to the petrophysical database.

Increased fracturing is indicated along the section 10–30 m, and minor sections of alteration are indicated between 150 m and 190 m depth.

5.2.8 HSH03

The result of the pseudofracture calculation together with geophysical logging data, interpreted salinity and vertical temperature gradient logs for the borehole HSH03 is presented in Appendix 7.

Correction of loggings and apparent porosity

The geometric mean of the measured lateral resistivity is 2.29 kΩm (± 0.37 decades) and after correction it is 1.83 kΩm (± 0.37 decades). The geometric mean of the measured short normal resistivity (N16) is 0.18 kΩm (± 0.53 decades) and after correction it is 0.14 kΩm (± 0.53 decades).

The median porosity calculated on basis of the lateral resistivity data is 0.9% and it is 4.9% calculated on basis of the short normal resistivity (N16) data.

Vertical temperature gradient and salinity

The fluid temperature data is rather noisy and the irregular variations may indicate non-stable conditions. The average temperature gradient is ca 3.2°C/km. One of the larger anomalies occurs at 65–75 m depth, which corresponds well with a major low resistivity section possibly indicating a water bearing fracture (see fracture below).

Along the uppermost ca 60 m of the borehole the salinity level is estimated at ca 230 ppm NaCl. At ca 70 m depth there is a rapid stepwise increase in salinity to ca 2800 ppm NaCl.

Interpretation of rock types and fractures

No pseudogeology is calculated for the borehole. One possible deformation zone is indicated by increased pseudofracture frequency along the section 63–71 m.

5.3 Comparison between logging and petrophysical data in KSH01A and KSH01B

A quality control of the gamma-gamma, magnetic susceptibility and the resistivity (short and long normal) loggings is performed by comparing the logging data to the petrophysical data at the corresponding depths. In Figure 5-14 the gamma-gamma (density) logging is plotted versus wet density sample measurements. As seen in the figure the correlation between logging and petrophysical data is excellent, even though there is some scatter in the data. The slope of the regression line is very close to 1.0, which indicates that the two data sets also are in the same range. A similar cross plot for the magnetic susceptibility also shows good correlation (Figure 5-15), but the slope of the fitted line is 0.653 and not 1.0 as it should be. This indicates that the logging data underestimates the susceptibility by ca 35%, which may be a result of an incorrect calibration of the logging tool. All susceptibility loggings measured with this tool have been corrected for this prior to the interpretation.

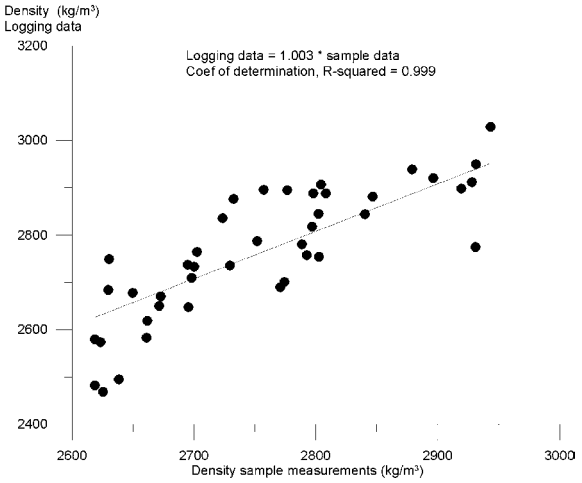

Figure 5-14. *Gamma-gamma (density) logging data versus sample measurement at corresponding depth.*

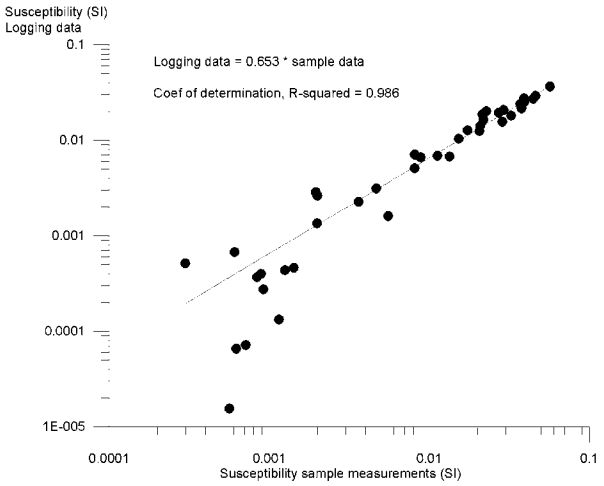

Figure 5-15. *Magnetic susceptibility logging data versus sample measurement at corresponding depth.*

The procedure of calculating the true resistivity of the rock in the vicinity of the borehole also involves a calculation of the apparent porosity. In Figure 5-16 above the apparent porosity loggings calculated on basis of the short normal (blue curve) and long normal (black curve) resistivity loggings of KSH01a and KSH01b are displayed together with porosities measured on rock samples from the cores of the two boreholes. The apparent porosity based on the short normal resistivity (N16) loggings are in the same range as the sample data and there is a fair correlation between corresponding anomalies. The apparent porosity based on the long normal resistivity (N64) logging overestimates the true porosity by a factor of ca 3.

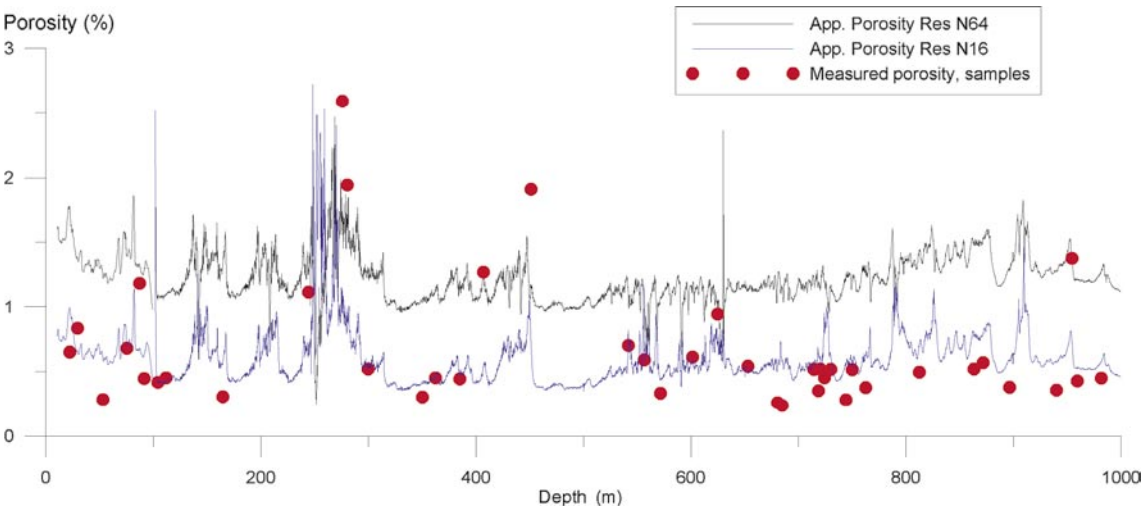

Figure 5-16. *Apparent porosity loggings calculated on basis of the short and long normal resistivity (N64) loggings of KSH01a and KSH01b, displayed together with porosity measured on rock samples from the cores of the two boreholes.*

6 Discussion and conclusions

A summation of some of the petrophysical parameters gained from KSH01A and KSH01 B is presented in Table 6-1. The compilation of the petrophysical parameters indicates that the data distribution agrees well with the results obtained from corresponding rock types at the surface /6/, apart from the fact that the magnetic susceptibility of the fine-grained dioritoid is generally lower in the borehole data /3/. The low susceptibility is most likely explained by the alteration that, according to the geological core logging (Boremap), has affected this rock type along major sections of the core. The single sample of Ävrö granite with a density of 2931 kg/m^3 suggests a possible erroneous rock classification, since this high density indicates a composition corresponding to diorite to gabbro. This borehole section ought to be re-examined.

AMS and electric resistivity data, independently from each other, indicate that the rocks of the lowermost ca 300 m of KSH01A (section 700–1000 m) may have suffered from plastic deformation. The lithology along this section is more heterogenic than for the uppermost 600 m, and there are some sections of relatively higher densities and higher natural gamma radiation levels at ca 700–1000 m depth. This is likely related to the results of the petrophysical data since variations in mineralogy will affect the petrophysical properties of the rocks. However, the lithological heterogeneity is unlikely to be the very cause of the "deformation indication" since the petrophysical data covers different rock types and the variations in properties are consistent regardless of type of rock.

Table 6-1. Average values of some petrophysical parameters from rock samples in KSH01A and KSH01B.

Rock type	Number of samples	Wet density (kg/m^3)	Magnetic susceptibility (Logarithm 10^{-5} SI)	Q-value (unit less)	Electric resistivity, fresh water 0.1 Hz (Logarithm Ωm)	Induced polarization, fresh water 0.1 Hz (mrad)	Porosity (%)
Ävrö granite	1	2931	3.34	0.16	3.06	11.8	1.4
Fine-grained dioritoid	7	2753 ± 39	2.40 ± 0.56	0.28 ± 0.09	3.95 ± 0.56	11.2 ± 4.5	0.9 ± 0.6
Quartz monzodiorite	18	2807 ± 72	3.12 ± 0.69	0.27 ± 0.10	4.05 ± 0.42	11.0 ± 3.8	0.7 ± 0.6
Granite, fine- to medium-grained	9	2633 ± 15	2.27 ± 0.61	0.41 ± 0.31	4.12 ± 0.34	7.0 ± 2.1	0.5 ± 0.2
Granite, medium- to coarse-grained	5	2685 ± 18	3.18 ± 0.10	0.34 ± 0.14	3.81 ± 0.27	10.6 ± 3.9	0.5 ± 0.1
Fine-grained diorite to gabbro	2	2930	1.79	0.16	3.65	9.8	0.5

The pseudogeological rock classification of the three cored boreholes KSH01A (100–1000 m), KSH01B and KSH02 (0–100 m) generally indicates a dominance of quartz monzodiorite rocks in the vicinity of these boreholes. A number of fairly thin (generally <1 m wide) fine-grained granite dykes occur frequently in the boreholes. Below 600 m depth (KSH01A) the physical properties of the rocks show large variations, which indicate a more heterogeneous lithology. This is displayed in the pseudo geological logging as a mixture of ca 5–20 m long sections of mainly granite (medium to coarse grained), Ävrö granite, fine-grained granite and quartz monzodiorite, with minor occurrence of fine-grained mafic rock (diorite to gabbro) and fine-grained dioritoid. Comparing the results of the pseudogeology classification to the core logging Boremap shows a fair agreement regarding lithological boundaries (see example in Figure 6-1). When comparing rock types it is evident that the occurrence of fined-grained granite correlates very well between the pseudogeology classification and the core logging (Boremap). However, one major difference between the two classifications is that large sections of KSH01A classified as fine-grained dioritoid in the core logging (Boremap) are classified as quartz monzodiorite in the pseudogeological classification. The reason for this is that the fine-grained dioritoid and the quartz monzodiorite rocks have very similar petrophysical characteristics. The pseudogeology is a statistical classification solely based on petrophysical properties of rocks, and does therefore not manage to separate these two rock types.

The comparison between mapped and estimated fracture frequency in KSH01A indicates good co-variation in magnitude as well as in frequency variations (Figure 6-2). There is also a clear connection between sections with high fracture frequency and large fluid temperature gradients. This indicates that some of the fractures most likely are water bearing.

The poor data quality of the density and susceptibility loggings of HSH01 and HSH03 does not allow a pseudogeological interpretation of these boreholes. A pseudogeological logging is presented for the borehole HSH02, but the reliability of this classification is questionable due to the high number of unclassified sections and also due to the problems with the data from the other two percussion drilled boreholes.

The results of the pseudogeology classification together with geophysical logging data, interpreted porosity, salinity and vertical temperature gradient logs for the boreholes KSH01A, the percussion drilled part of KSH01A, KSH01B and the upper part of KSH02 (0–100 m), HSH01, HSH02 and HSH03 are presented in Appendices 1 to 7 respectively.

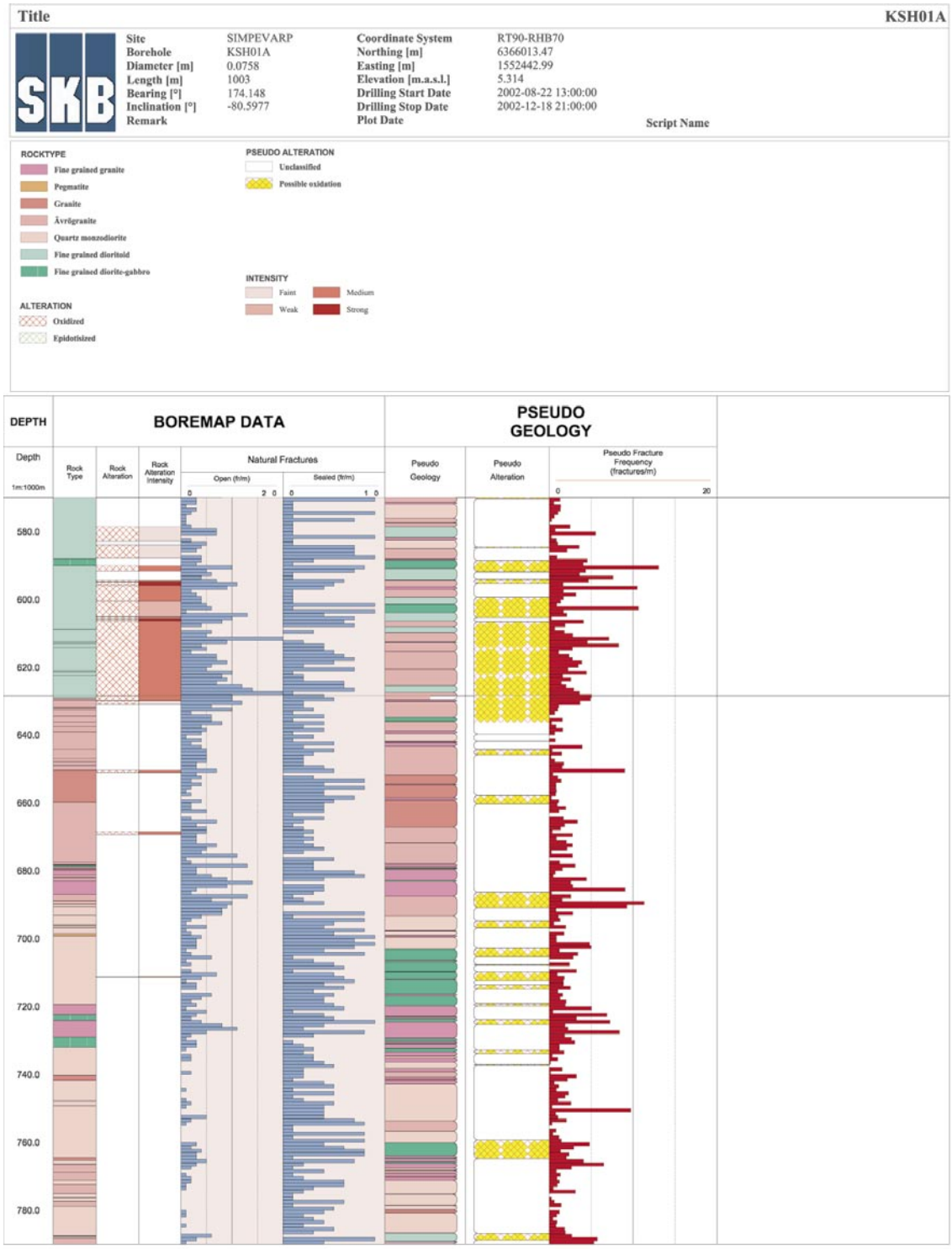

Figure 6-1. *Comparison between Boremap data and pseudogeological data along the section 570–790 m of the borehole KSH01A.*

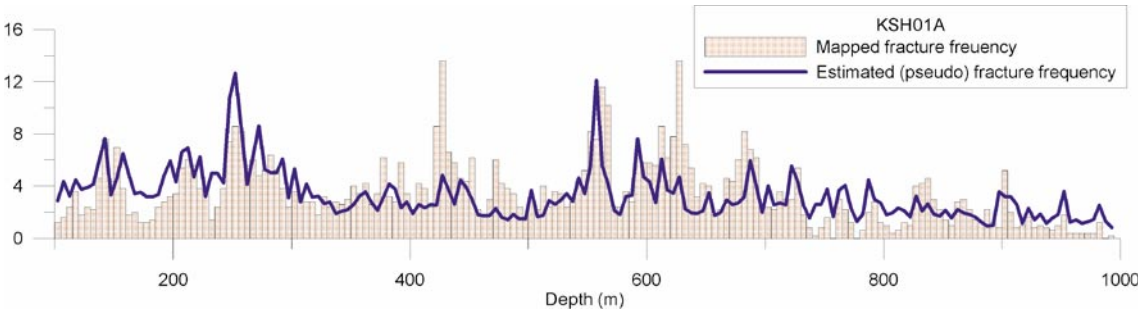

Figure 6-2. *Mapped and estimated fracture frequency for the borehole KSH01A (100–1000 m).*

References

/1/ **Nielsen U T, Ringgaard J, 2003.** Geophysical logging in borehole KSH01A, KSH01B and part of KSH02. SKB P-03-16, Svensk Kärnbränslehantering AB.

/2/ **Nilsson P, Gustafsson C, 2003.** Geophysical, radar and BIPS logging in borehole KSH01A, HSH01, HSH02 and HSH03. SKB P-03-15, Svensk Kärnbränslehantering AB.

/3/ **Mattsson H, Thunehed H, 2003.** Measurements of petrophysical parameters on rock samples during autumn 2002. SKB P-03-19, Svensk Kärnbränslehantering AB.

/4/ **Sehlstedt S, 1988.** Description of geophysical data on the SKB data base GEOTAB. SKB TR 88-05, Svensk Kärnbränslehantering AB.

/5/ **Henkel H, 1991.** Petrophysical properties (density and magnetization) of rock from the northern part of the Baltic Shield. Tectonophysics 192, 1–19.

/6/ **Mattsson H, Thunehed H, Triumf C A, 2003.** Compilation of petrophysical parameters from rock samples and in situ gamma-ray spectrometry measurements. SKB P-03-97, Svensk Kärnbränslehantering AB.

/7/ **Mattsson H, 2003.** Interpretation of borehole geophysical data from the percussion drilled part of the borehole KSH01A. SKB P-04-27, Svensk Kärnbränslehantering AB.

Appendix 1

Pseudogeology classification together with geophysical logging data for the borehole KSH01A

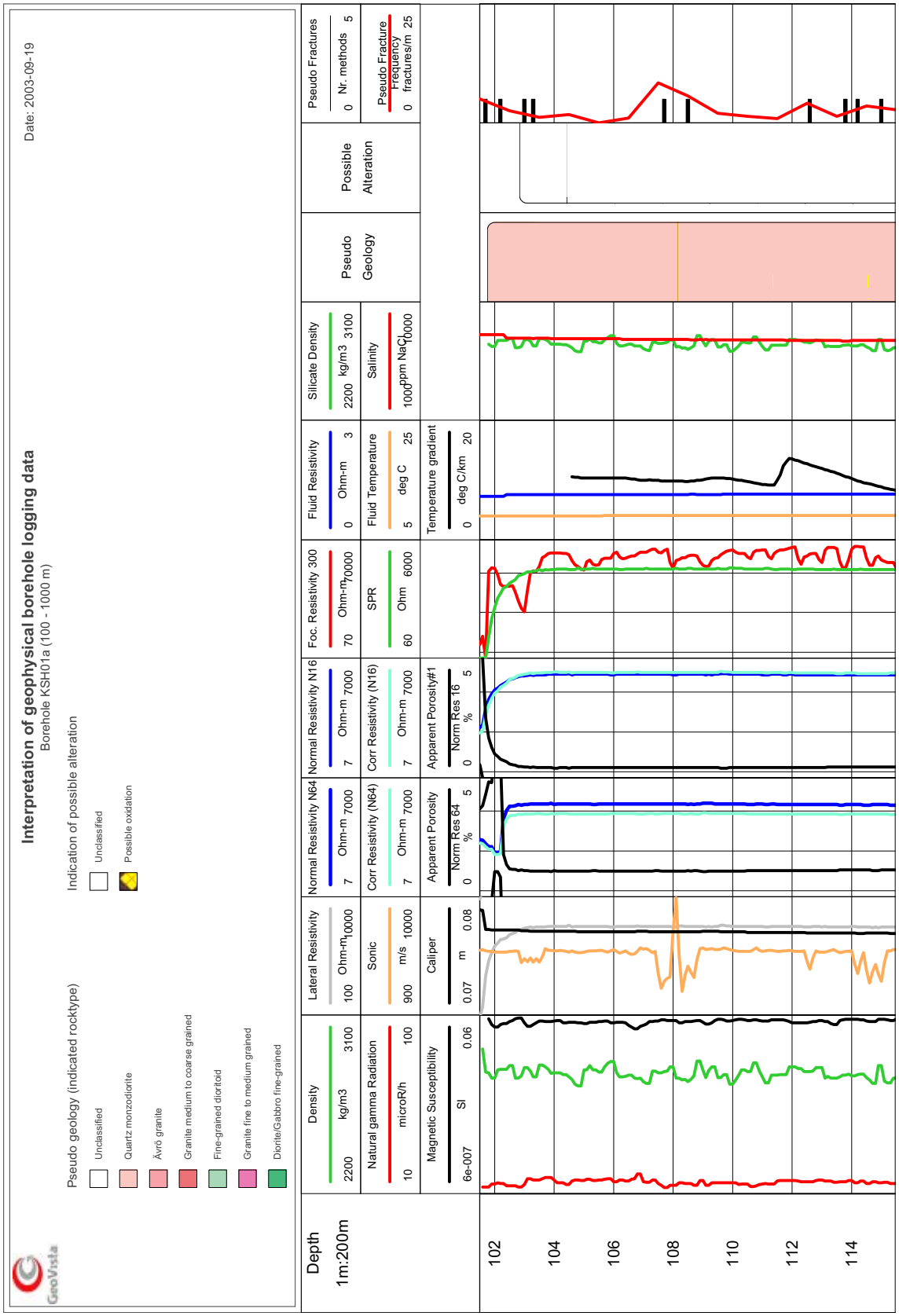

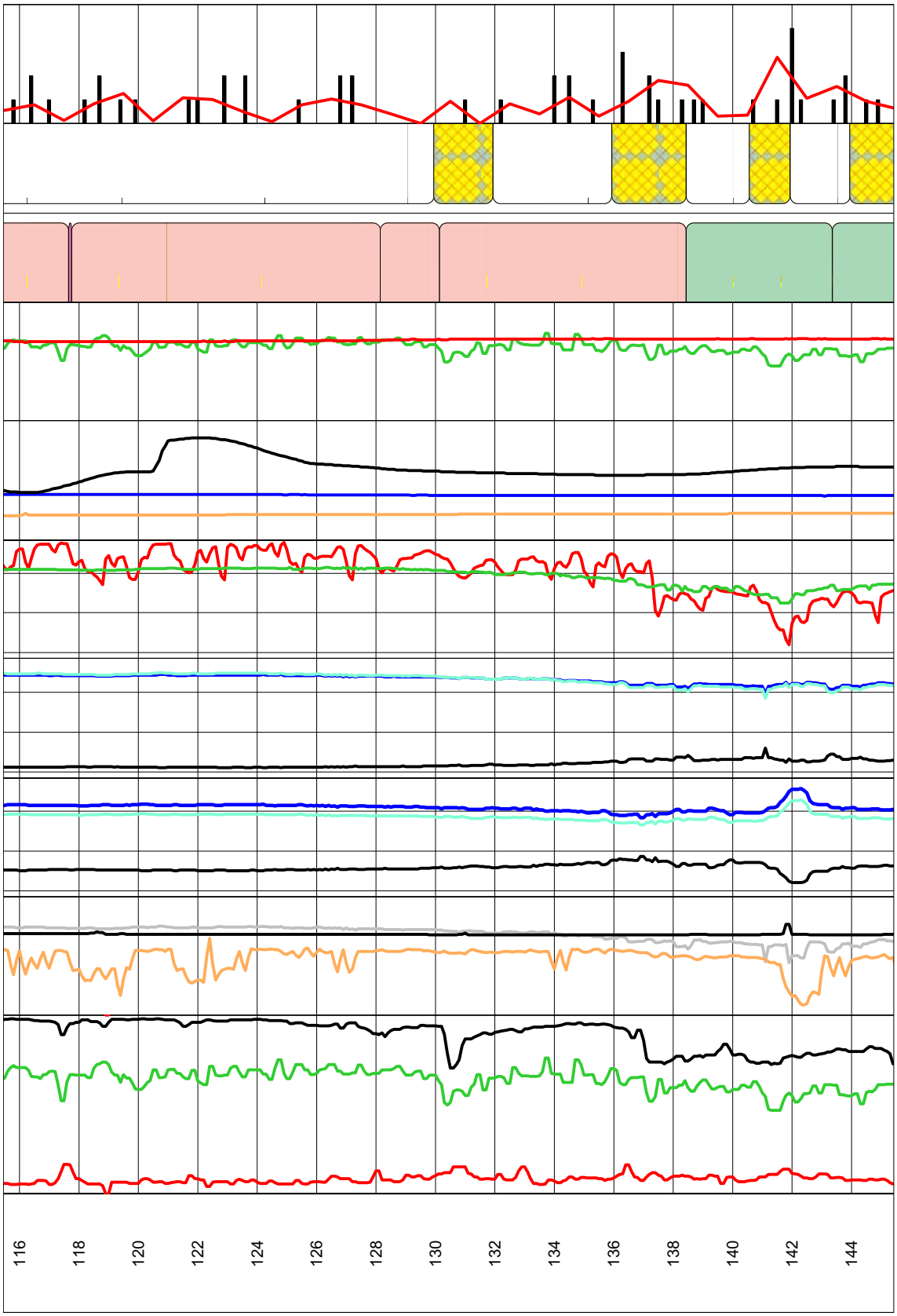
116
118
120
122
124
126
128
130
132
134
136
138
140
142
144

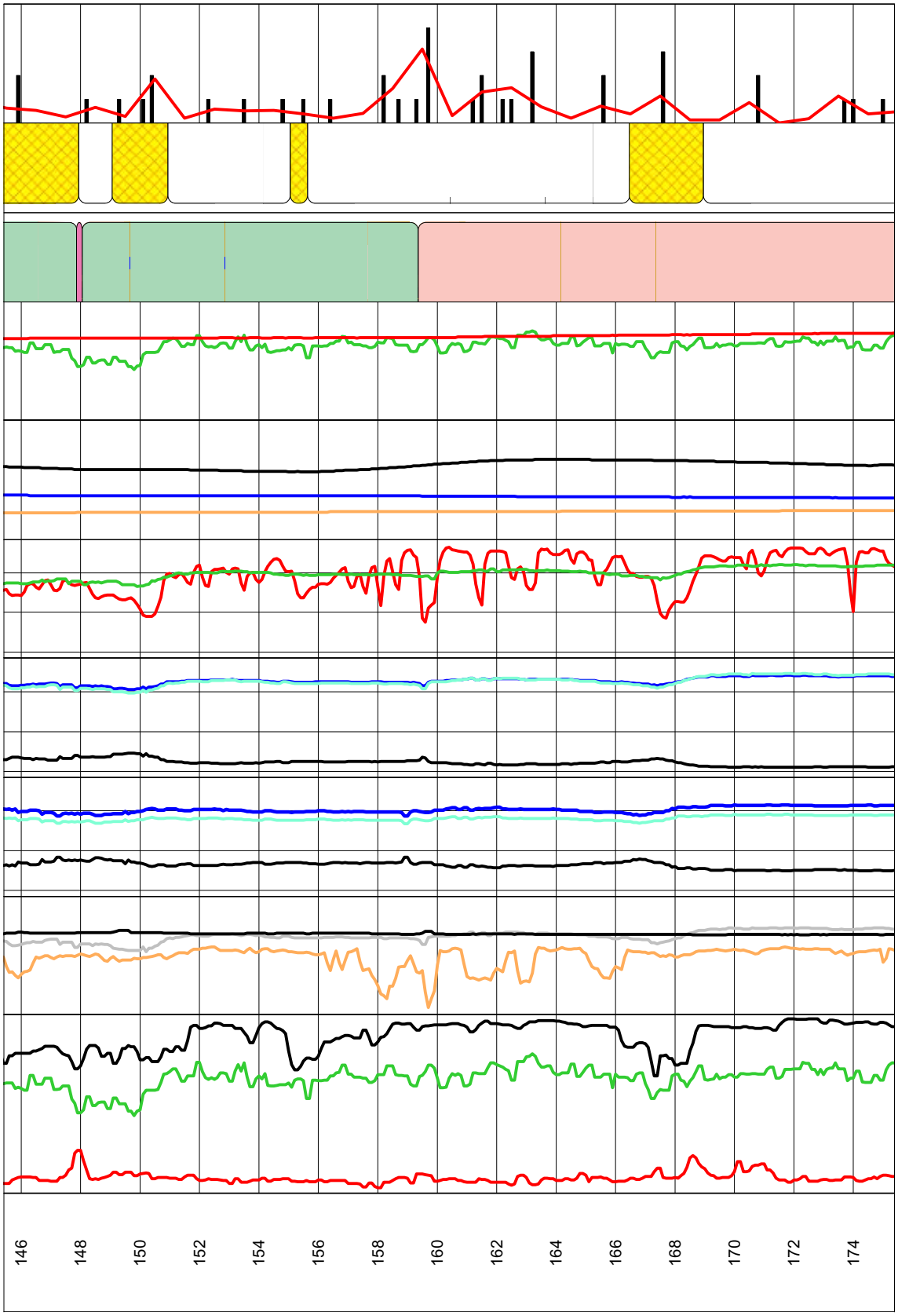
146
148
150
152
154
156
158
160
162
164
166
168
170
172
174

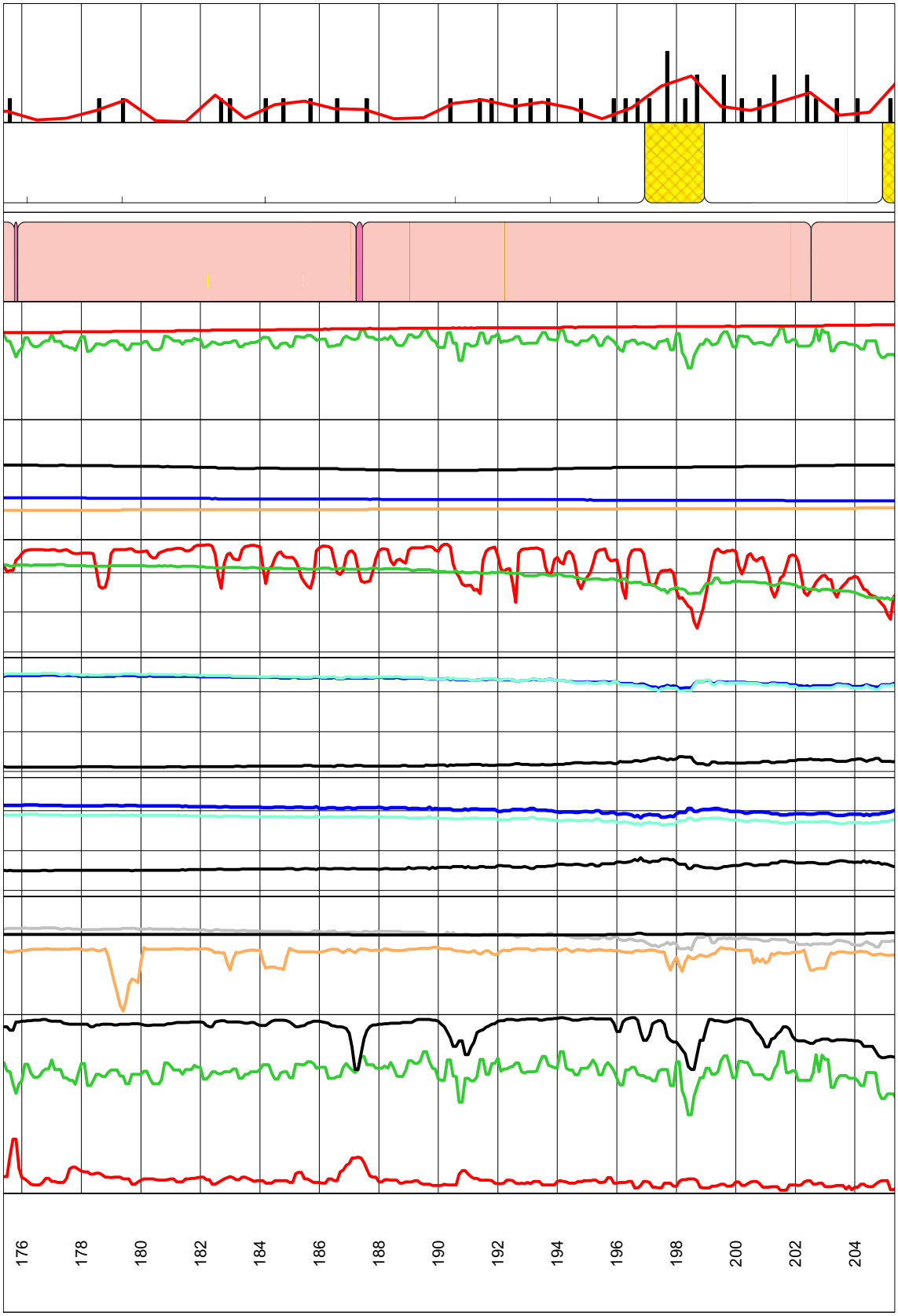
176
178
180
182
184
186
188
190
192
194
196
198
200
202
204

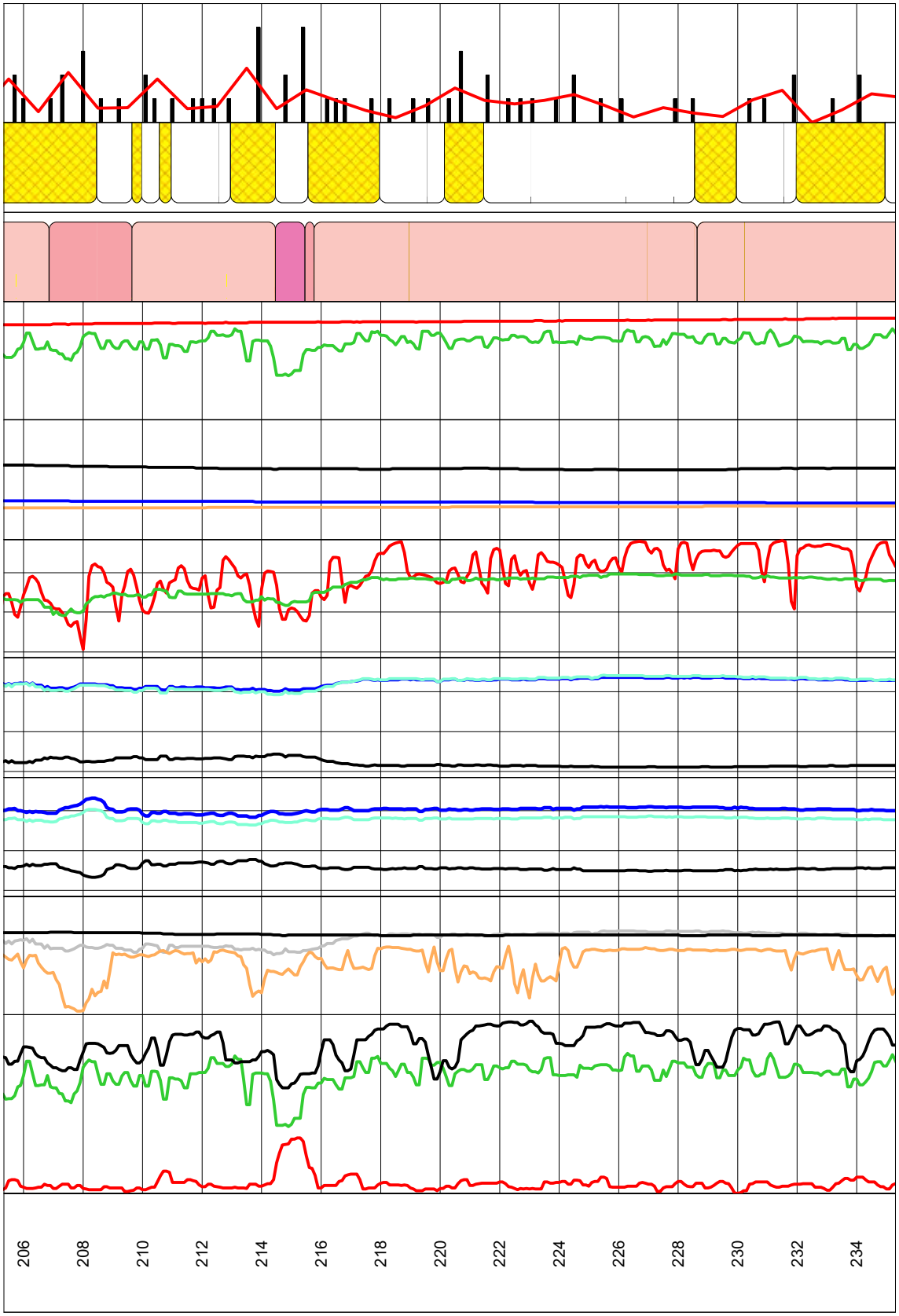
206
208
210
212
214
216
218
220
222
224
226
228
230
232
234

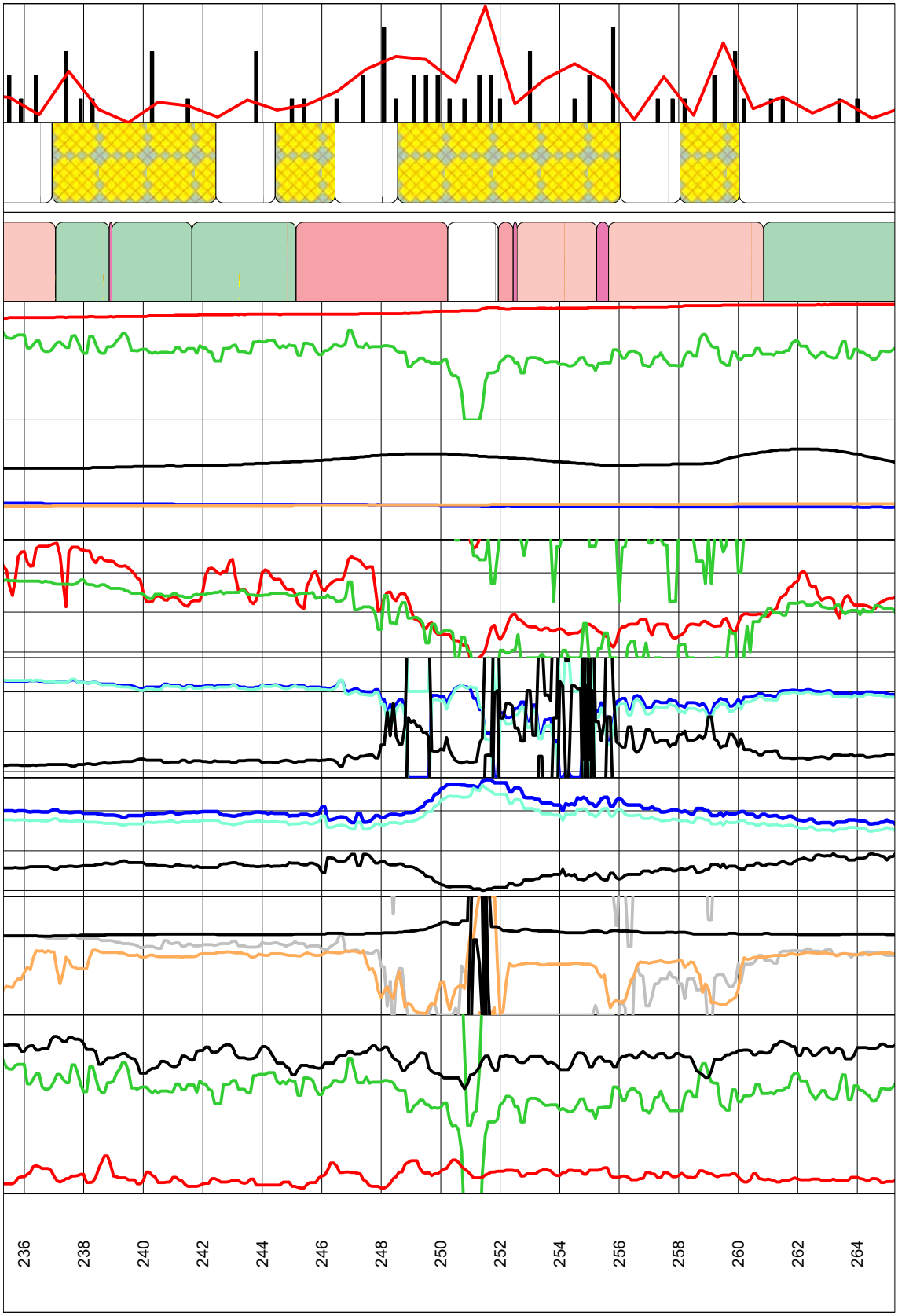
236
238
240
242
244
246
248
250
252
254
256
258
260
262
264

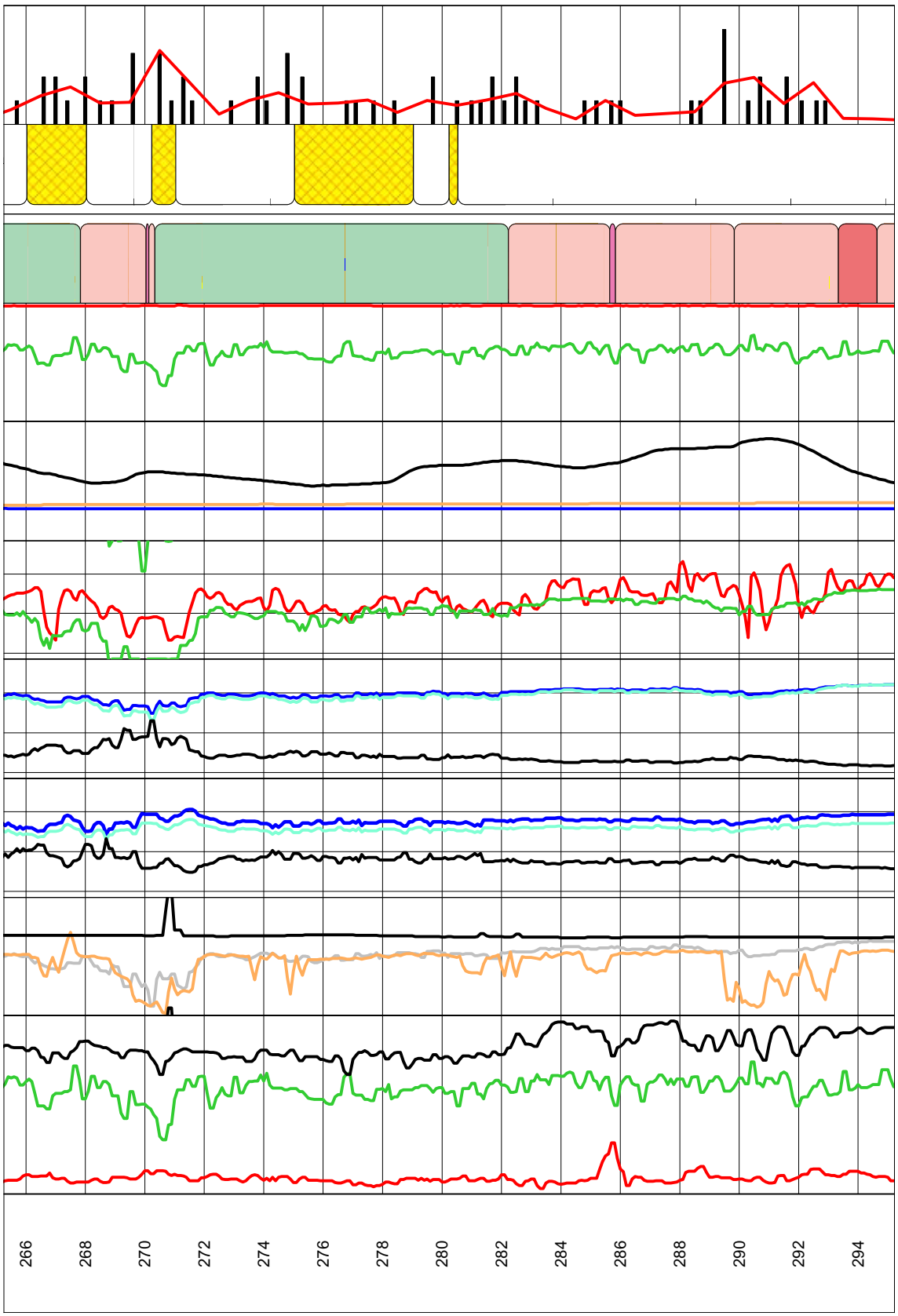
266
268
270
272
274
276
278
280
282
284
286
288
290
292
294

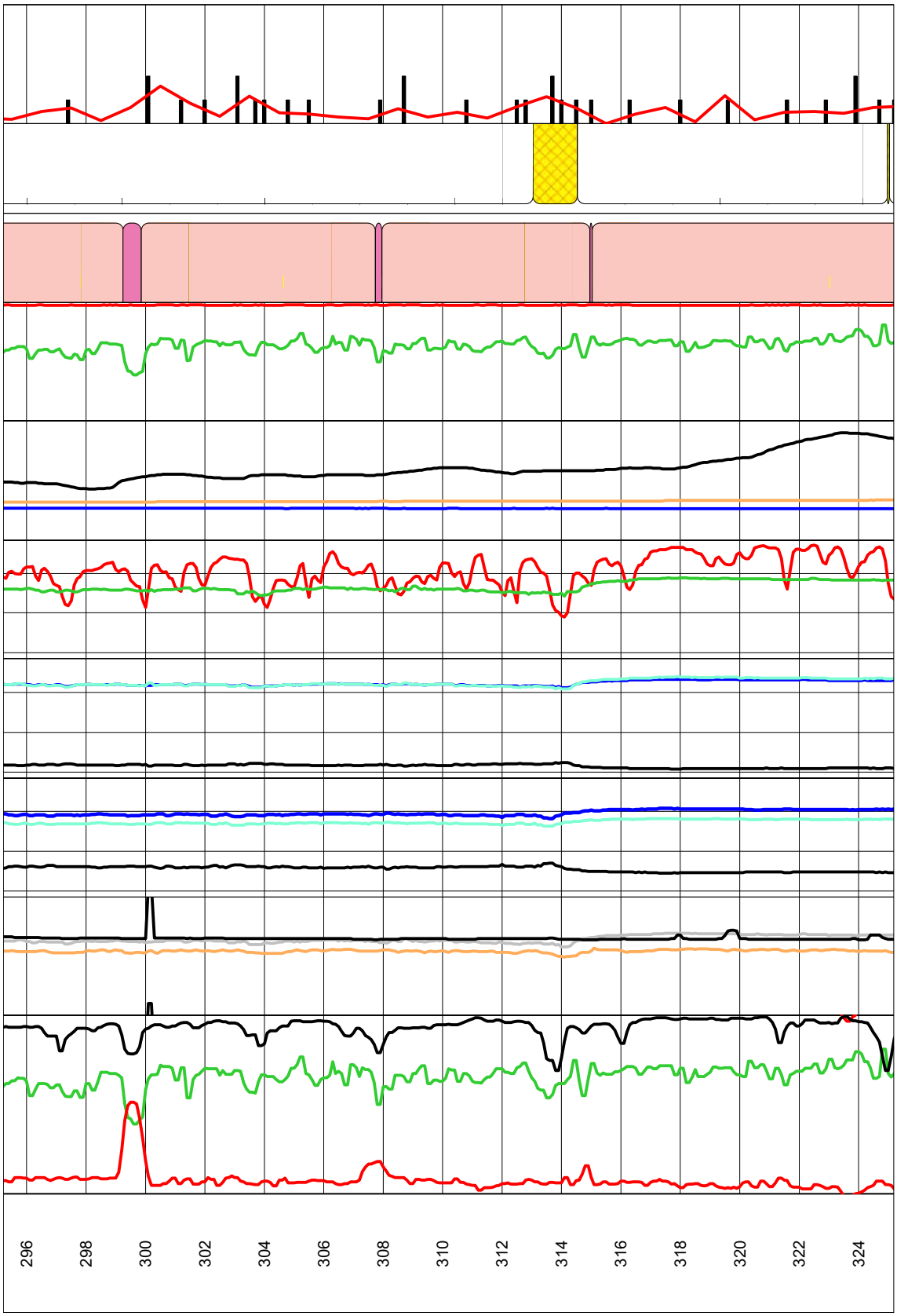
296
298
300
302
304
306
308
310
312
314
316
318
320
322
324

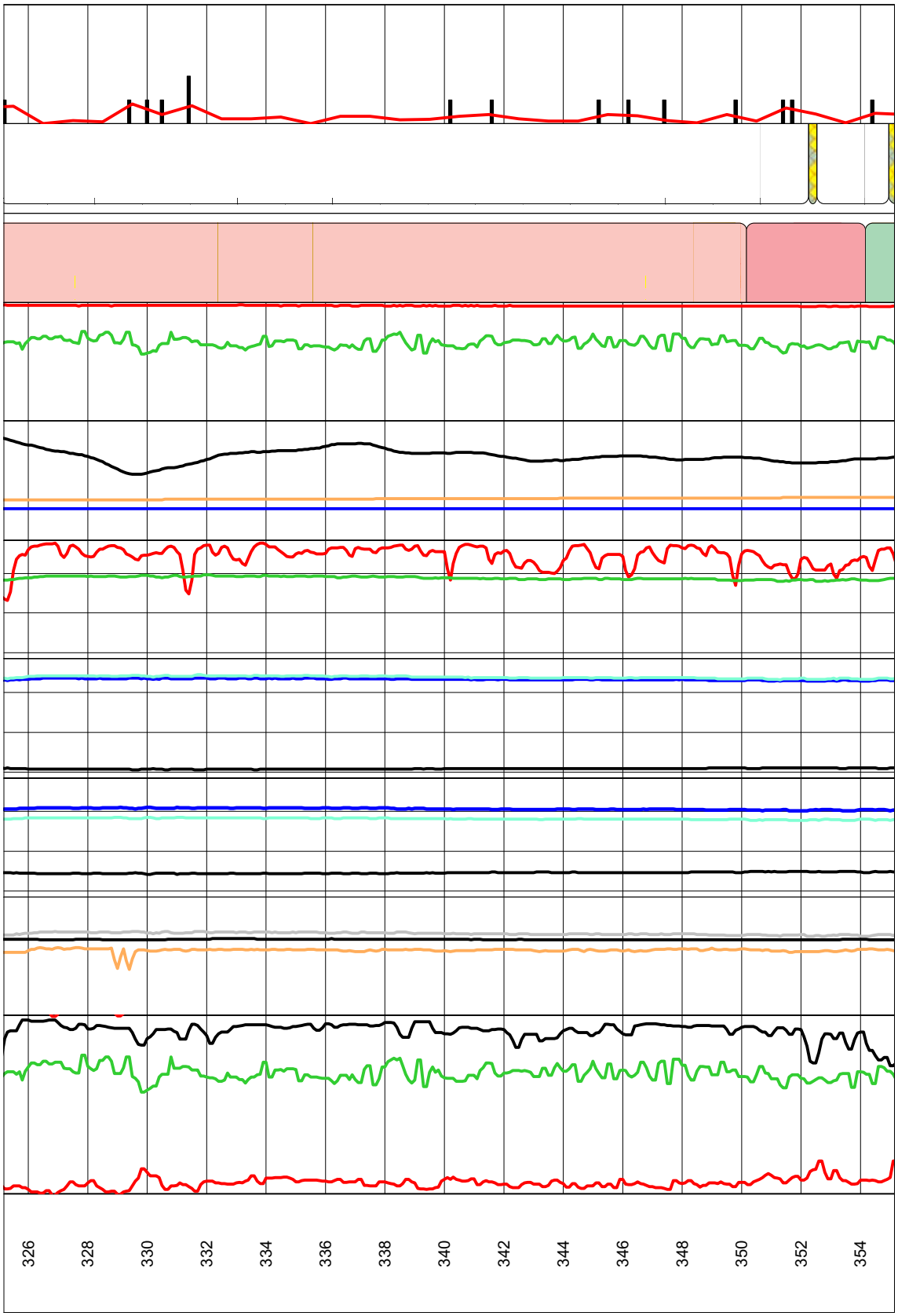
326
328
330
332
334
336
338
340
342
344
346
348
350
352
354

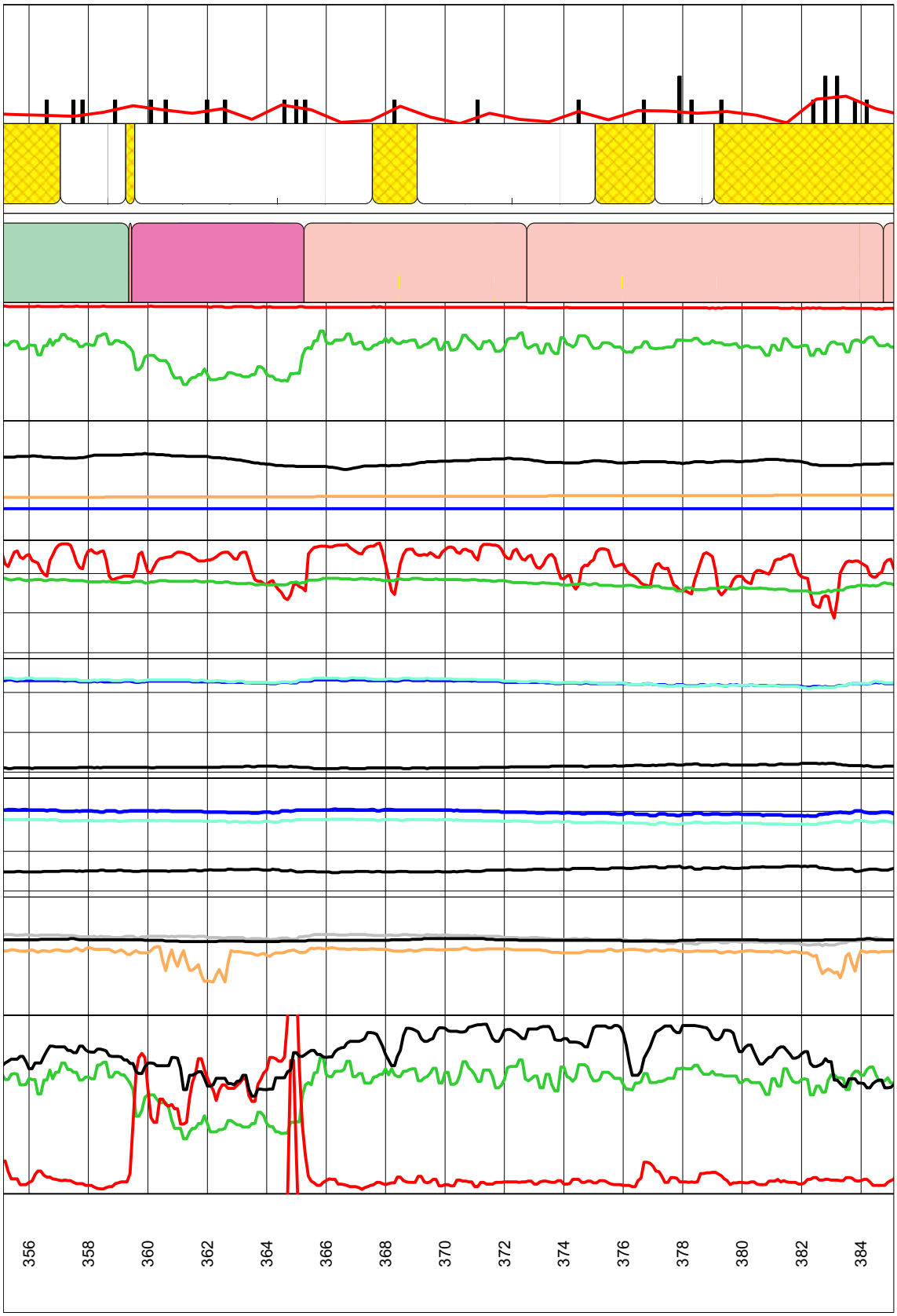
356
358
360
362
364
366
368
370
372
374
376
378
380
382
384

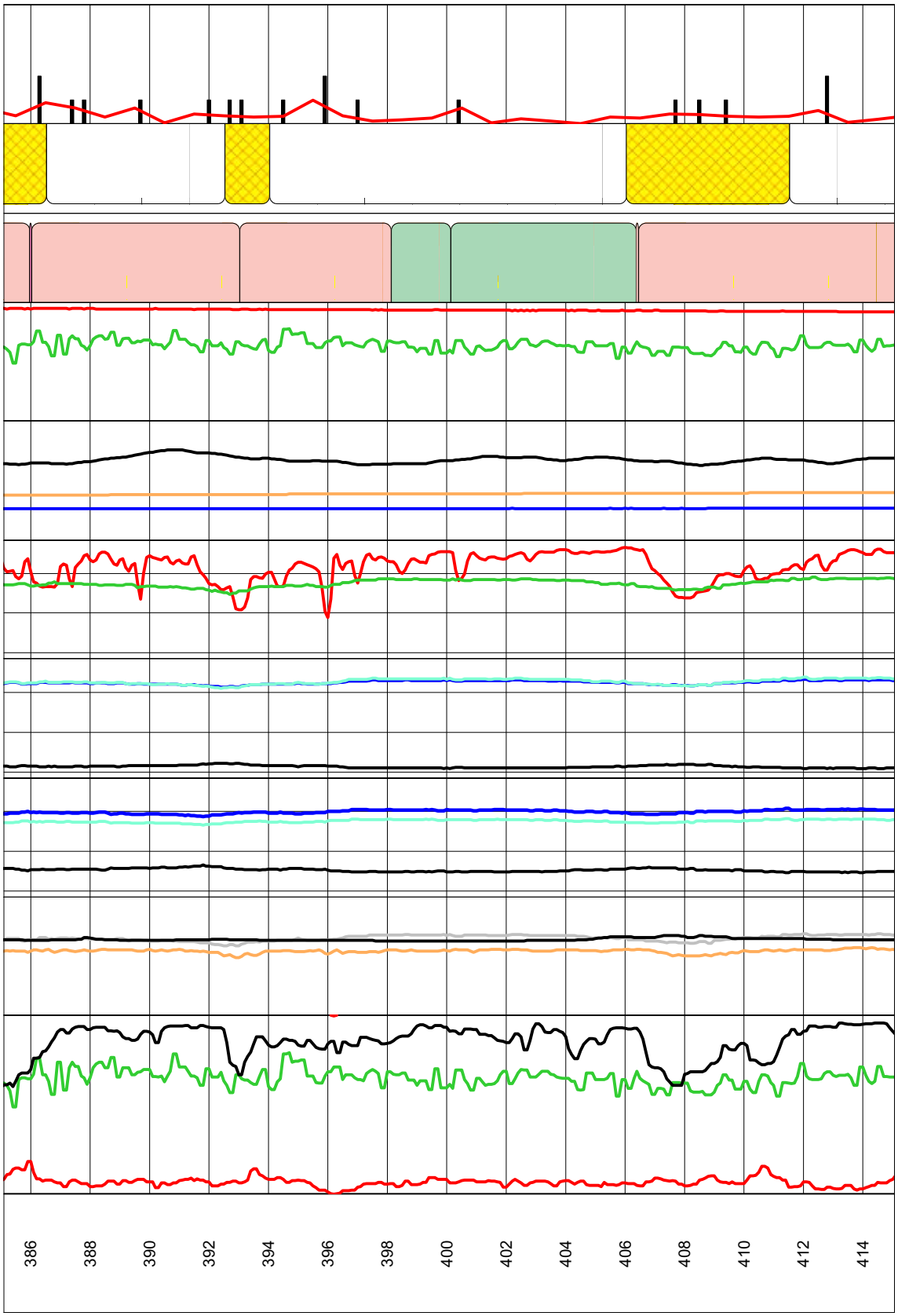
386
388
390
392
394
396
398
400
402
404
406
408
410
412
414

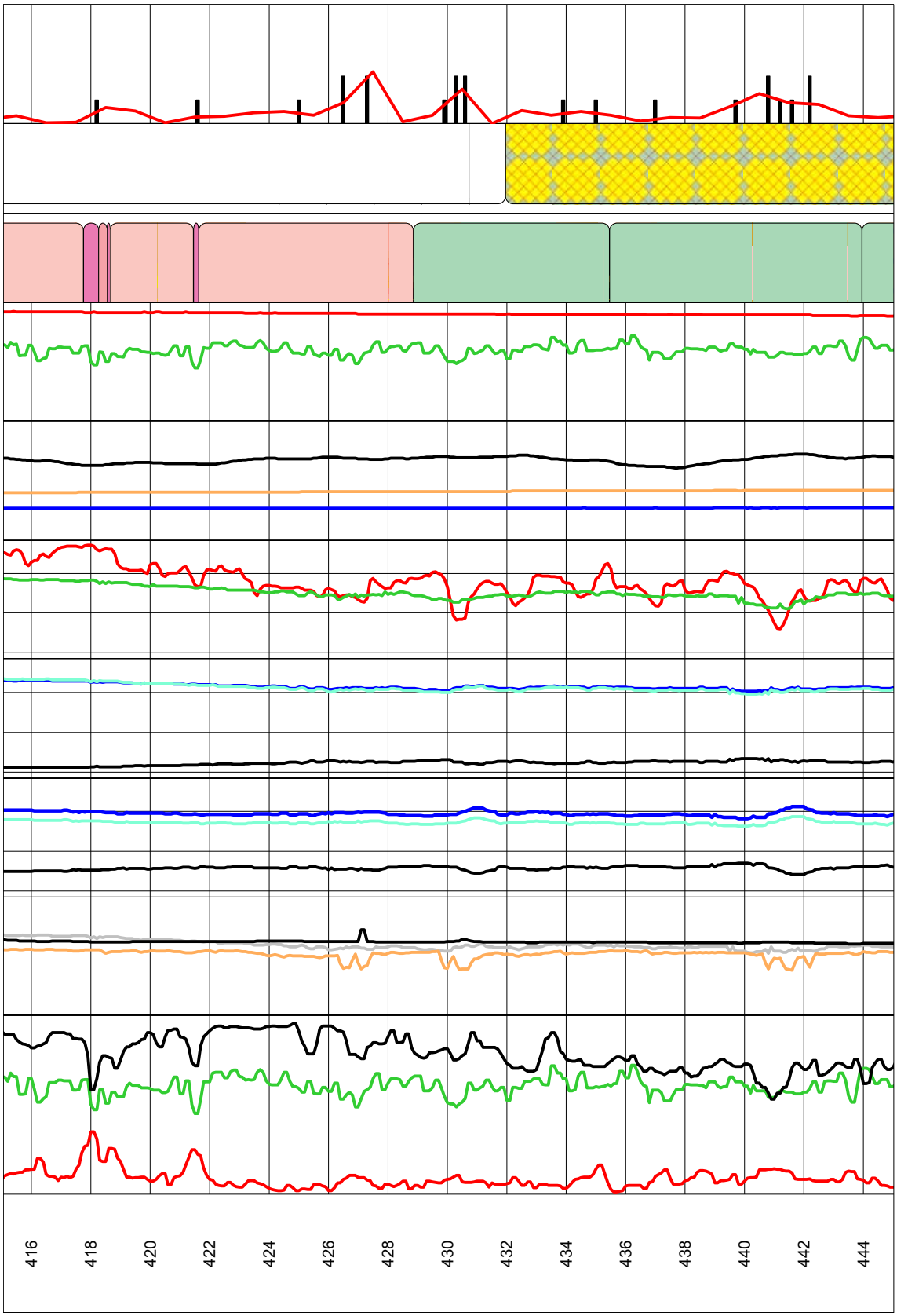
416
418
420
422
424
426
428
430
432
434
436
438
440
442
444

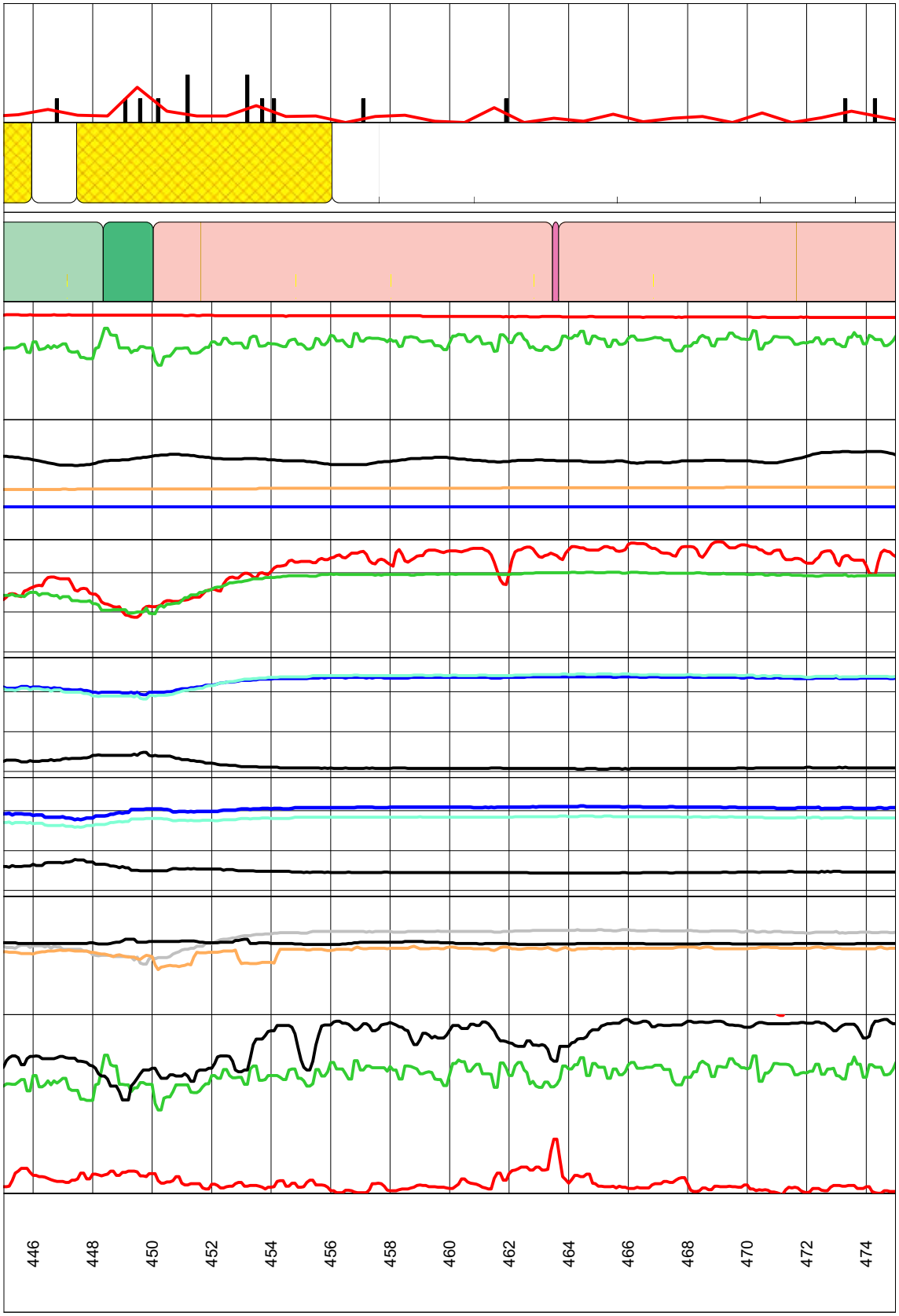
446
448
450
452
454
456
458
460
462
464
466
468
470
472
474

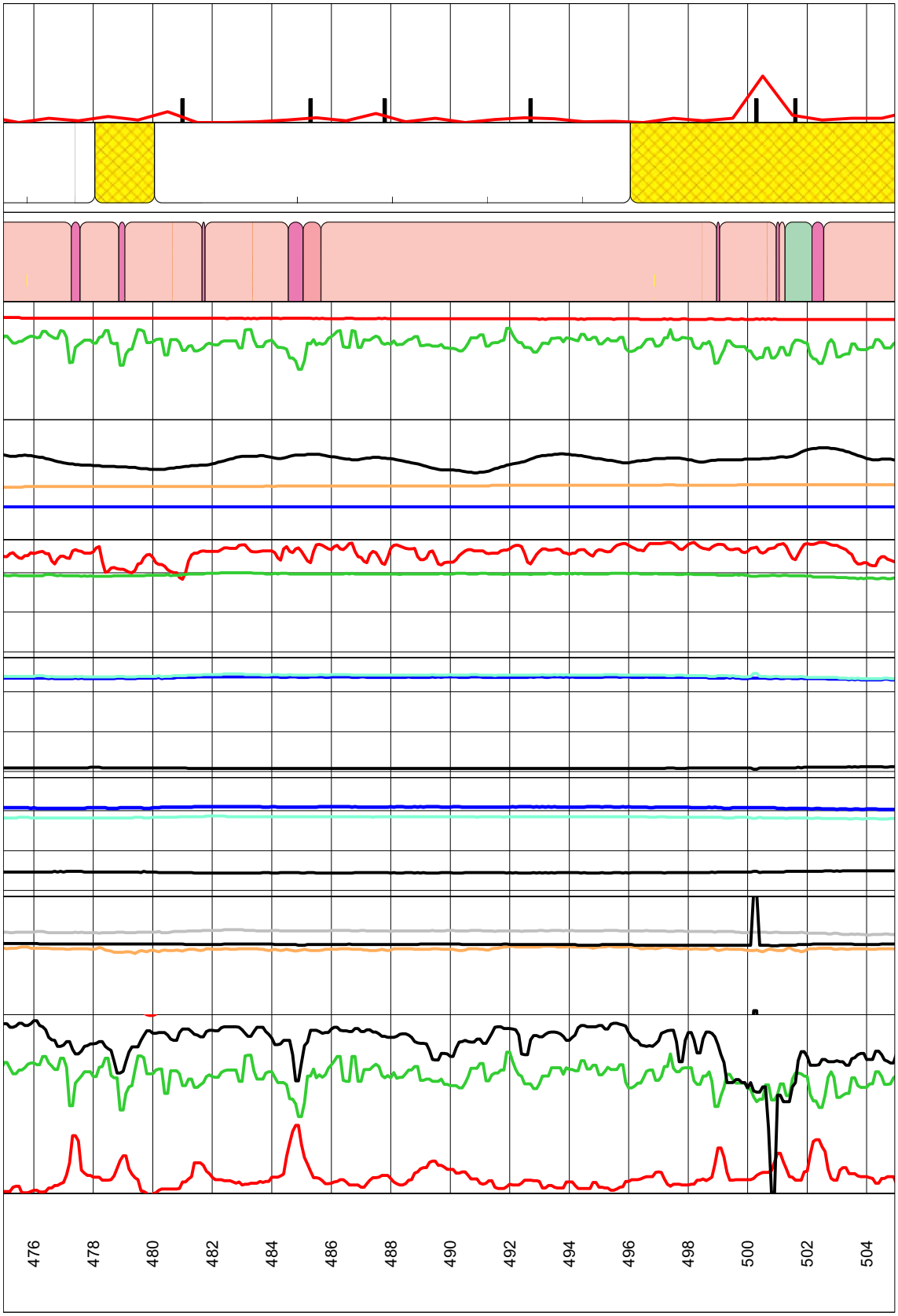
476
478
480
482
484
486
488
490
492
494
496
498
500
502
504

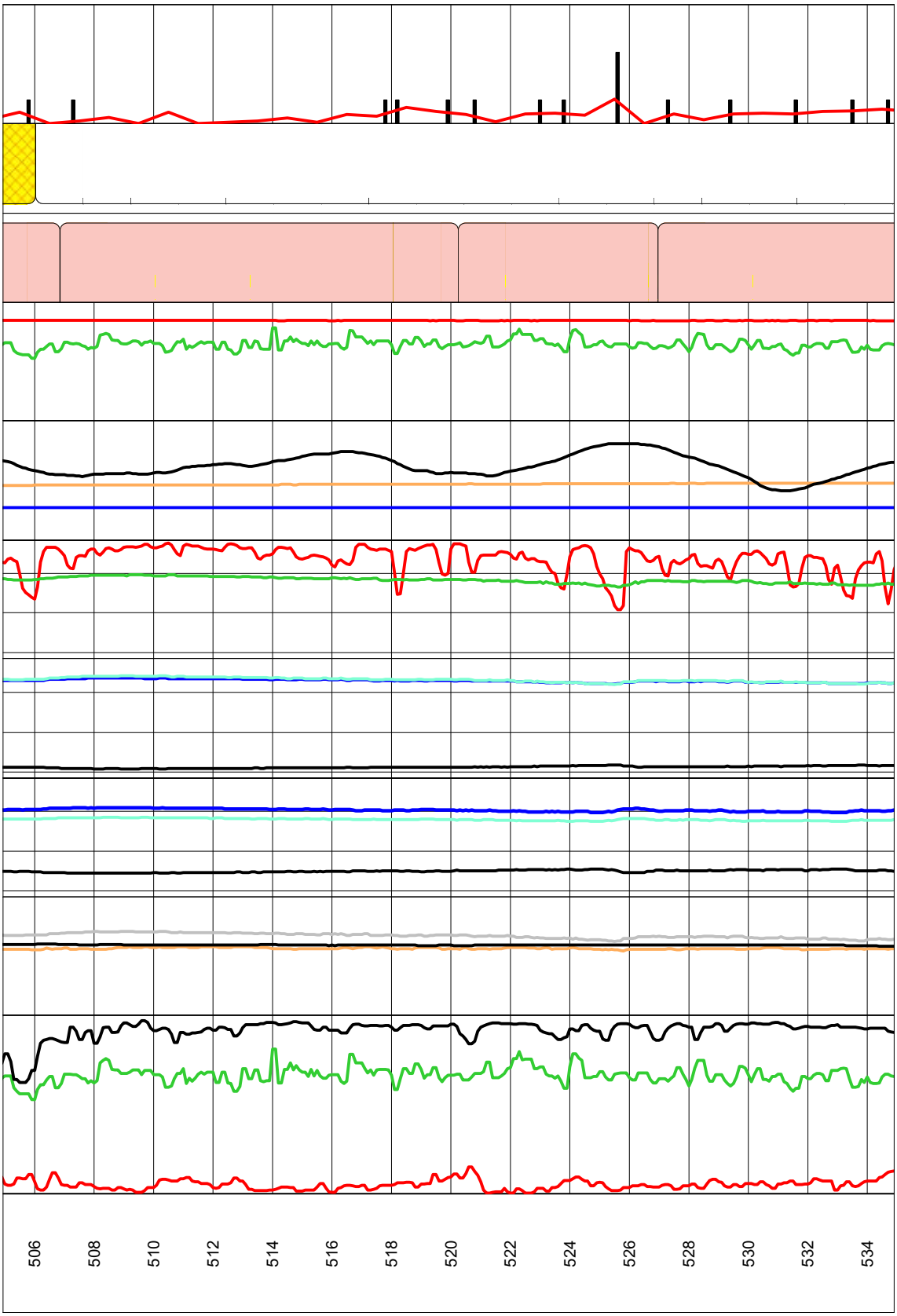
506
508
510
512
514
516
518
520
522
524
526
528
530
532
534

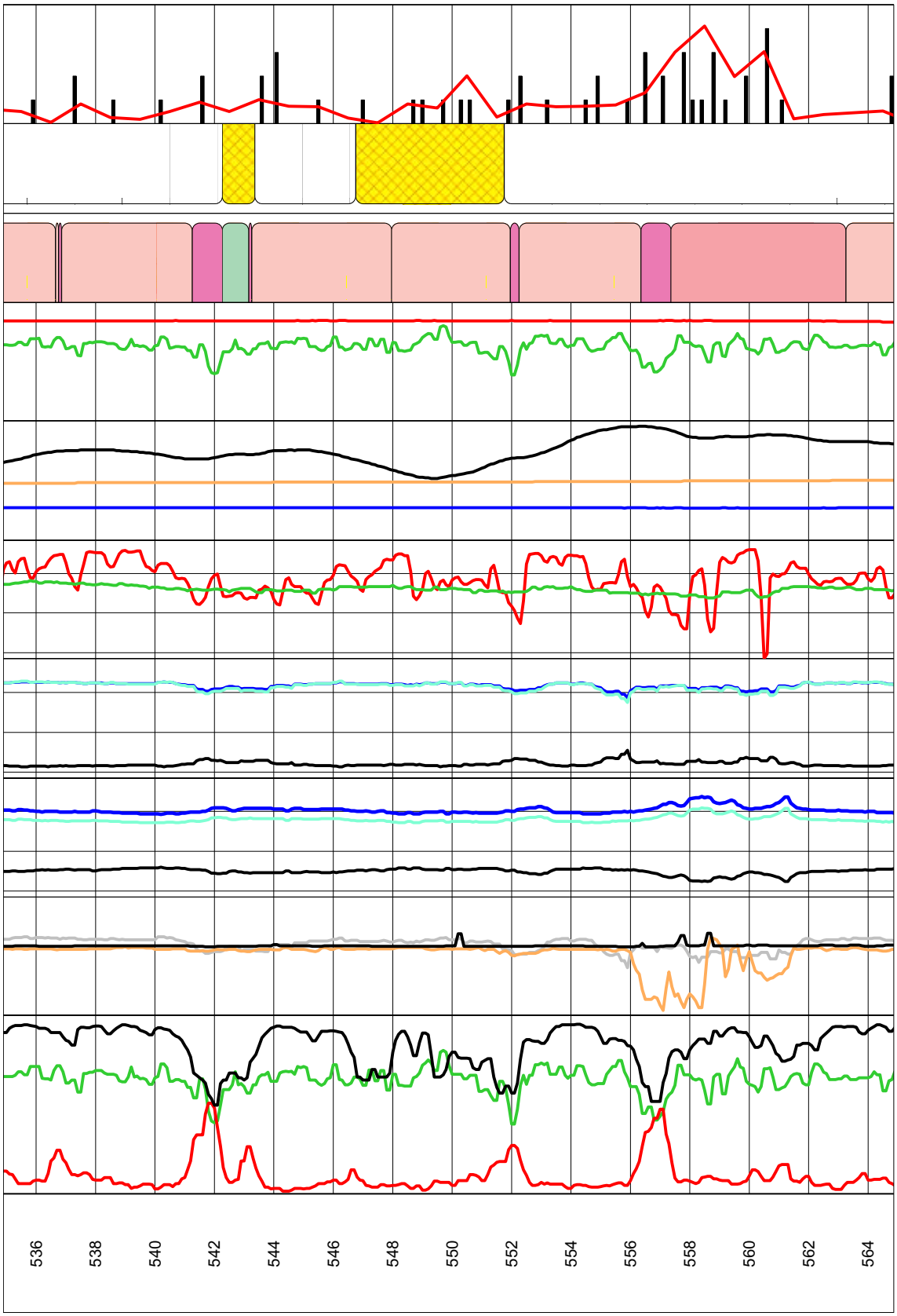
536
538
540
542
544
546
548
550
552
554
556
558
560
562
564

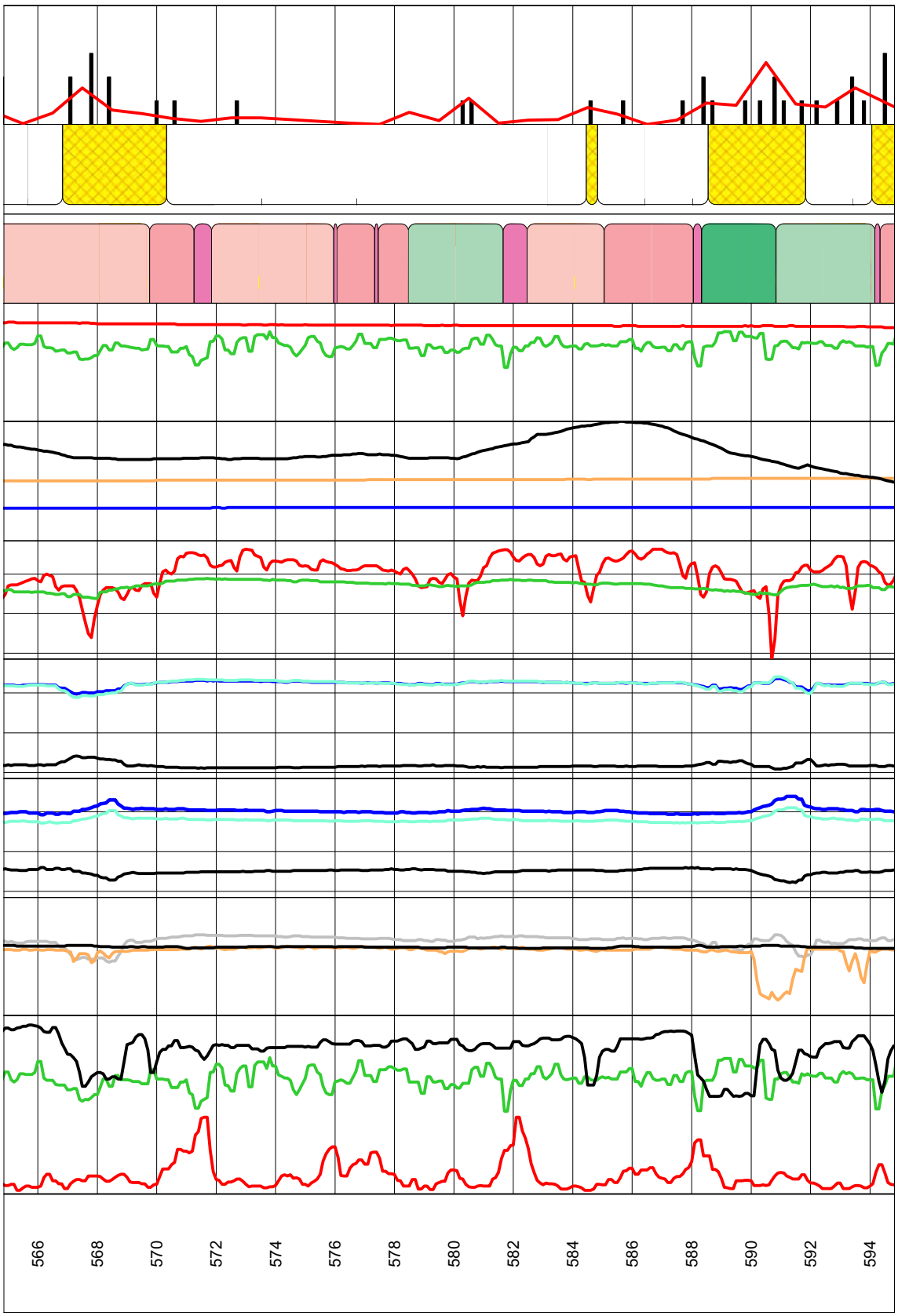
566
568
570
572
574
576
578
580
582
584
586
588
590
592
594

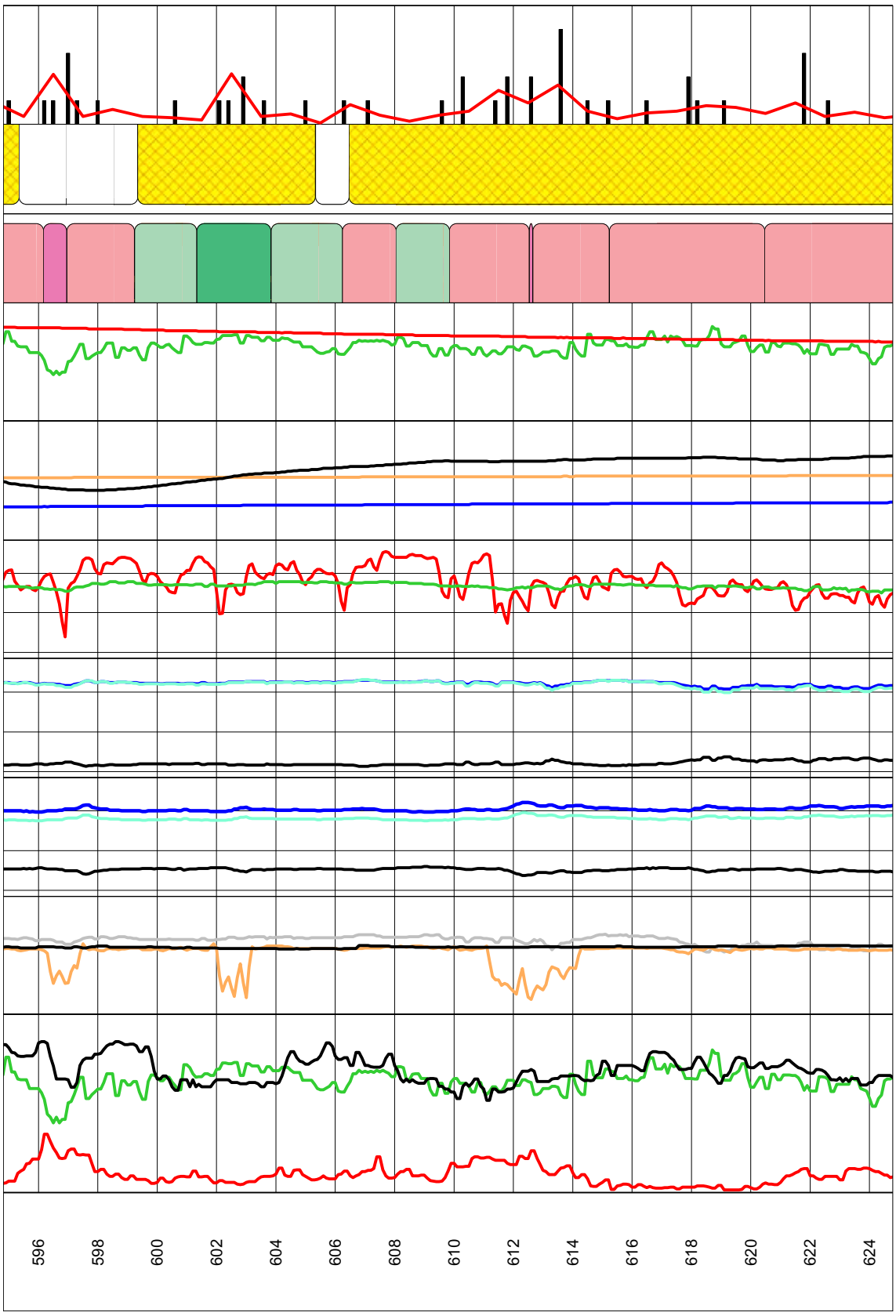
596
598
600
602
604
606
608
610
612
614
616
618
620
622
624

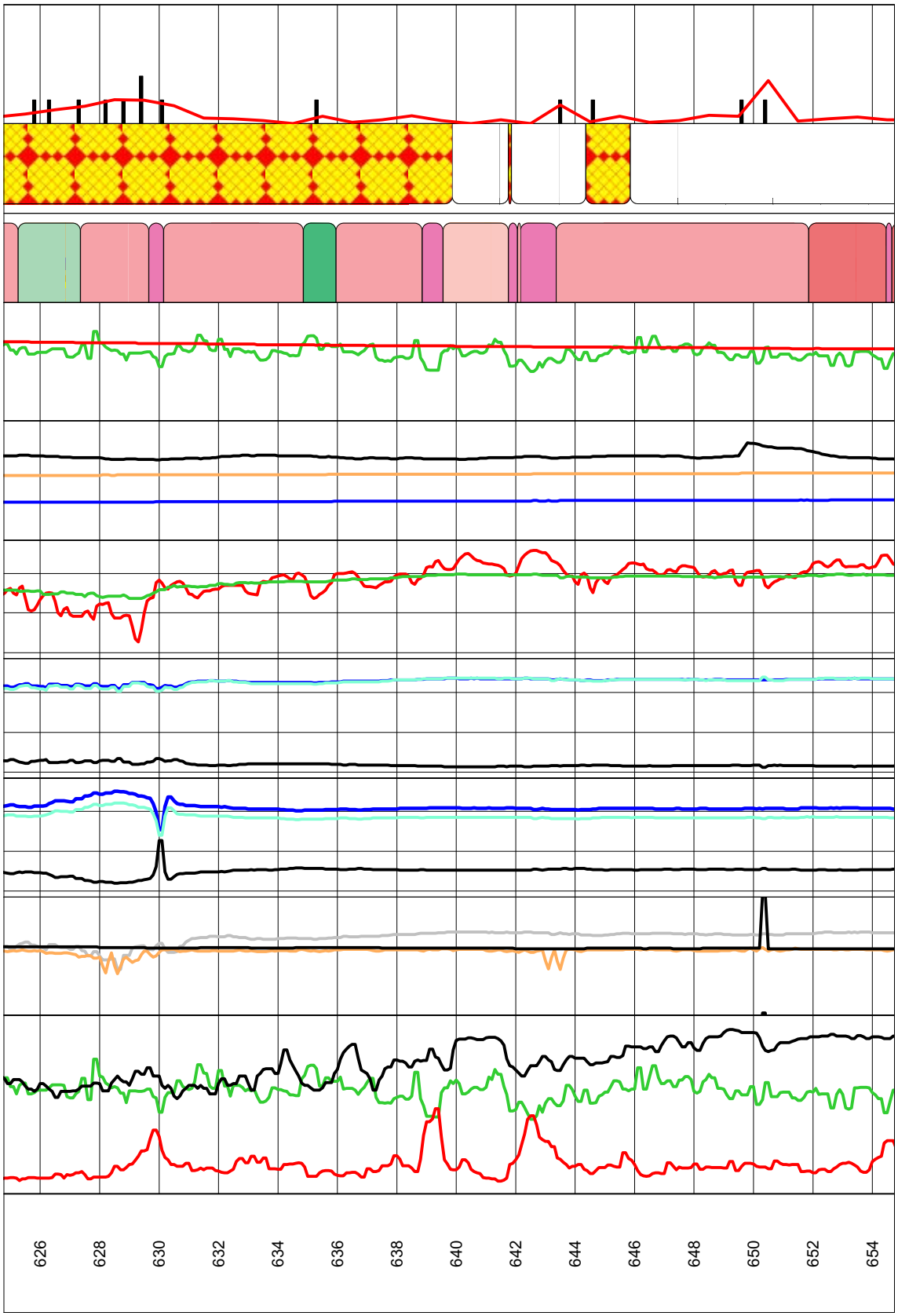
626
628
630
632
634
636
638
640
642
644
646
648
650
652
654

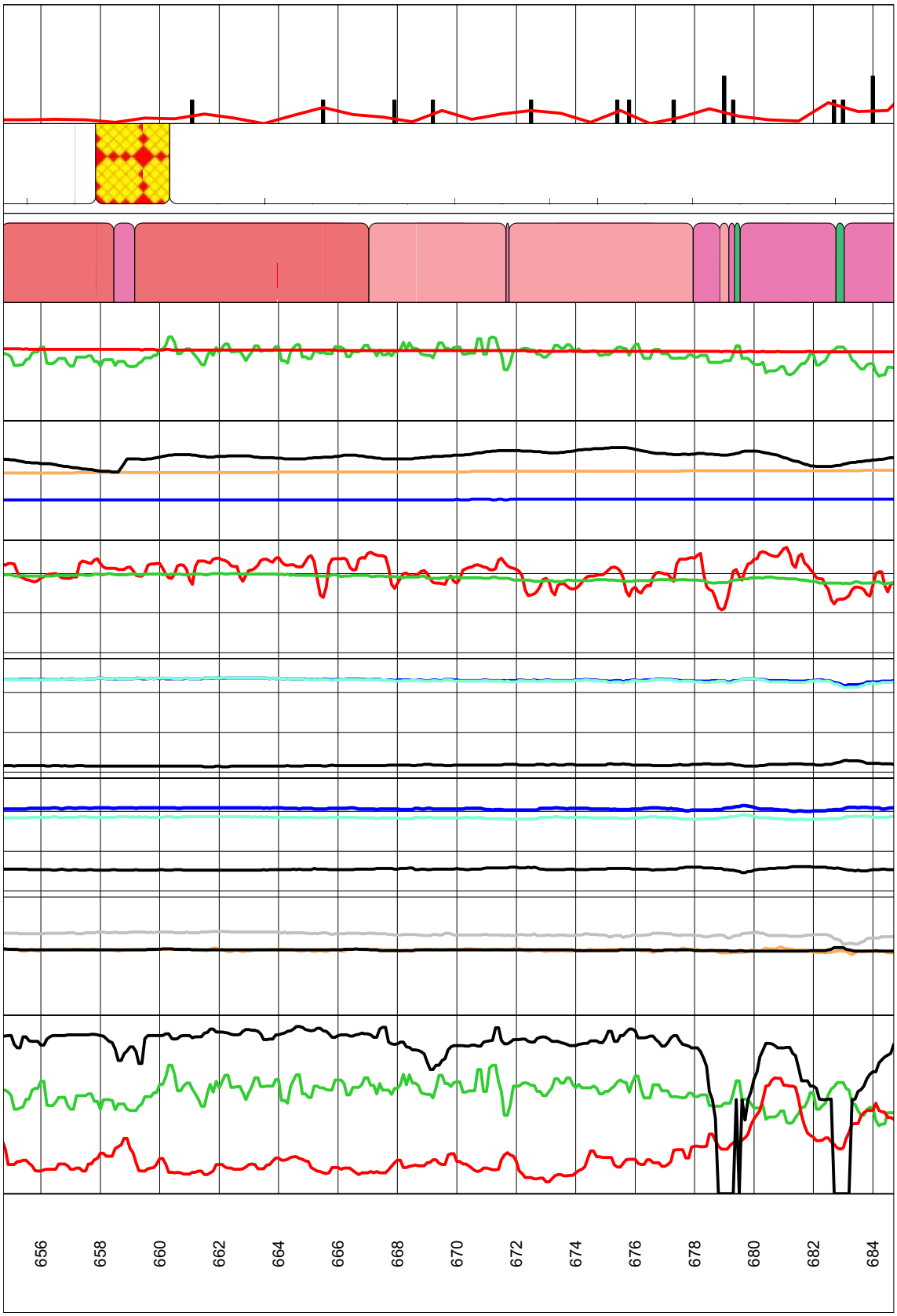
656
658
660
662
664
666
668
670
672
674
676
678
680
682
684

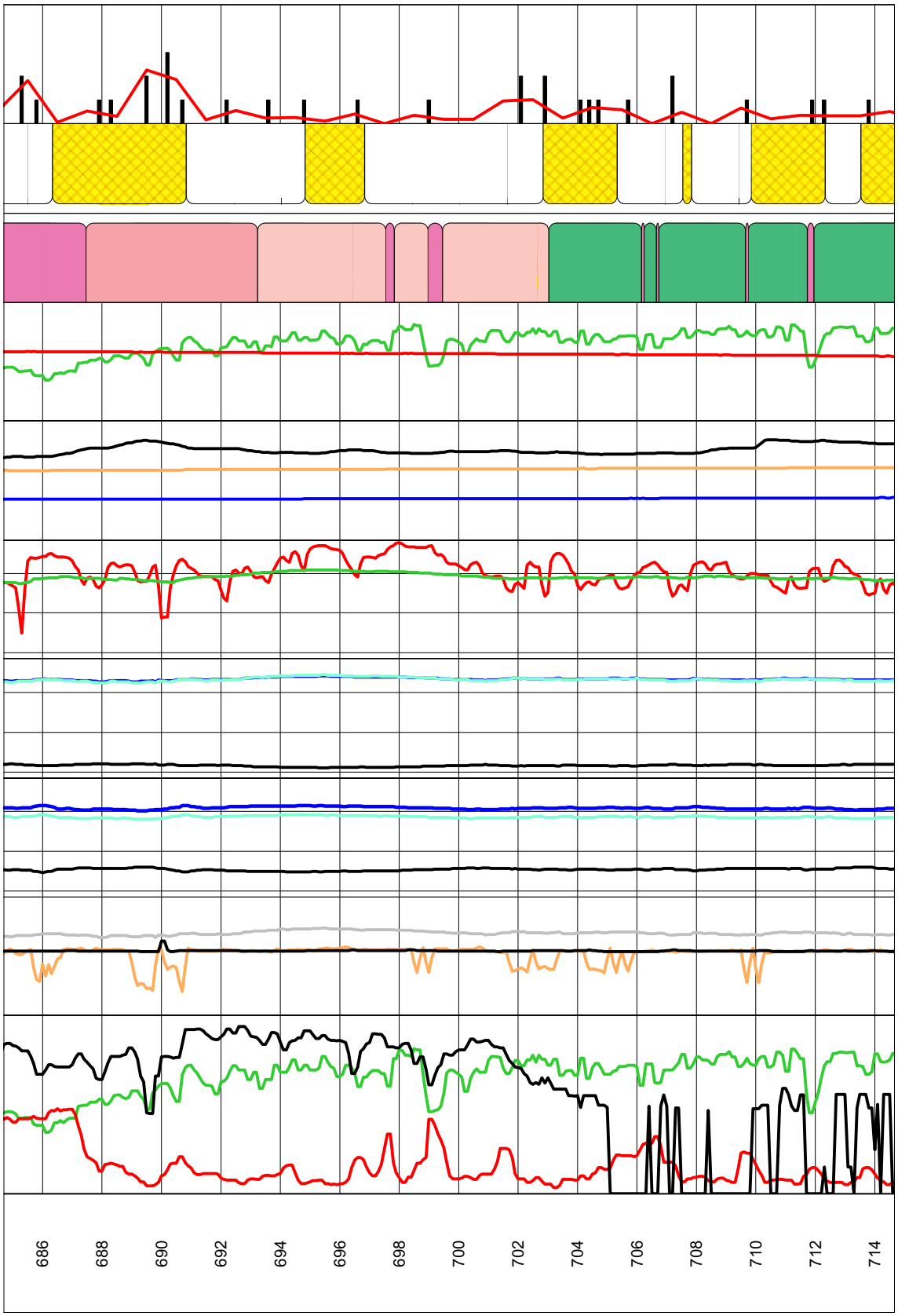
686
688
690
692
694
696
698
700
702
704
706
708
710
712
714

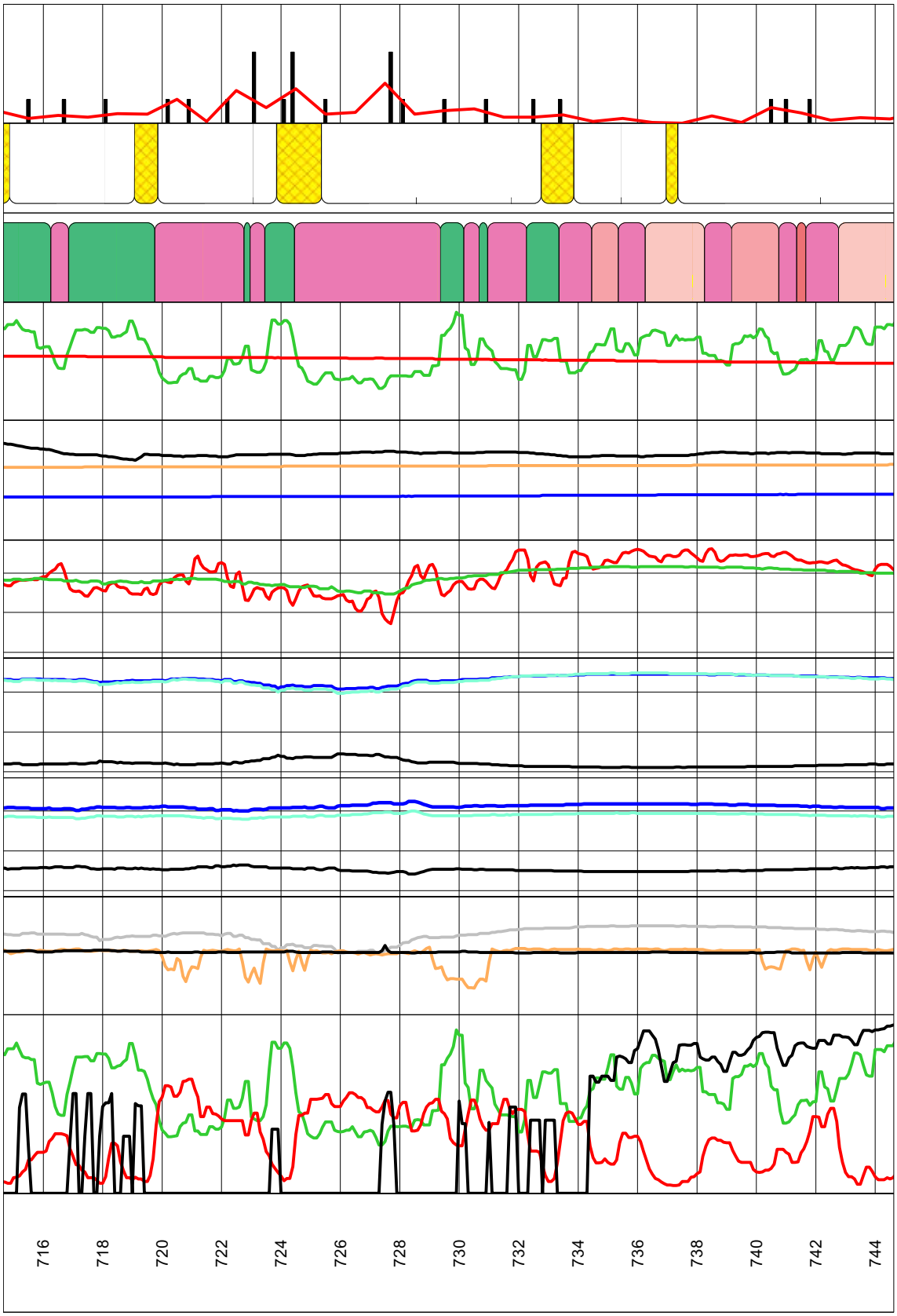
716
718
720
722
724
726
728
730
732
734
736
738
740
742
744

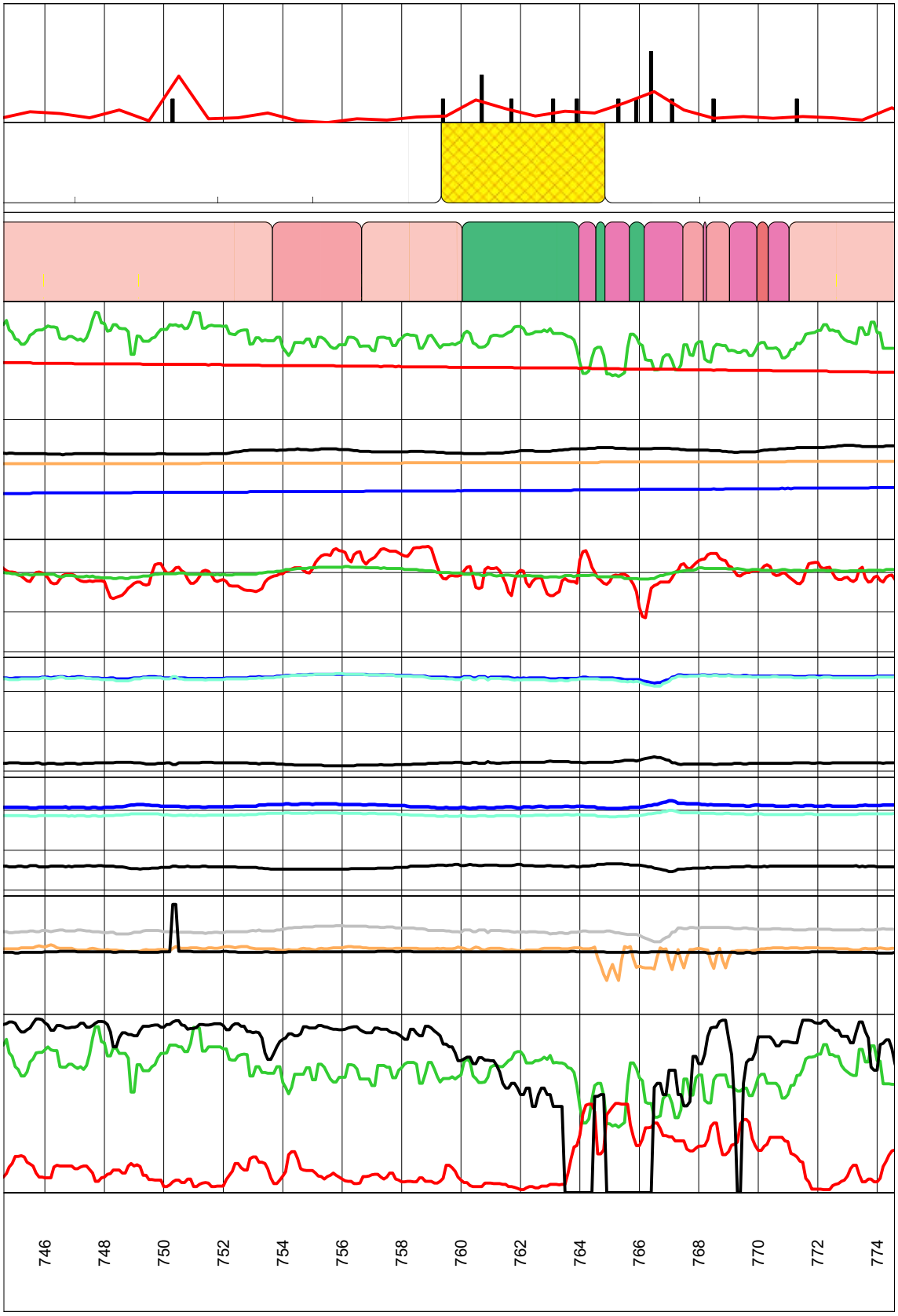
746
748
750
752
754
756
758
760
762
764
766
768
770
772
774

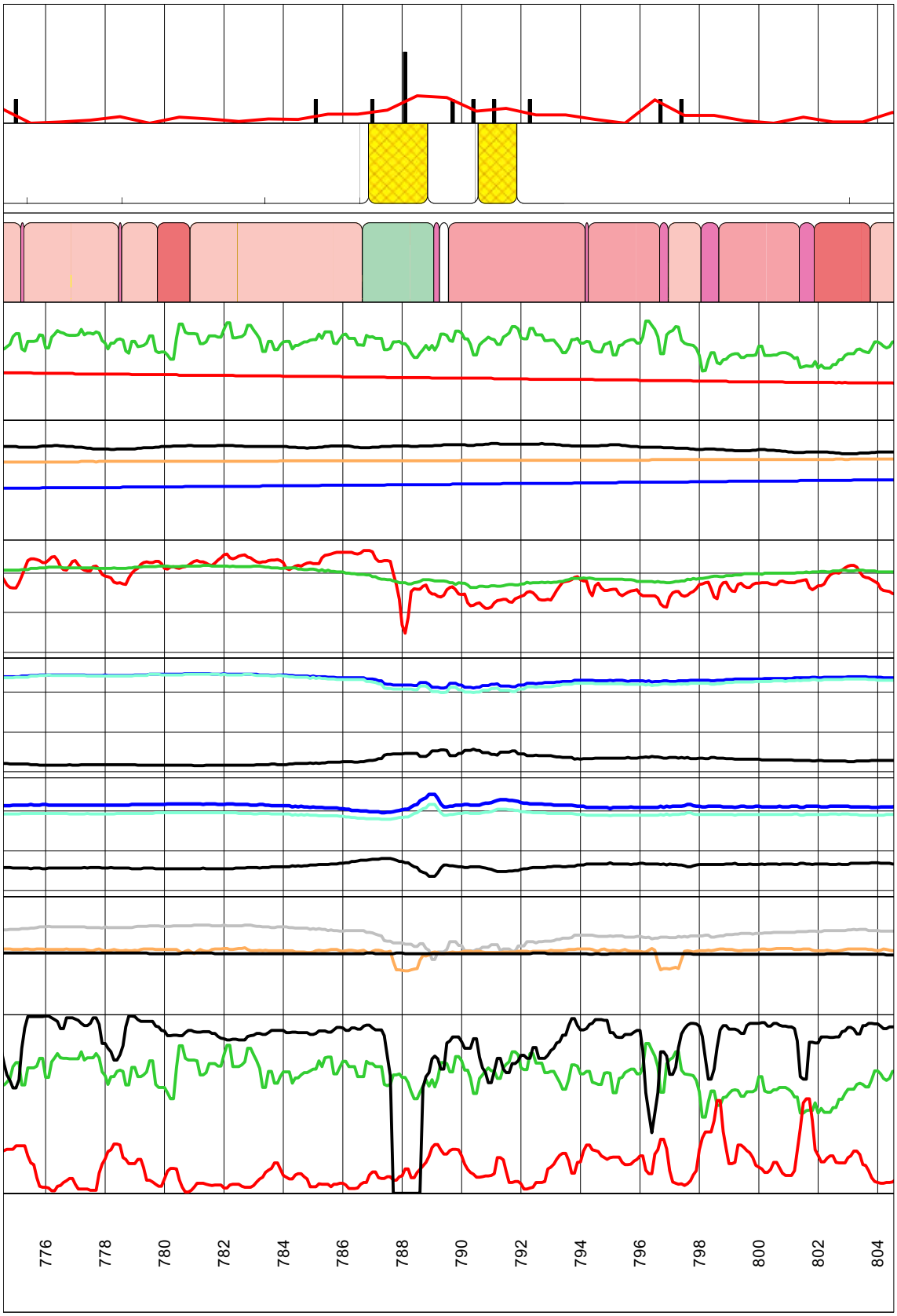
776
778
780
782
784
786
788
790
792
794
796
798
800
802
804

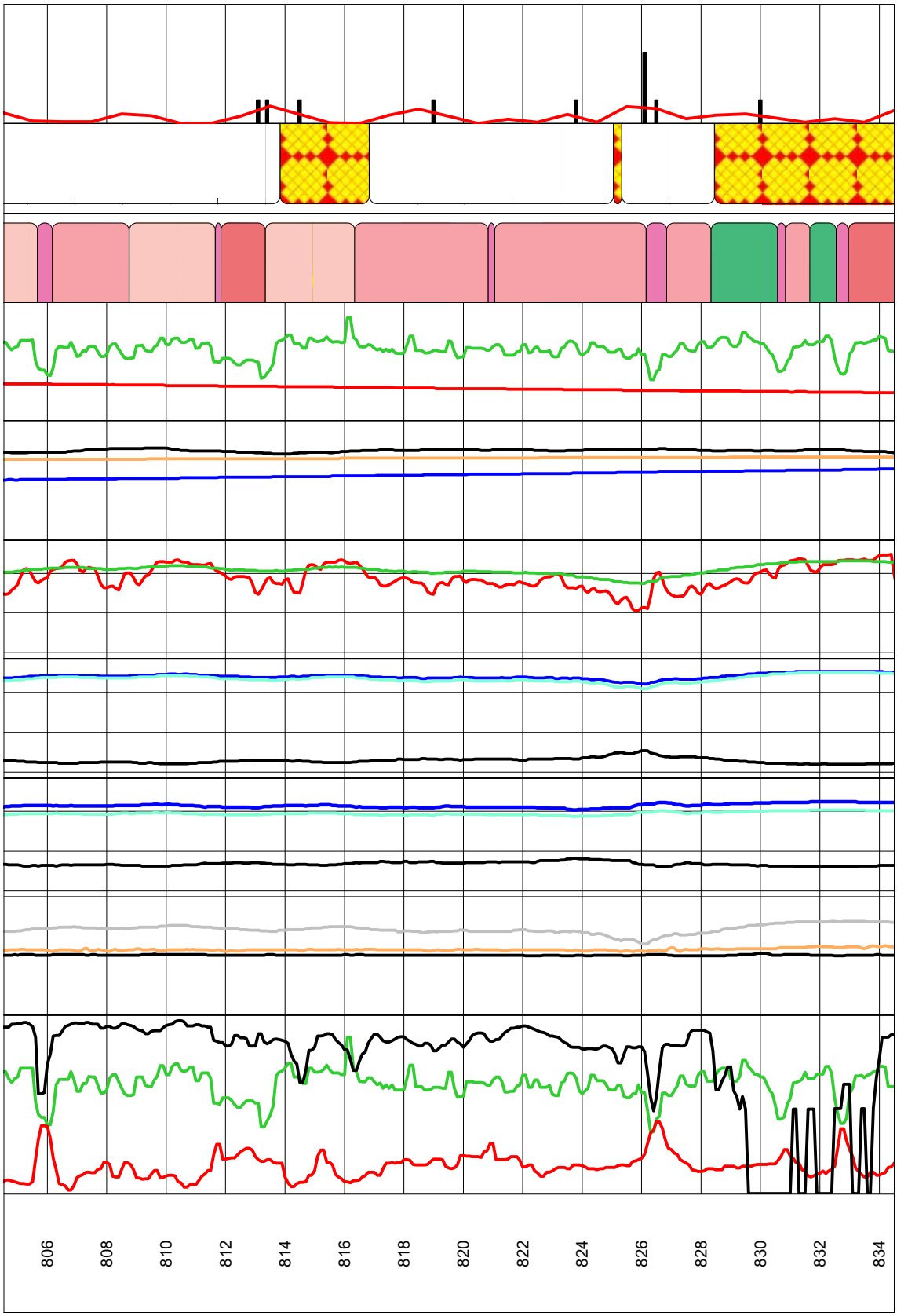
806
808
810
812
814
816
818
820
822
824
826
828
830
832
834

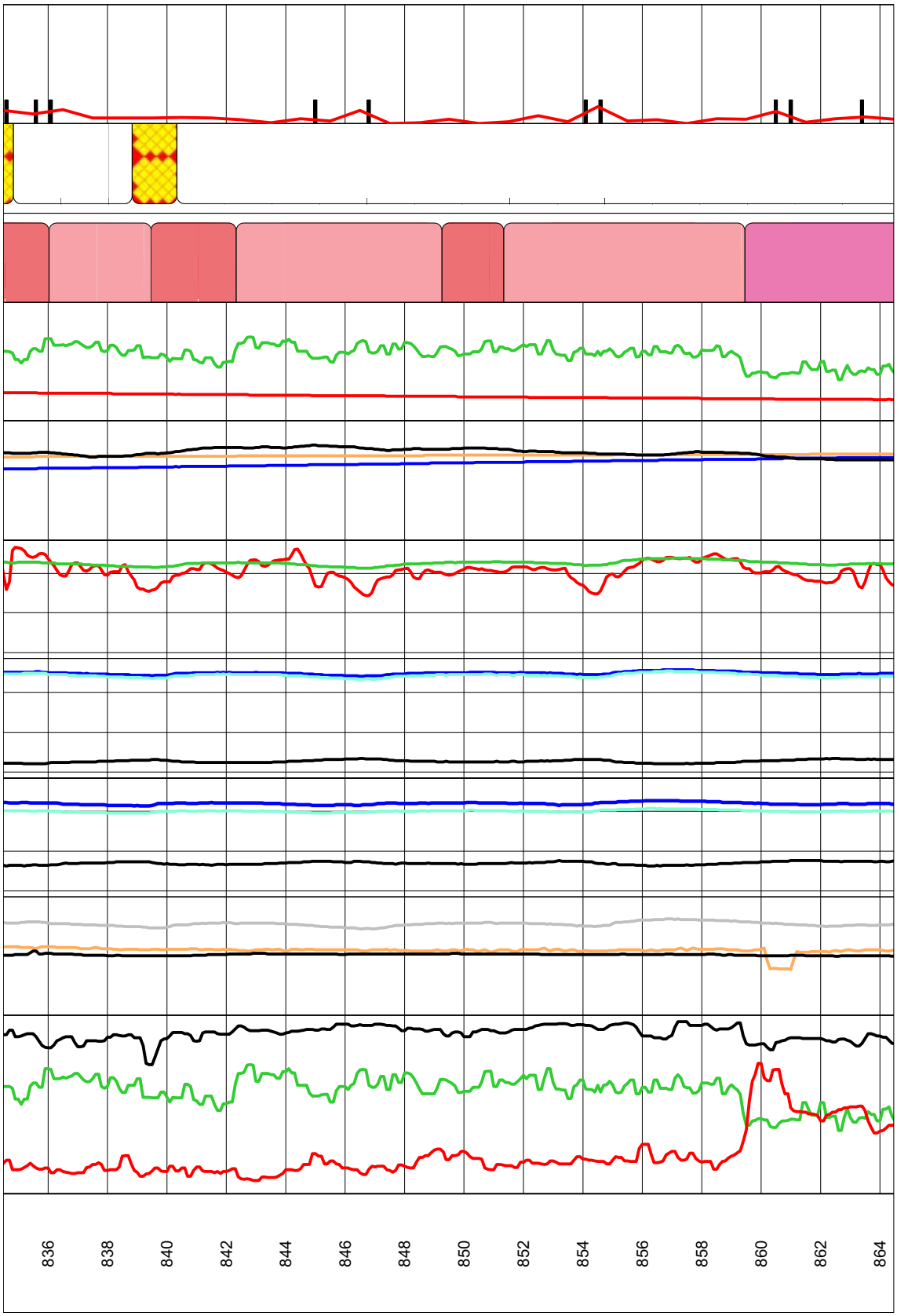
836
838
840
842
844
846
848
850
852
854
856
858
860
862
864

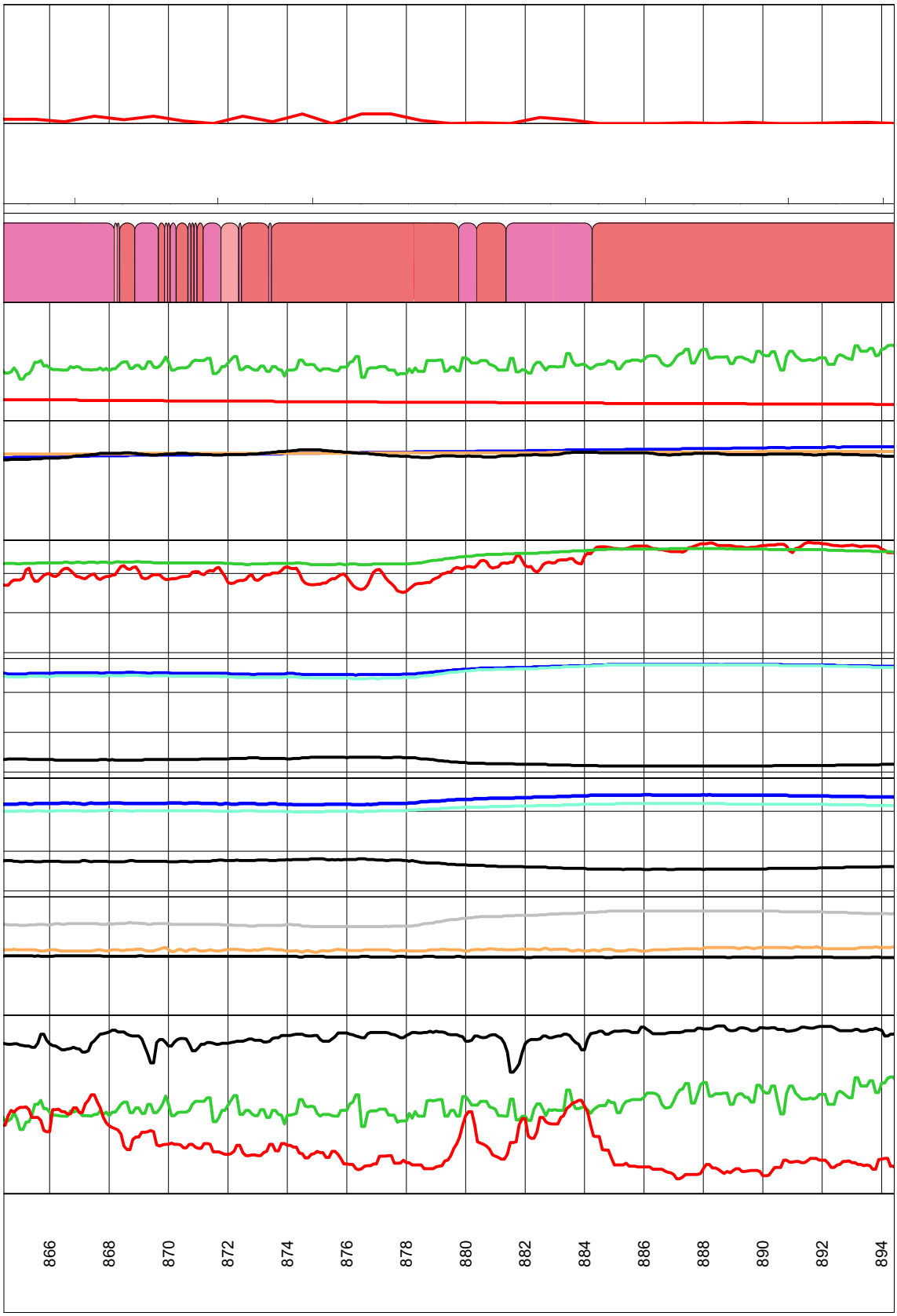
866
868
870
872
874
876
878
880
882
884
886
888
890
892
894

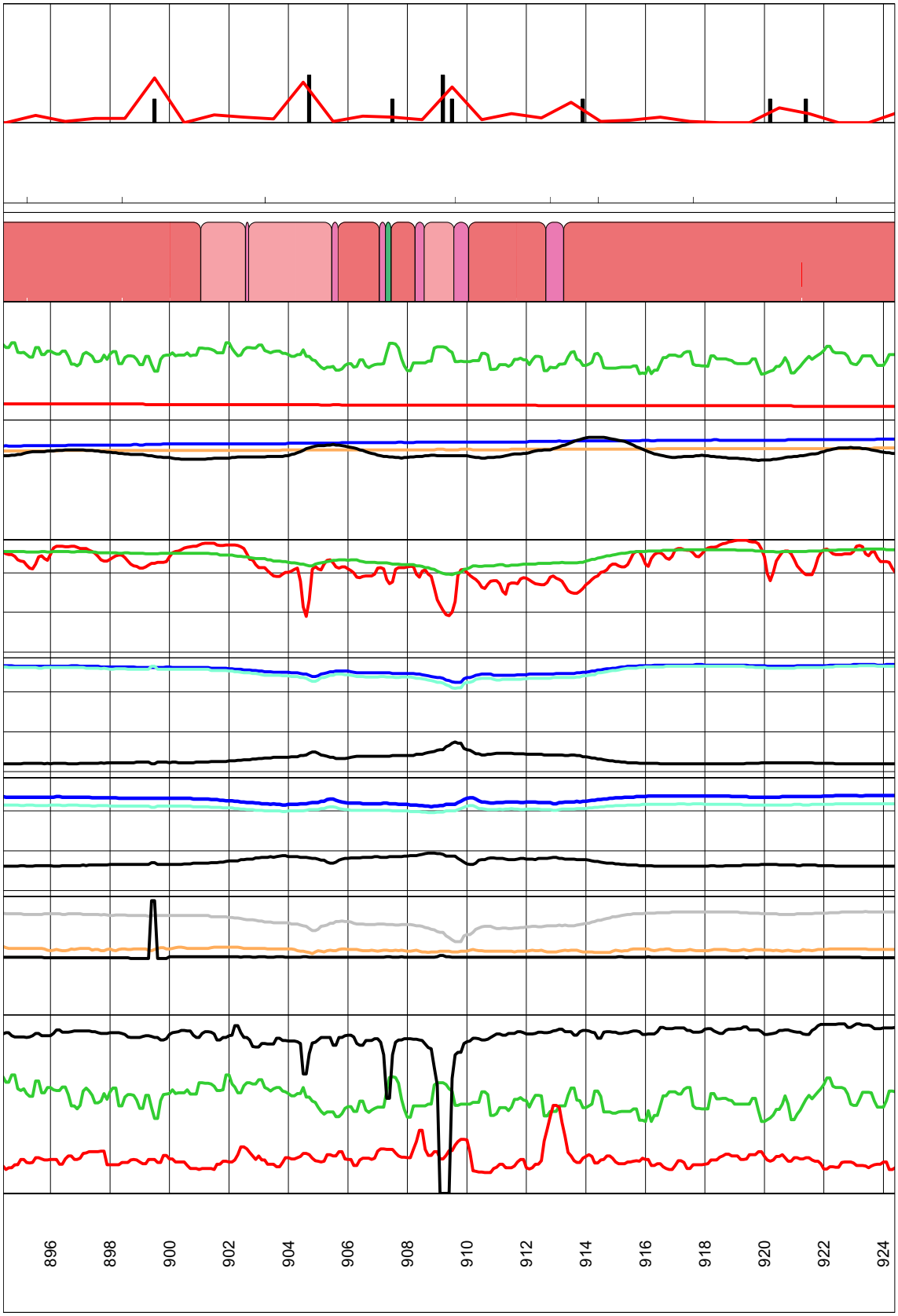
896
898
900
902
904
906
908
910
912
914
916
918
920
922
924

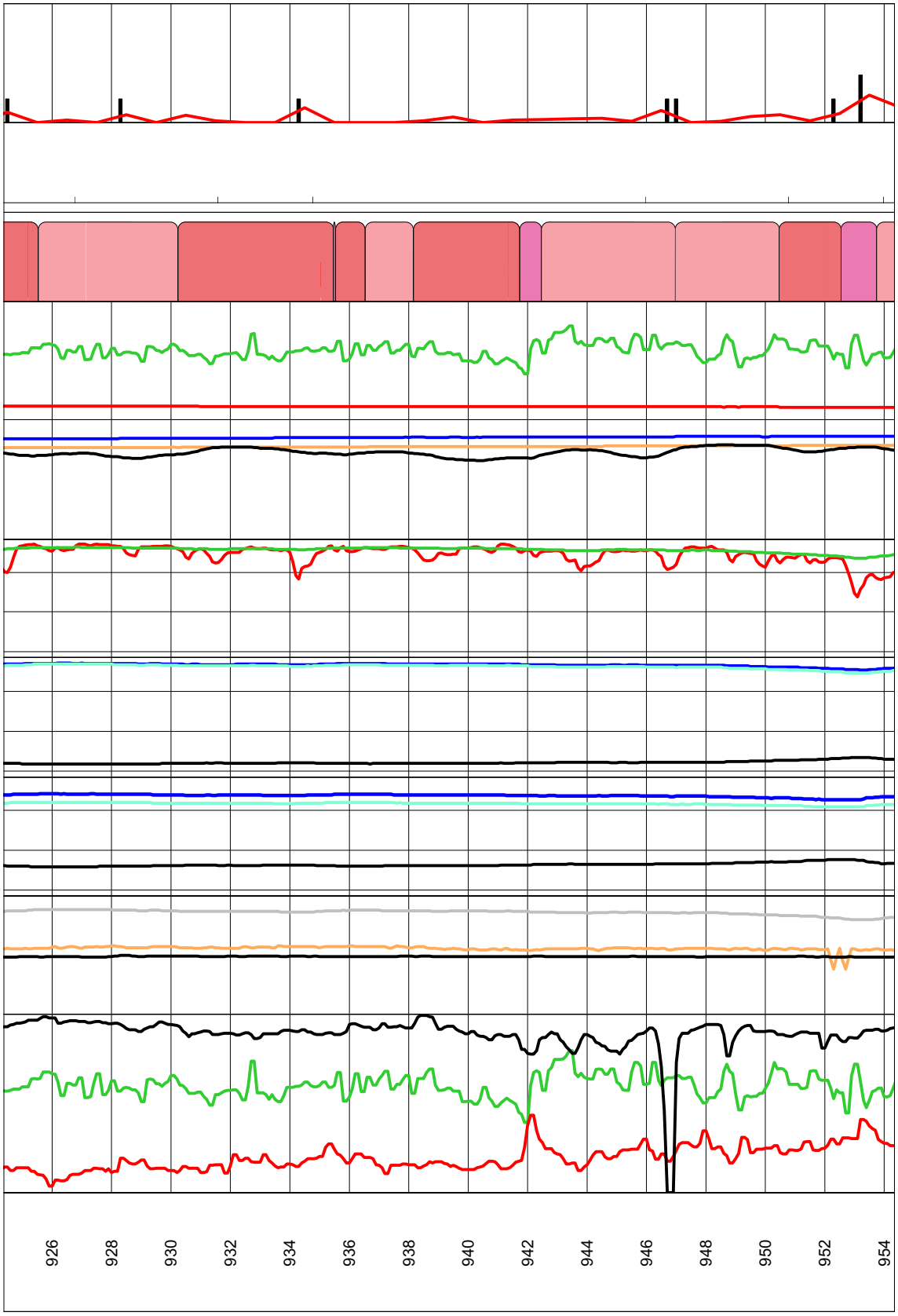
926
928
930
932
934
936
938
940
942
944
946
948
950
952
954

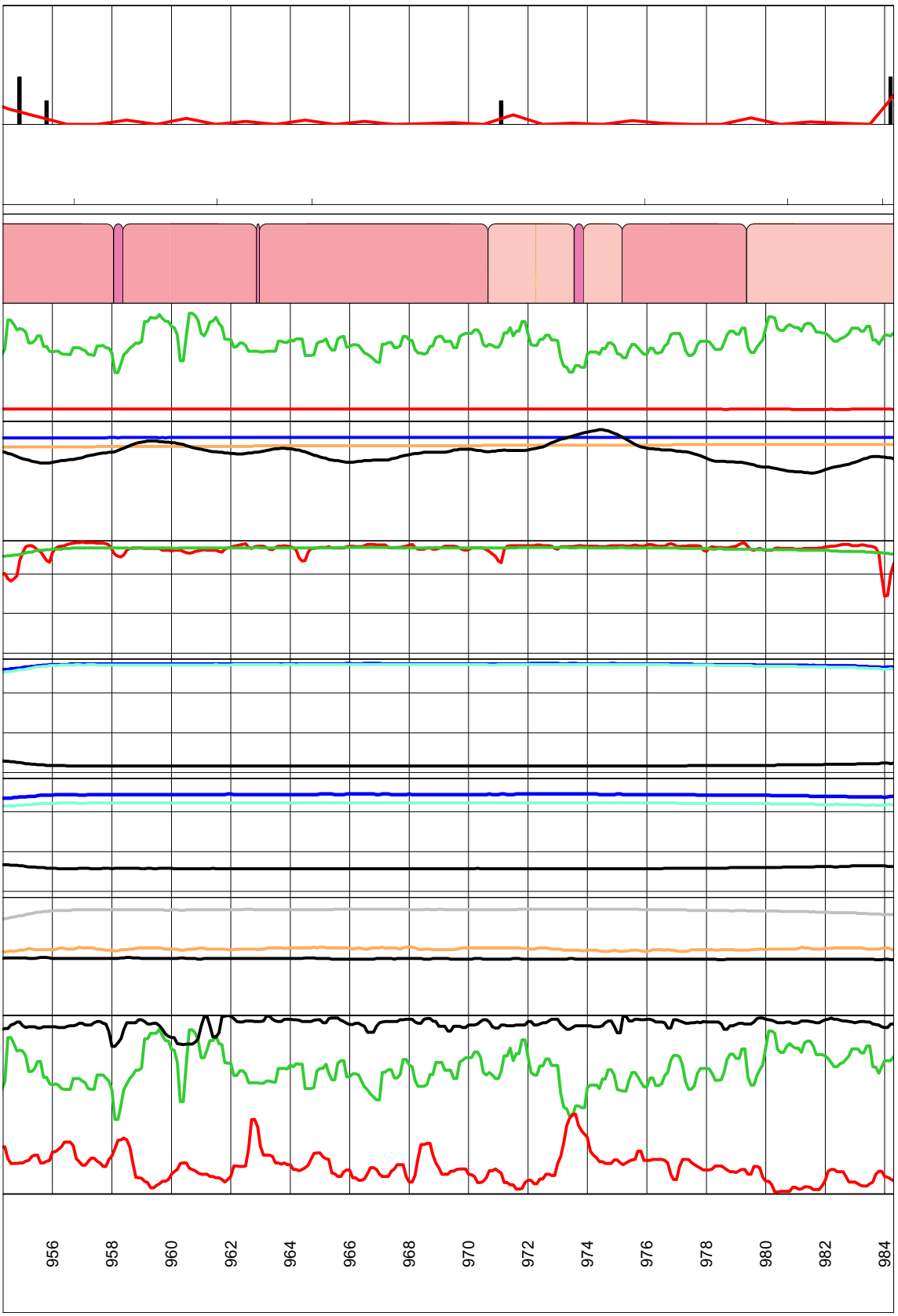
956
958
960
962
964
966
968
970
972
974
976
978
980
982
984

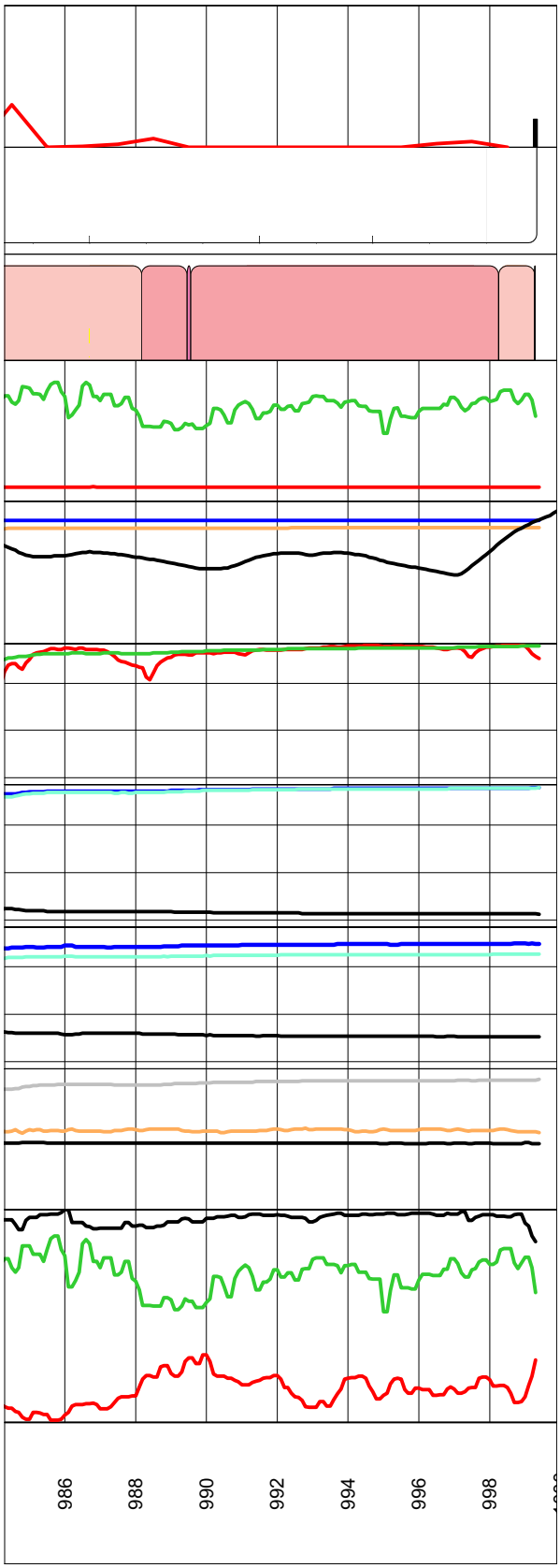
986
988
990
992
994
996
998

Appendix 2

Pseudogeology classification together with geophysical logging data for the percussion drilled part of KSH01A

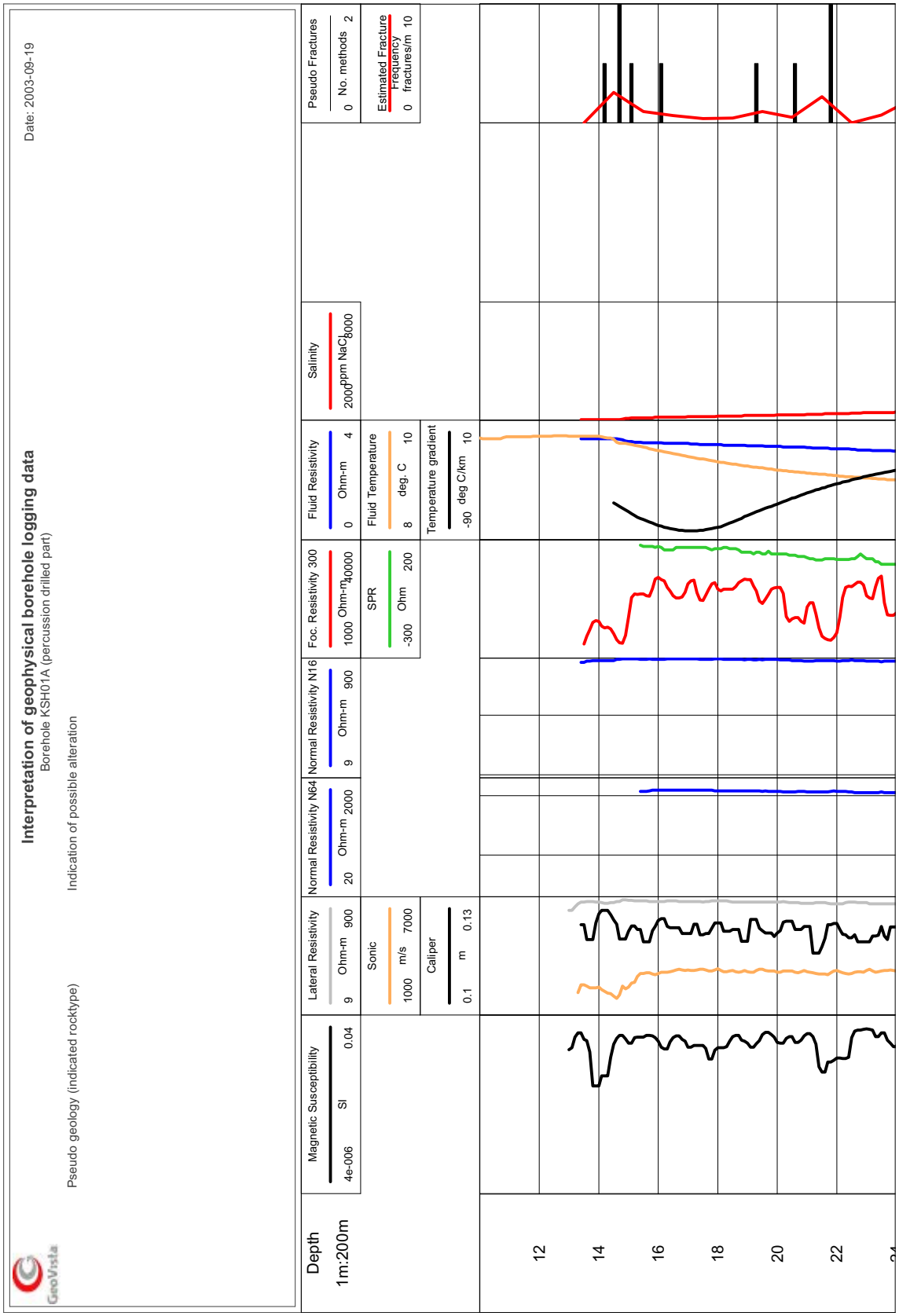


24
26
28
30
32
34
36
38
40
42
44
46
48
50
52

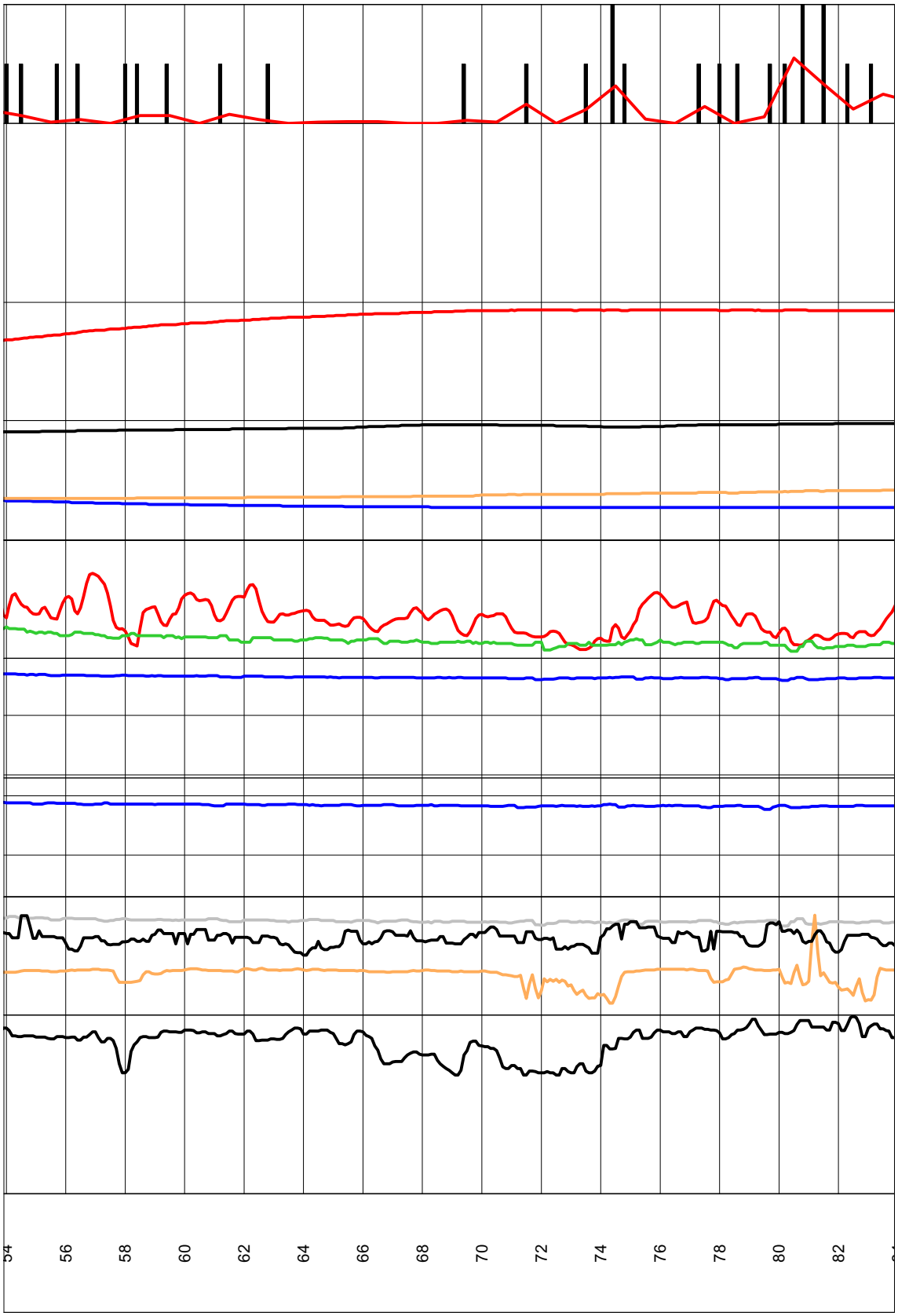
54
56
58
60
62
64
66
68
70
72
74
76
78
80
82

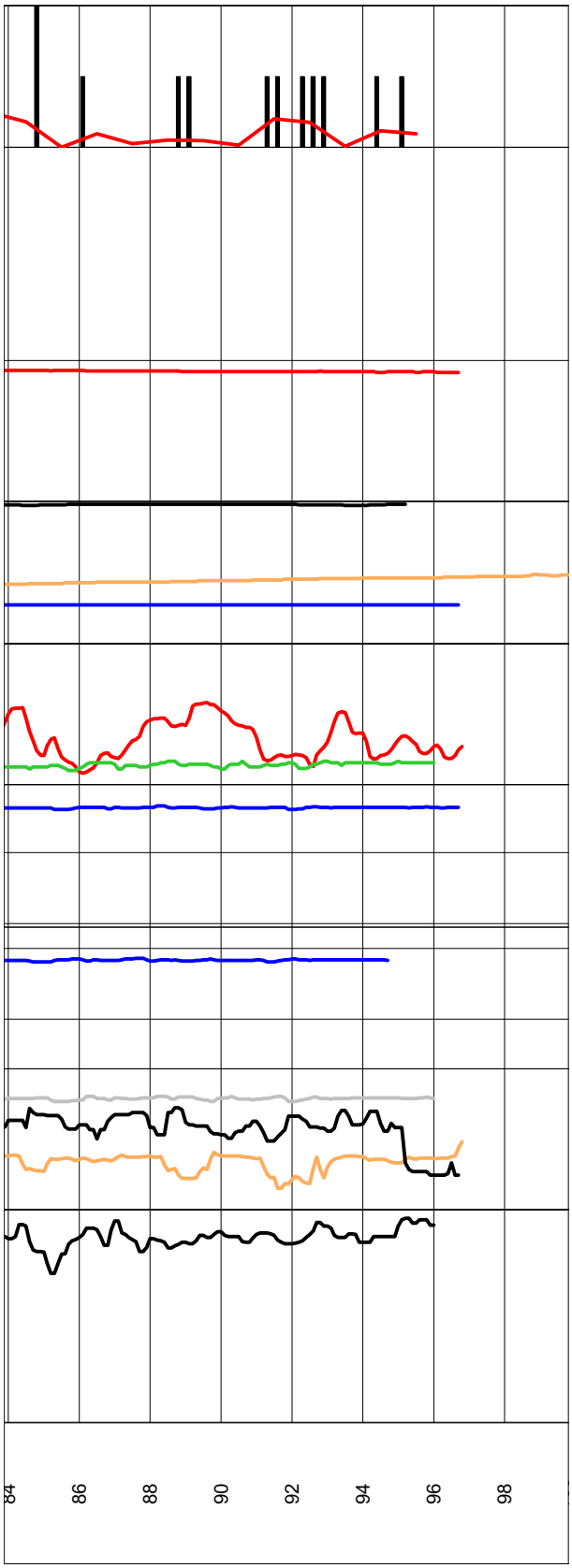
84
86
88
90
92
94
96
98

Appendix 3

Pseudogeology classification together with geophysical logging data for the borehole KSH01B

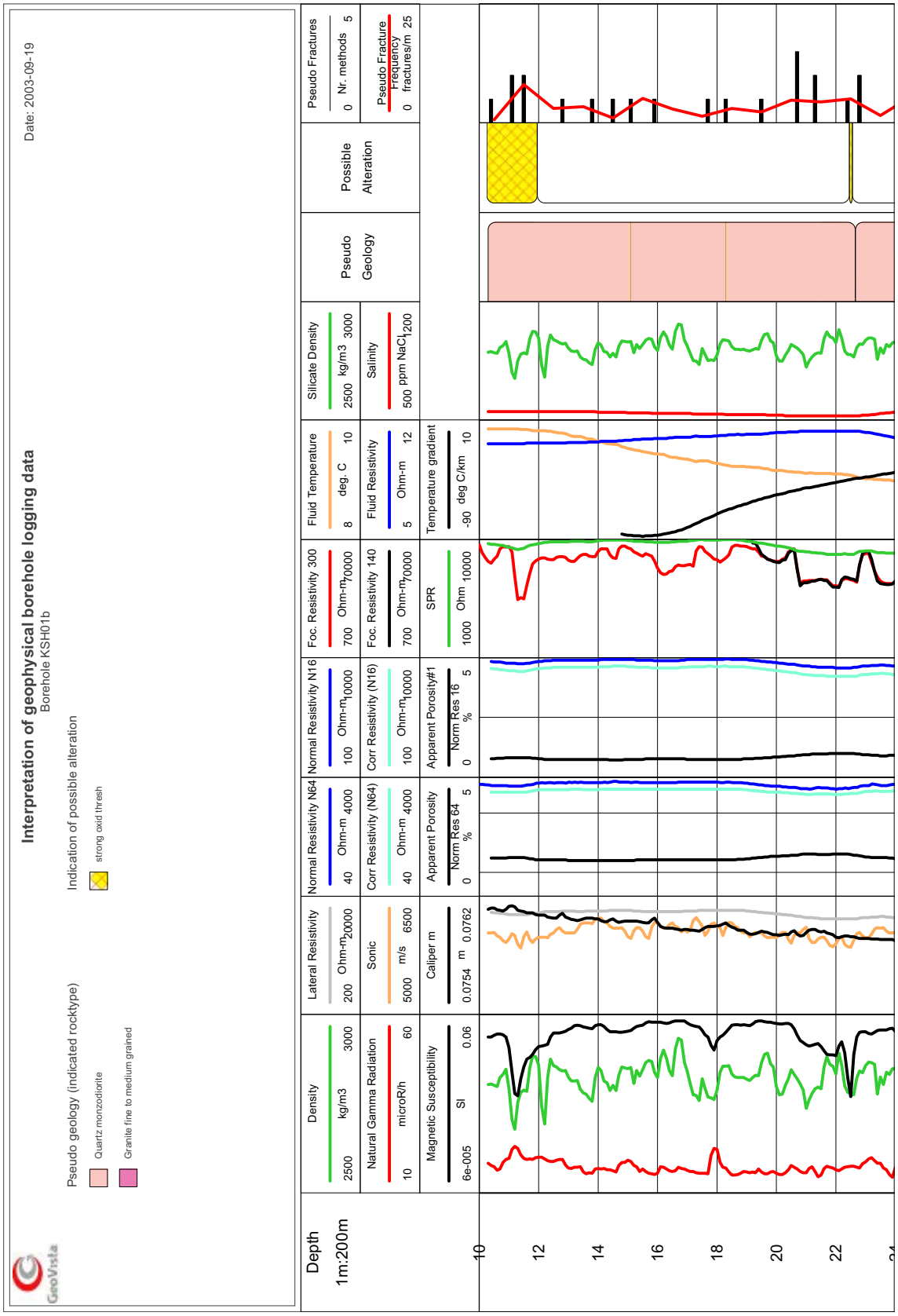

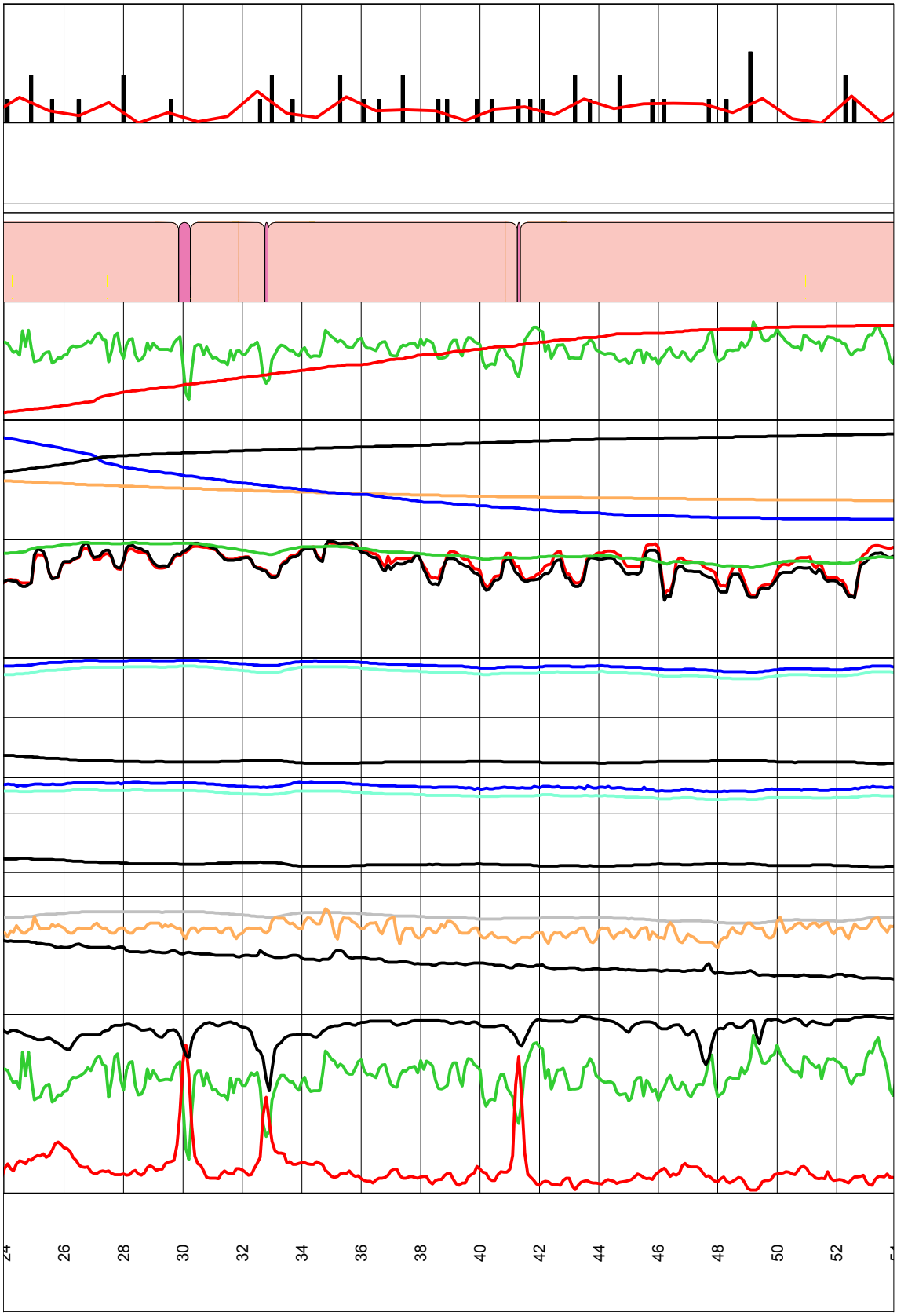
24
26
28
30
32
34
36
38
40
42
44
46
48
50
52

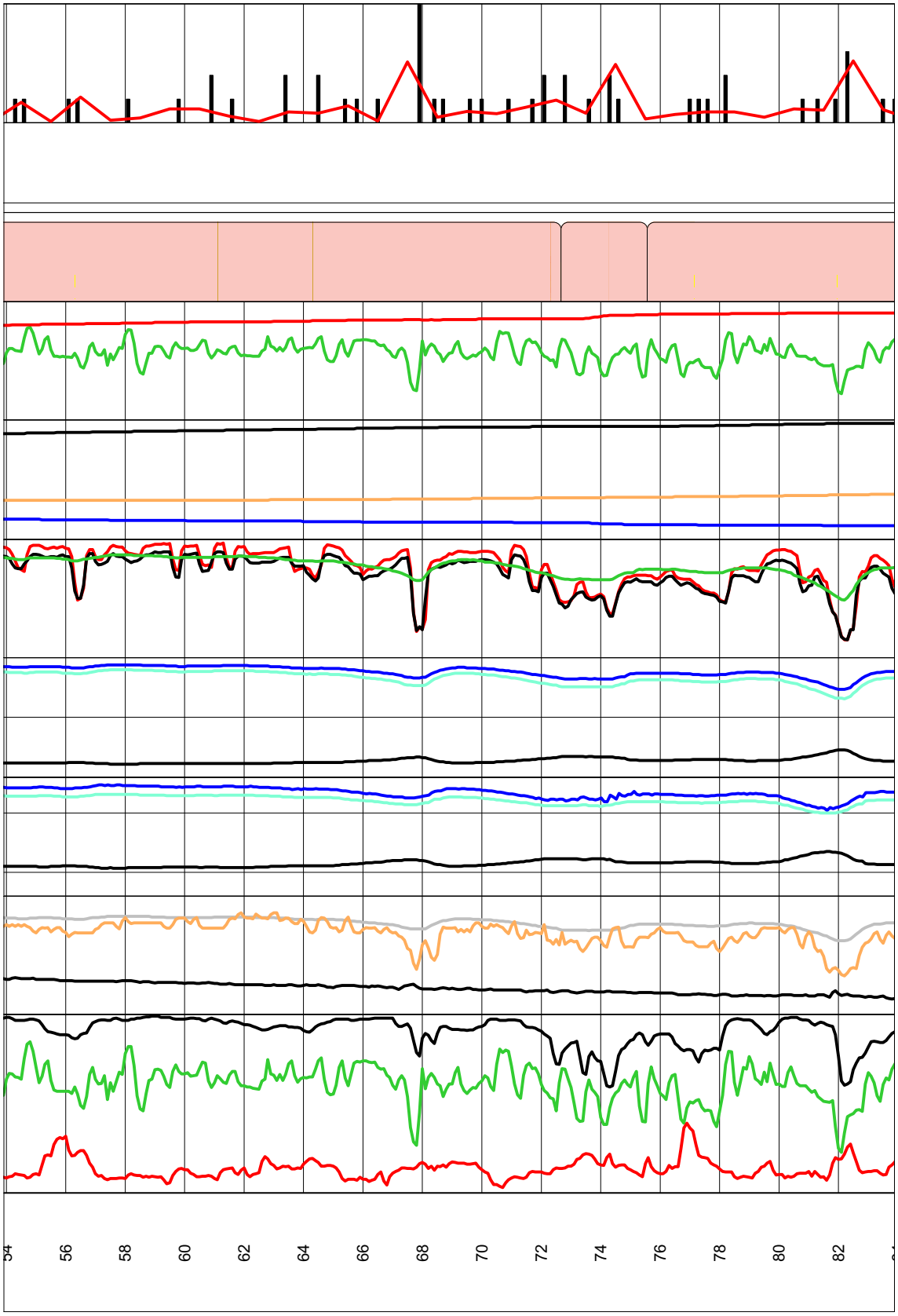
54
56
58
60
62
64
66
68
70
72
74
76
78
80
82

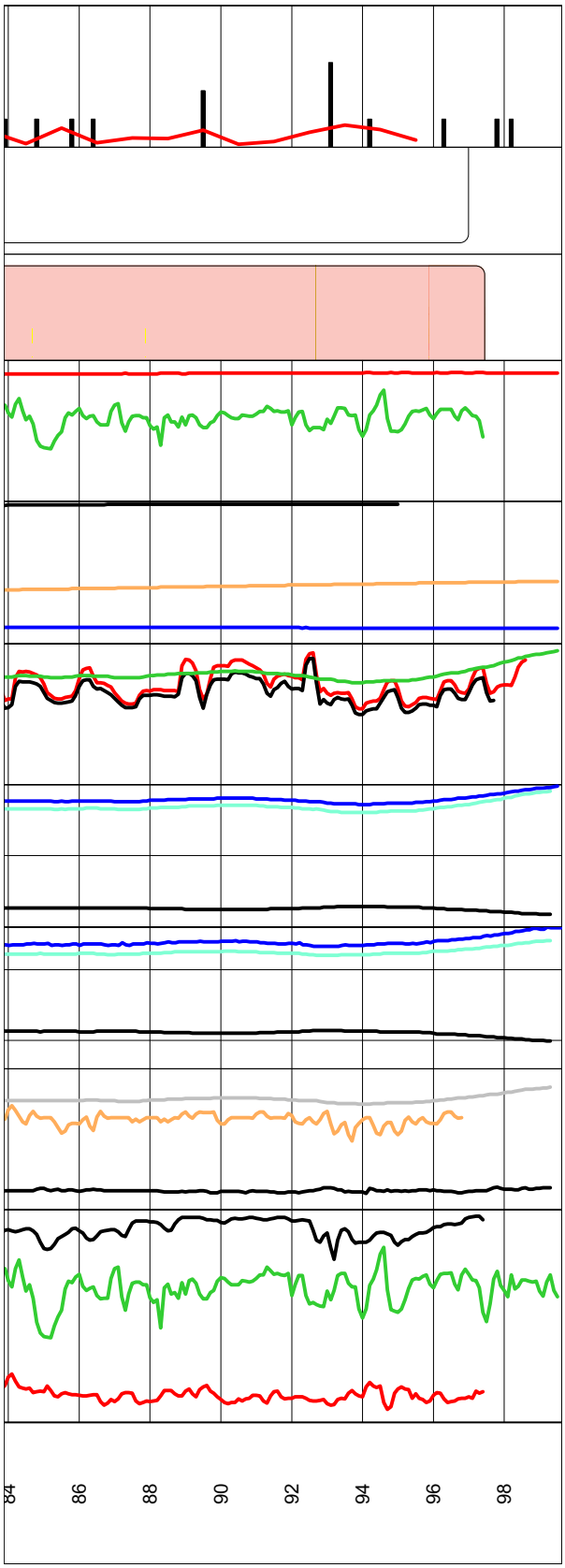
84
86
88
90
92
94
96
98

Appendix 4

Pseudogeology classification together with geophysical logging data for the upper 100 m of KSH02

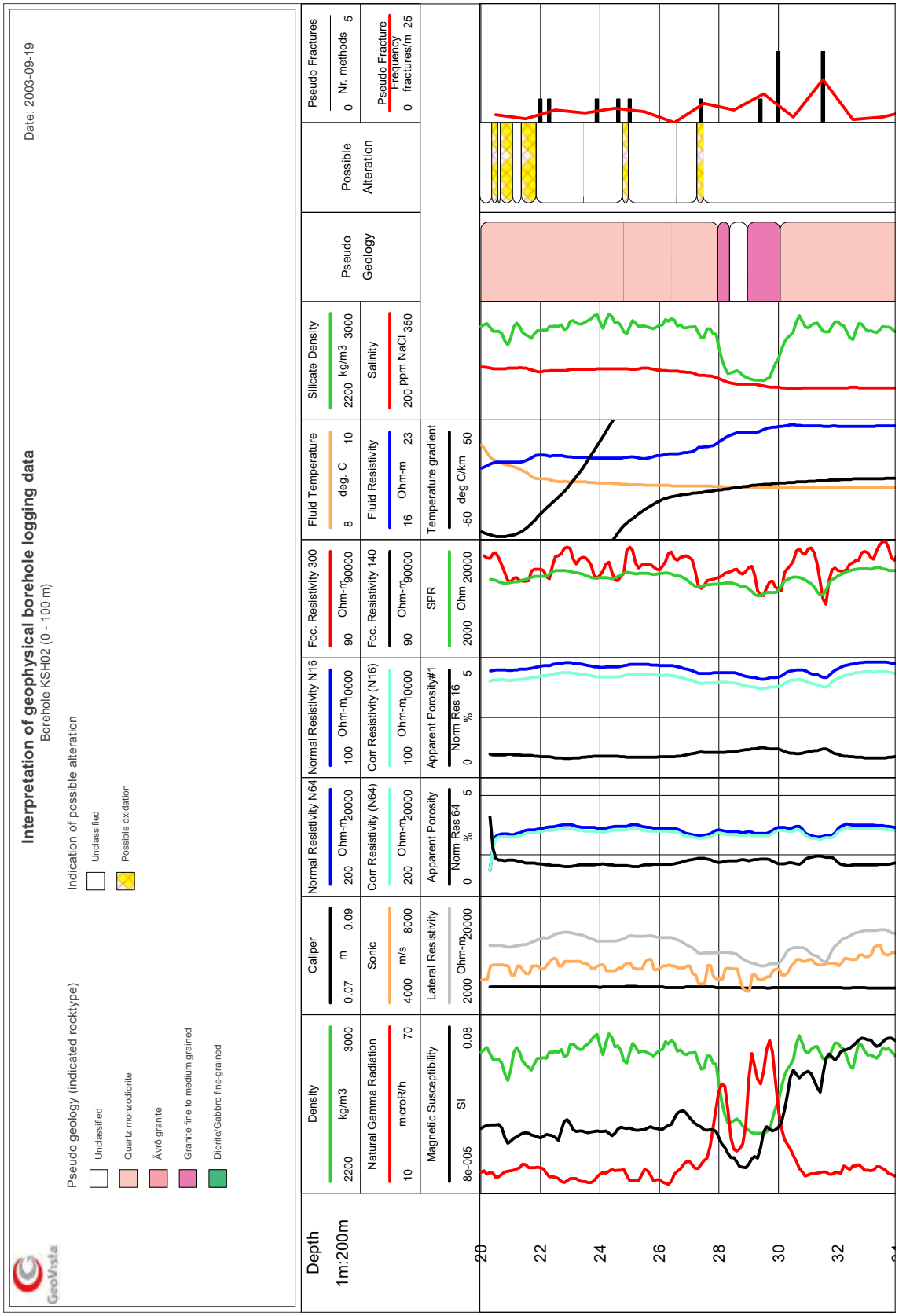

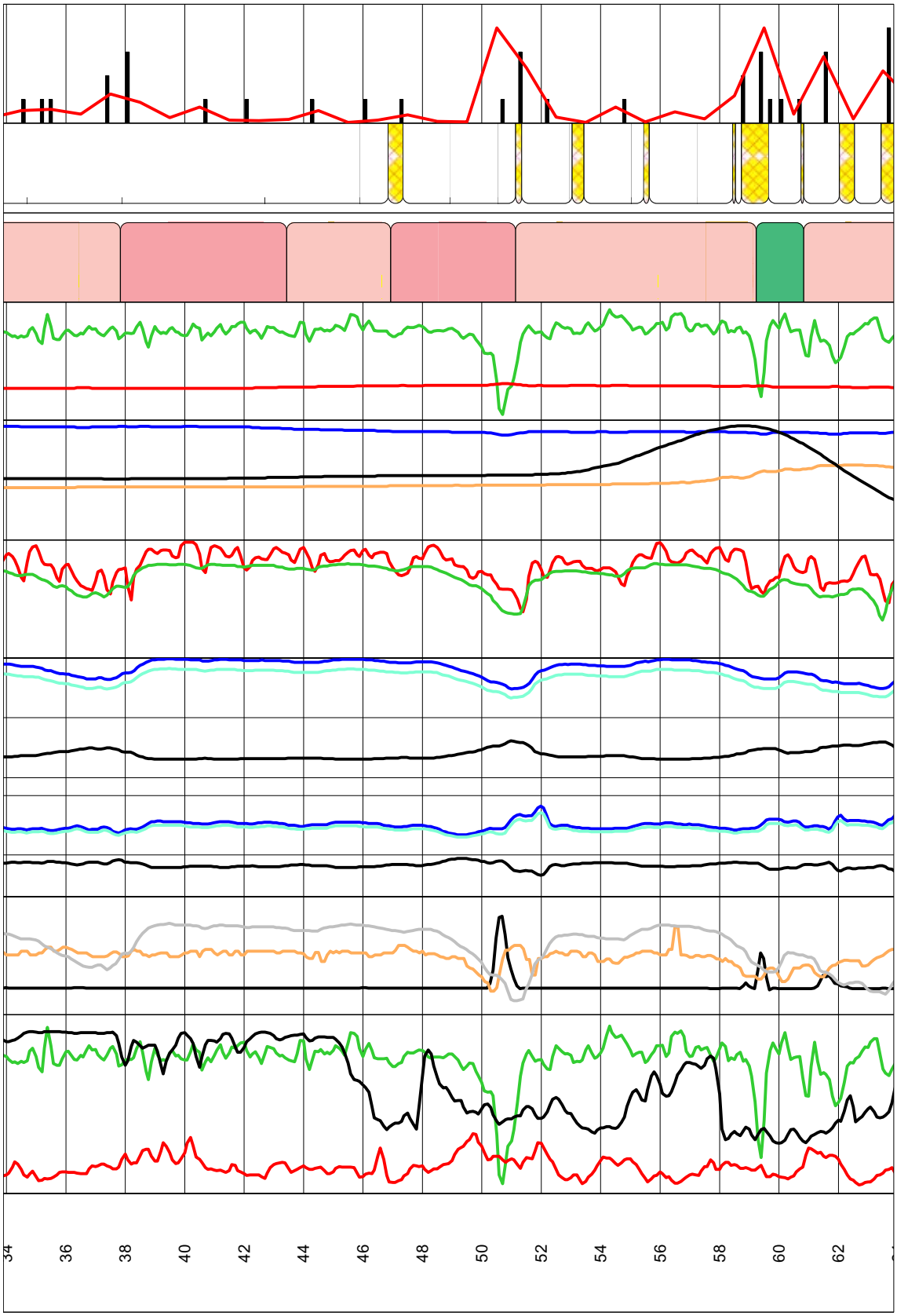
34
36
38
40
42
44
46
48
50
52
54
56
58
60
62

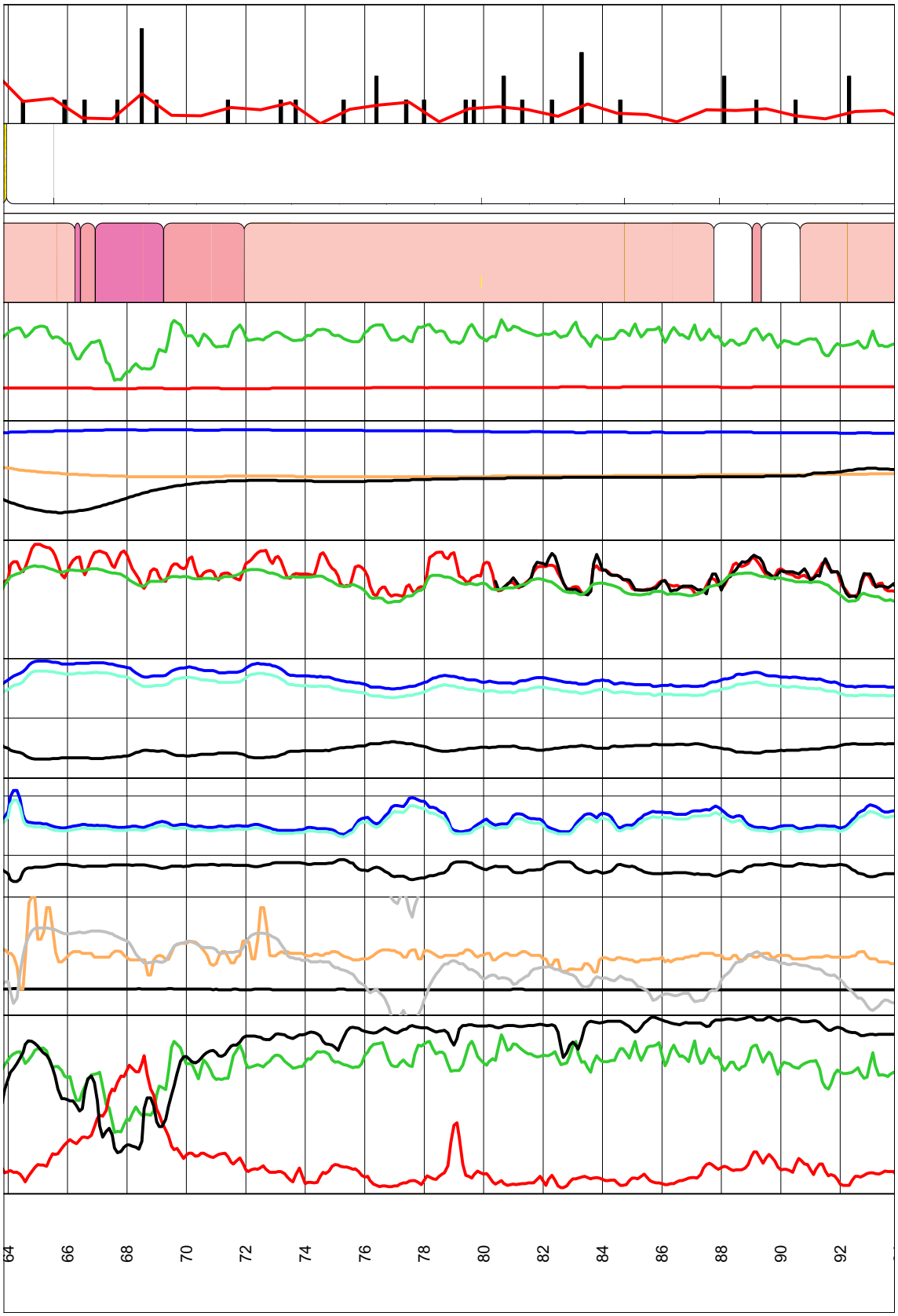
64
66
68
70
72
74
76
78
80
82
84
86
88
90
92

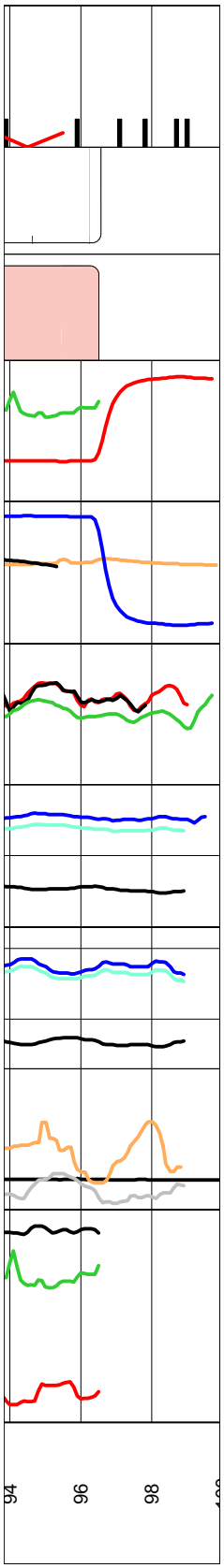
94
96
98

Appendix 5

Pseudogeology classification together with geophysical logging data for the borehole HSH01

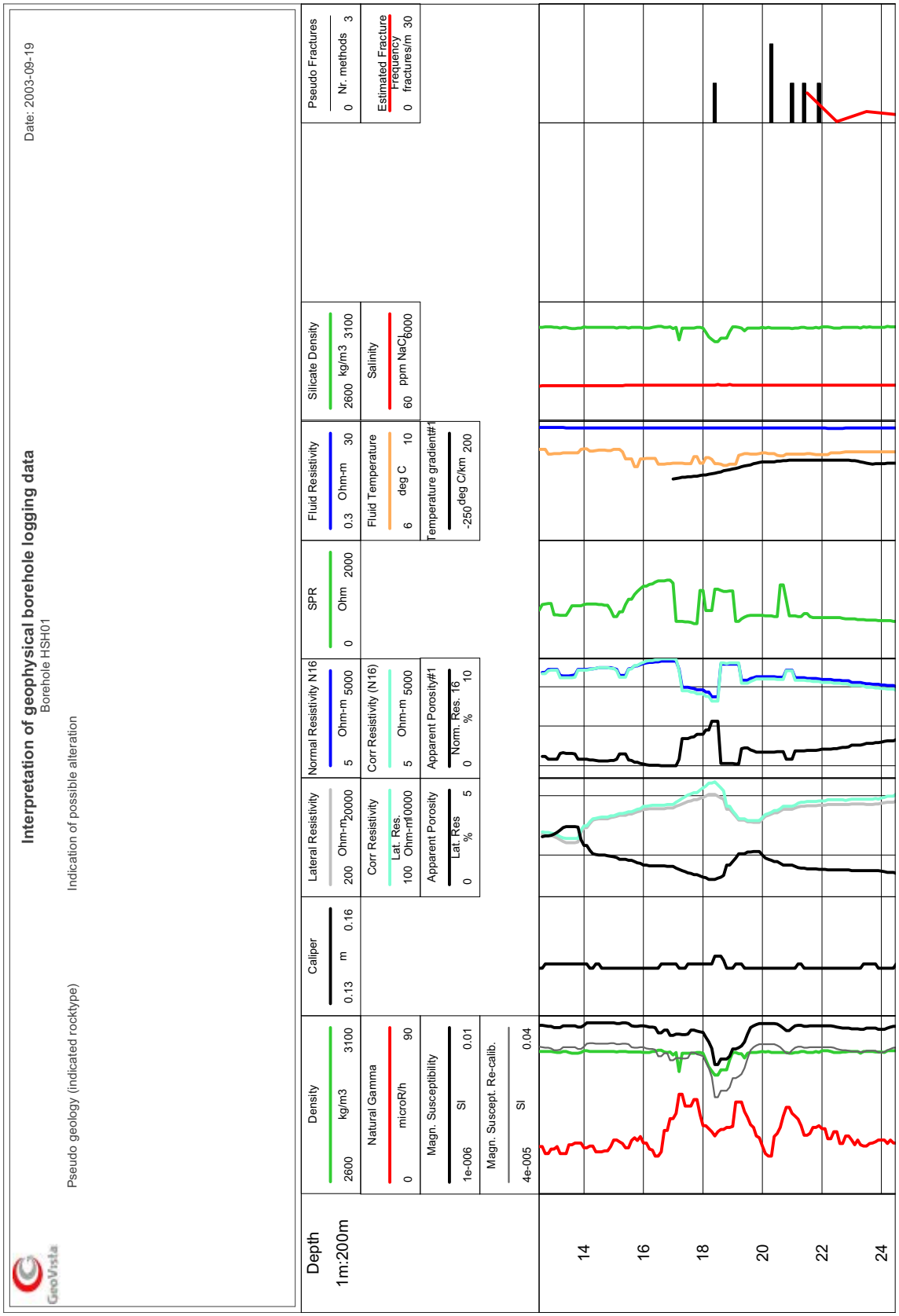

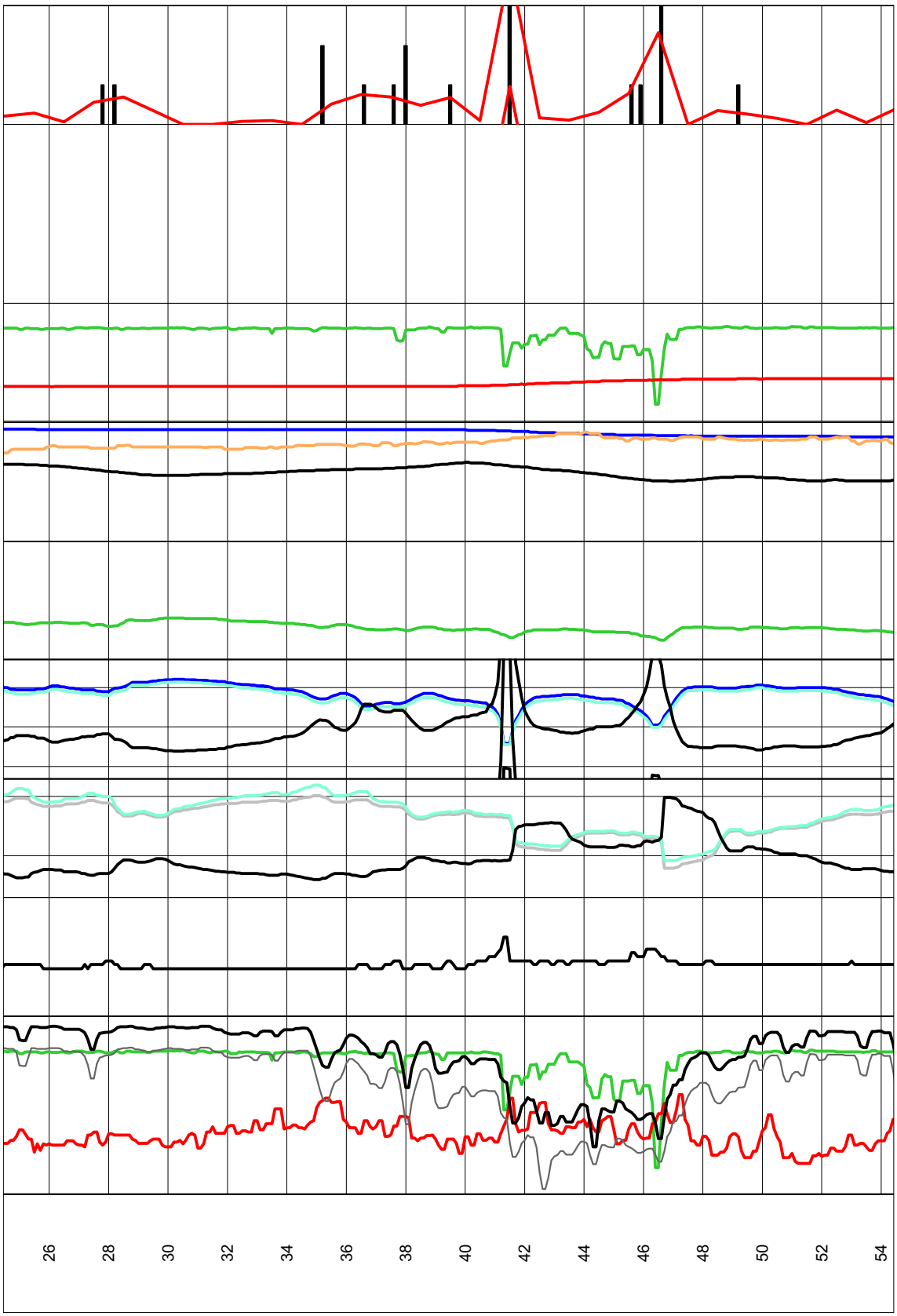
26
28
30
32
34
36
38
40
42
44
46
48
50
52
54

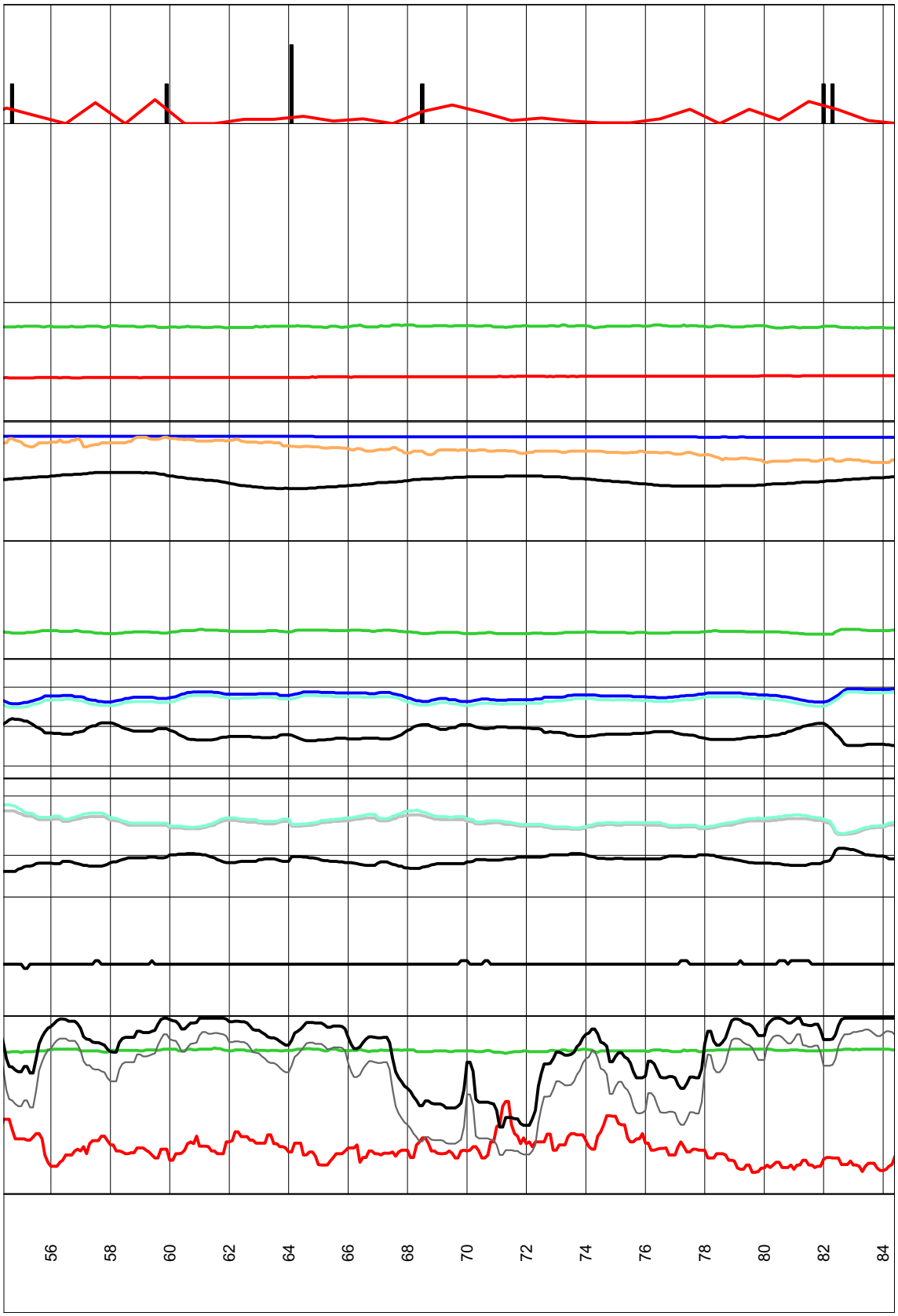
56
58
60
62
64
66
68
70
72
74
76
78
80
82
84

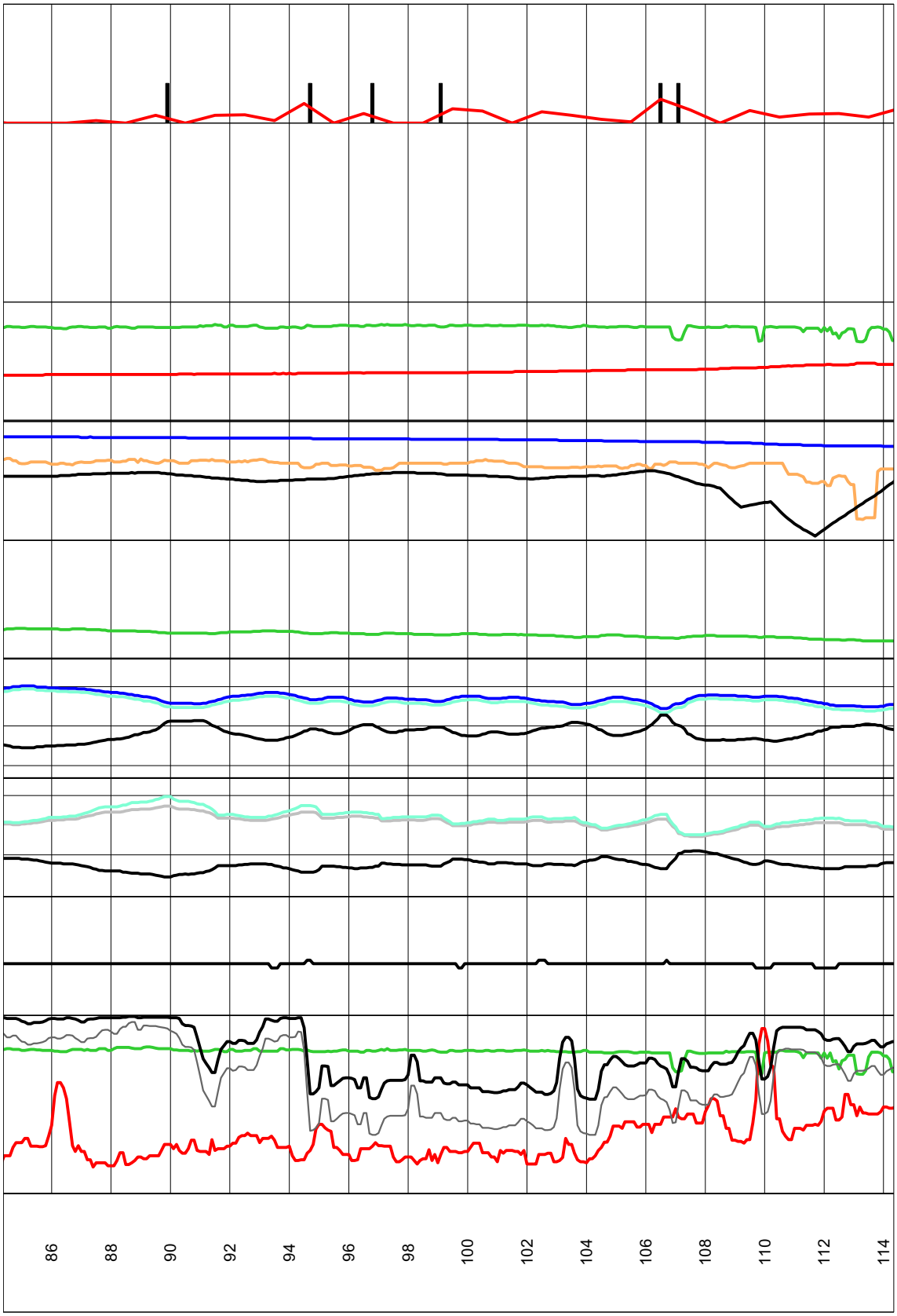
86
88
90
92
94
96
98
100
102
104
106
108
110
112
114

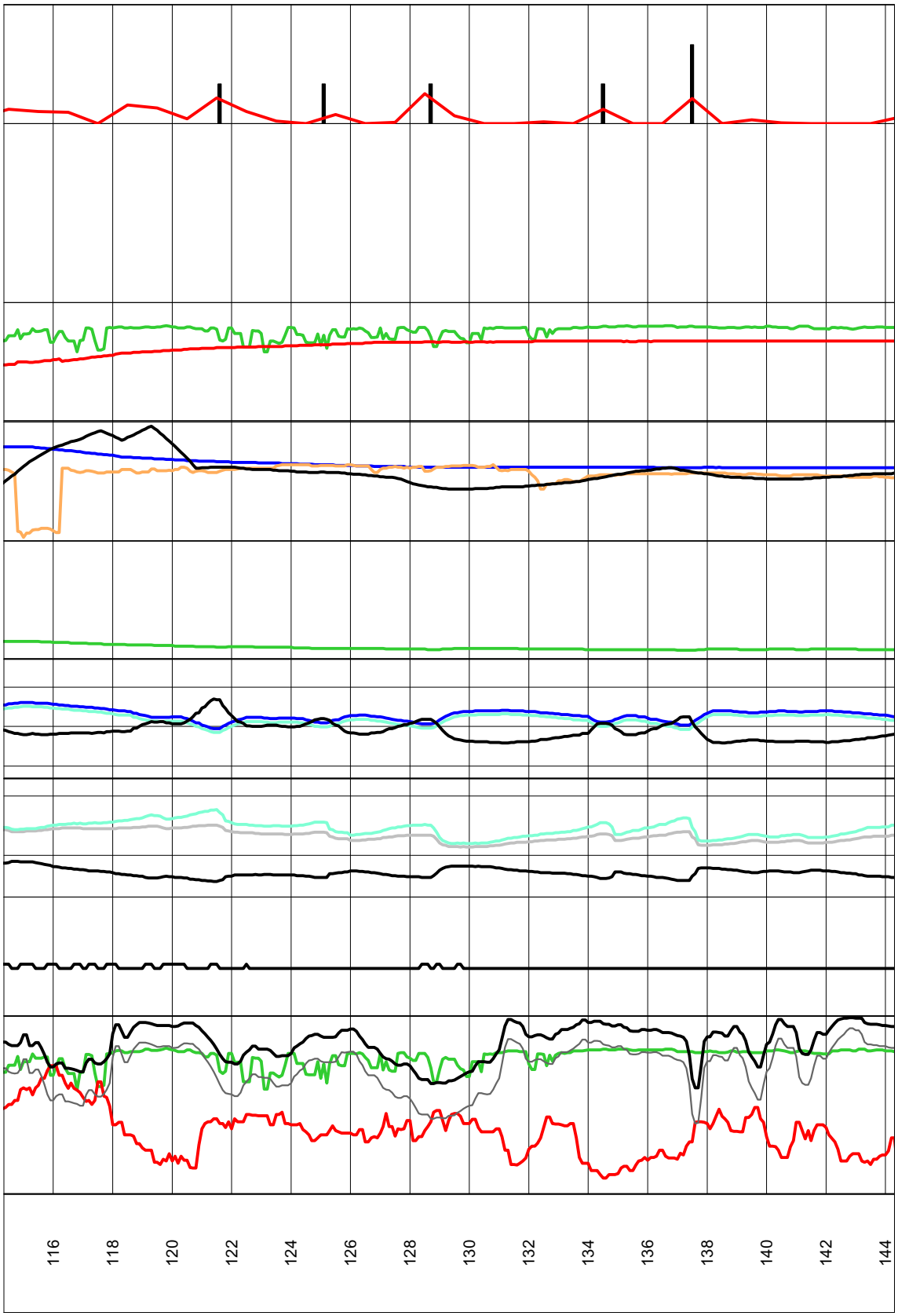
116
118
120
122
124
126
128
130
132
134
136
138
140
142
144

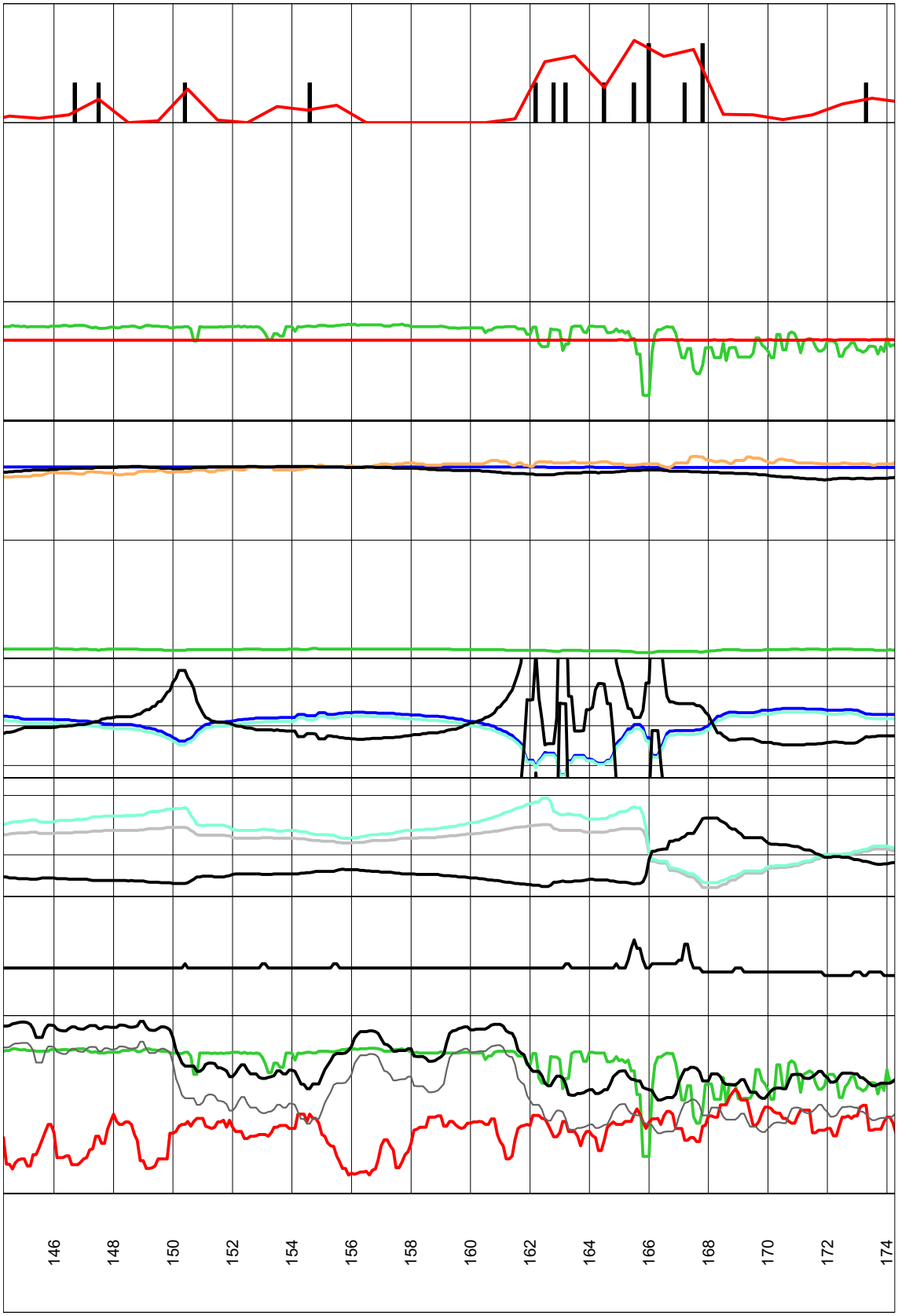
146
148
150
152
154
156
158
160
162
164
166
168
170
172
174

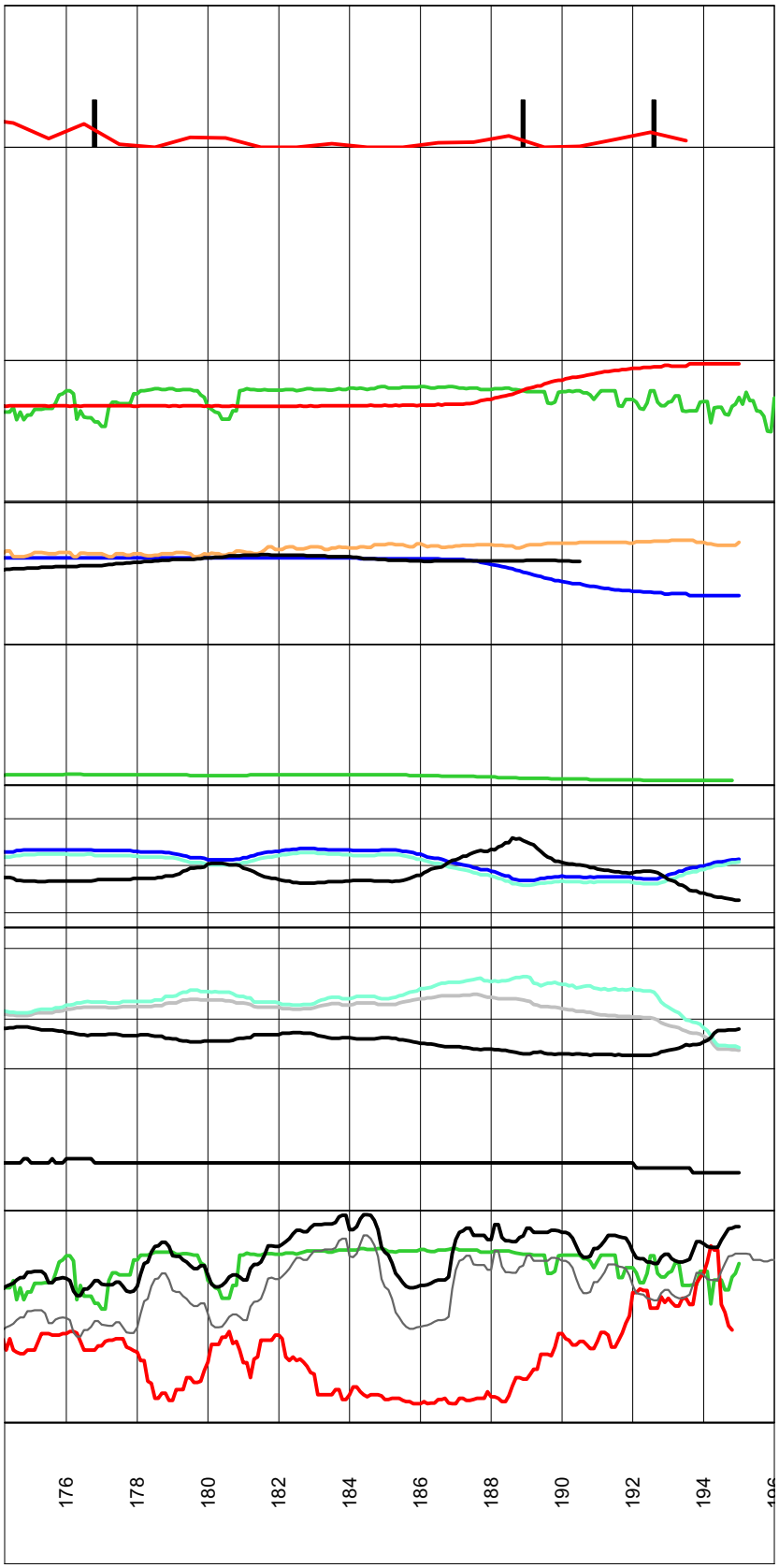
176
178
180
182
184
186
188
190
192
194

Appendix 6

Pseudogeology classification together with geophysical logging data for the borehole HSH02

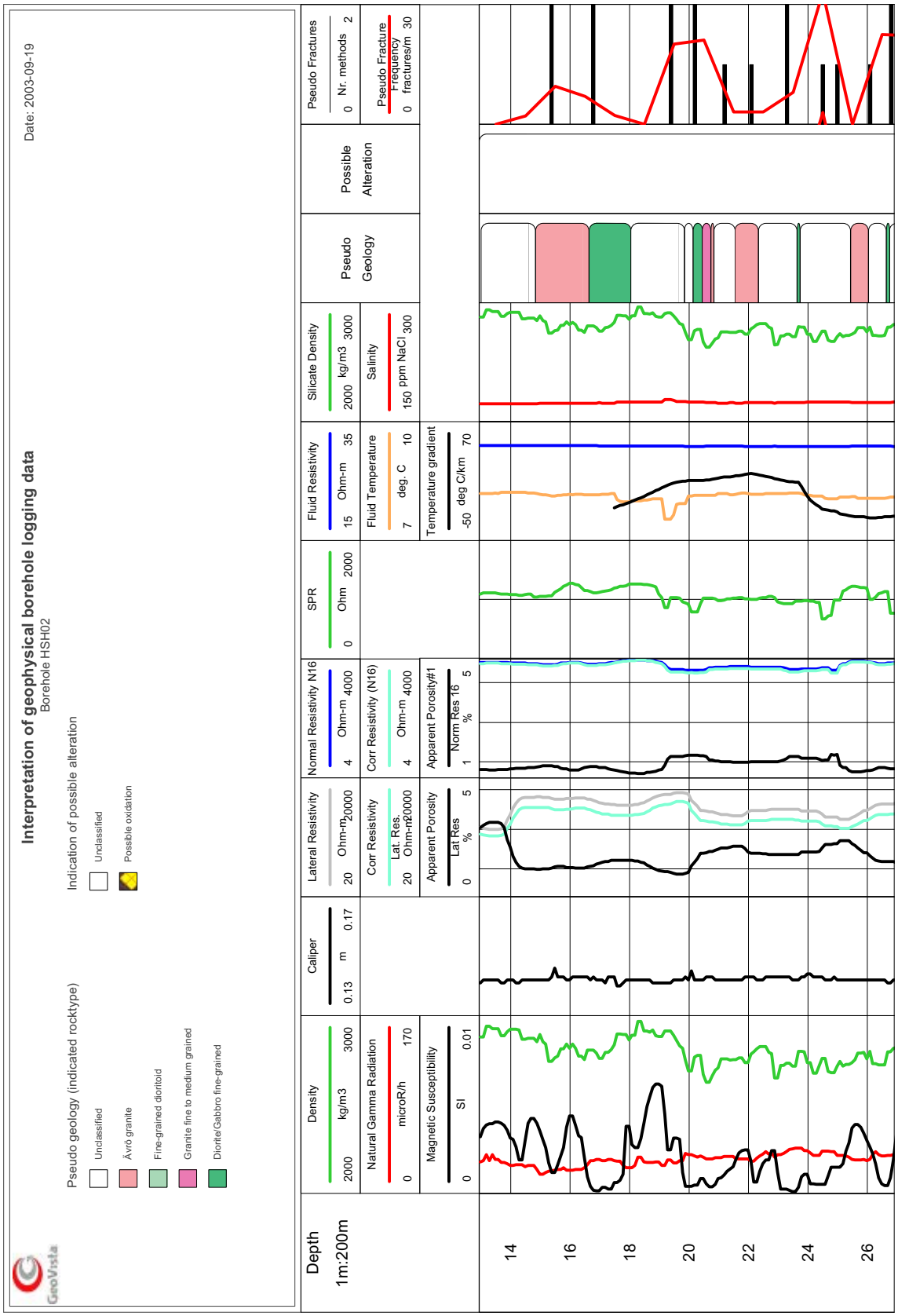

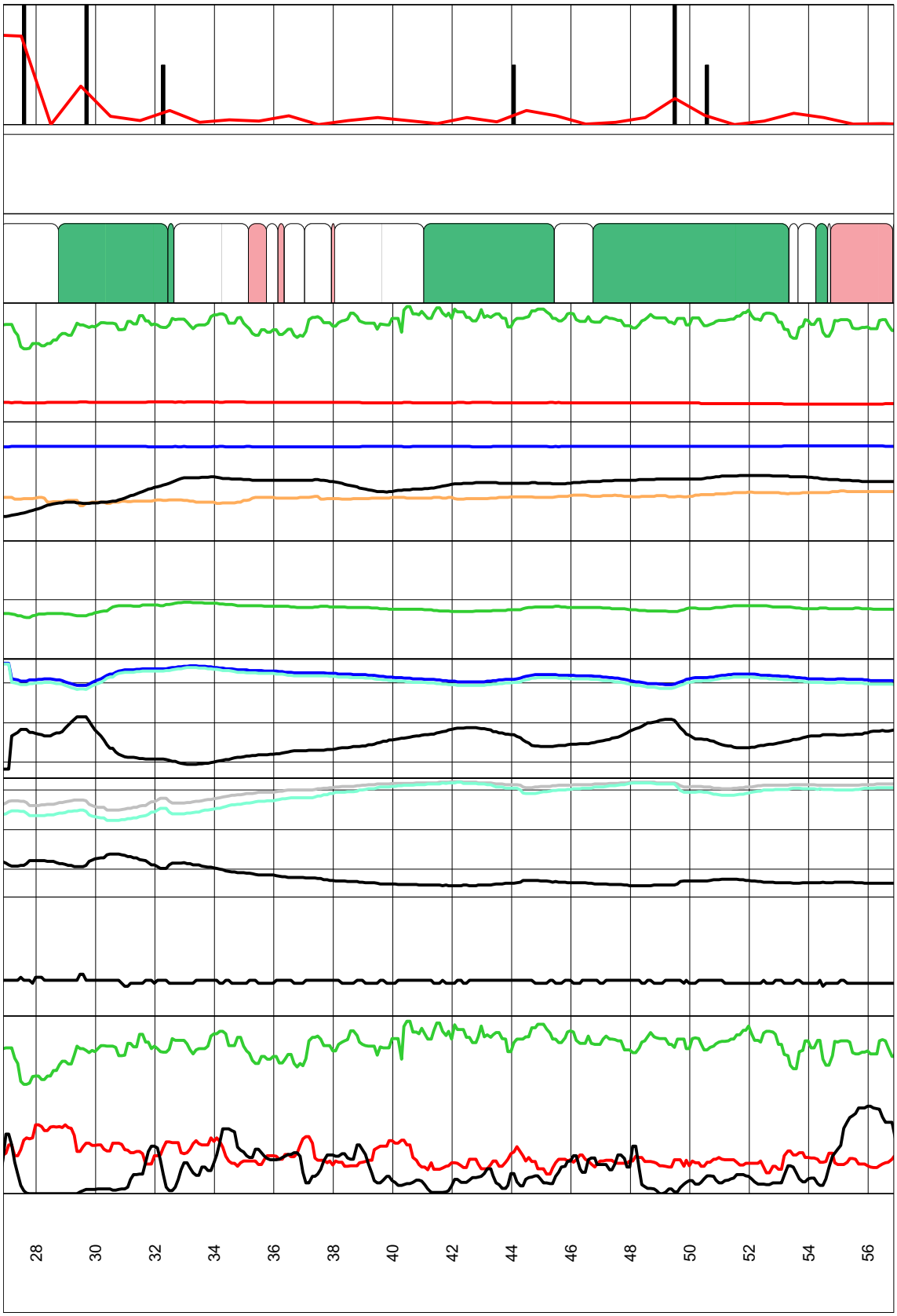
28
30
32
34
36
38
40
42
44
46
48
50
52
54
56

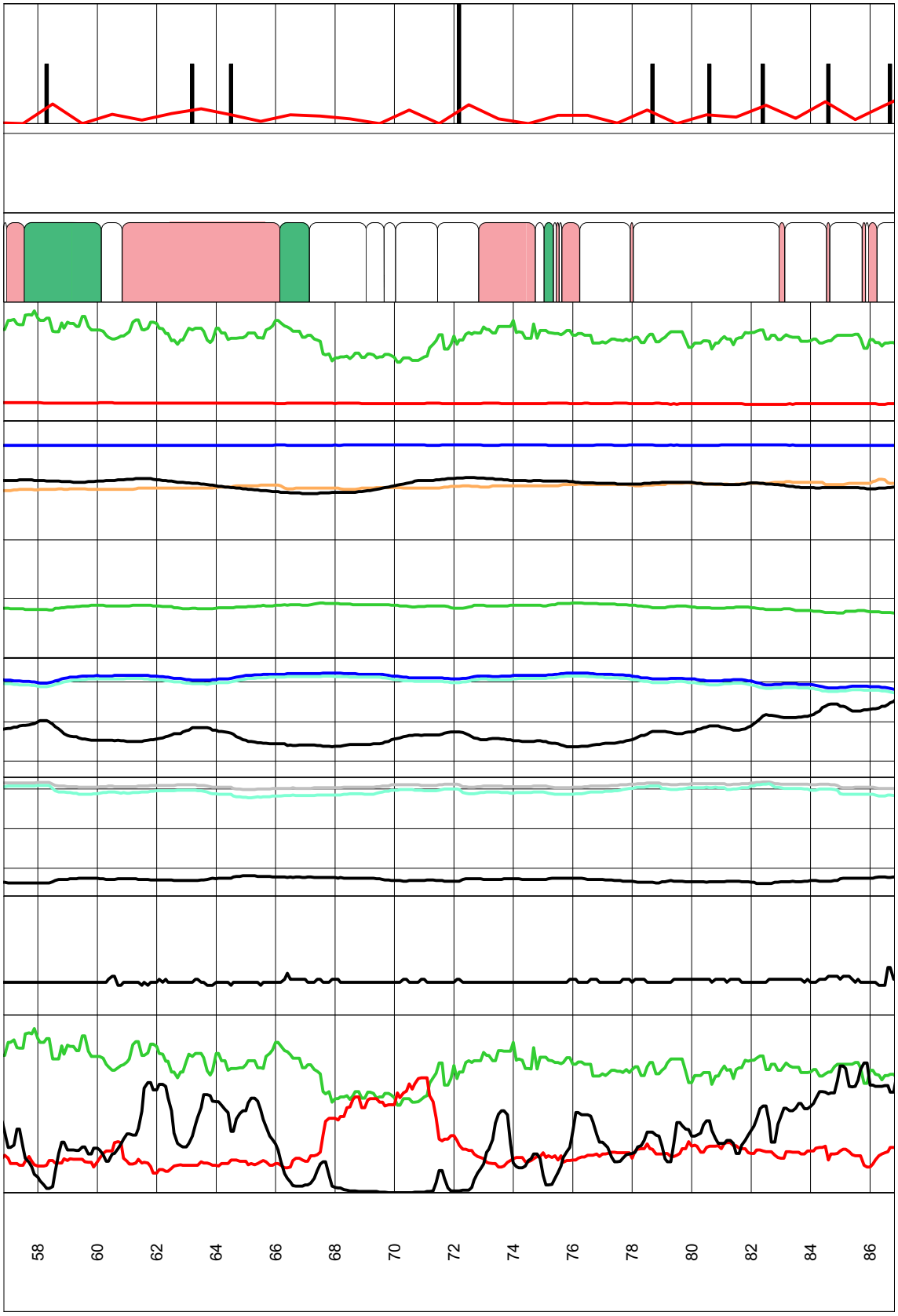
58
60
62
64
66
68
70
72
74
76
78
80
82
84
86

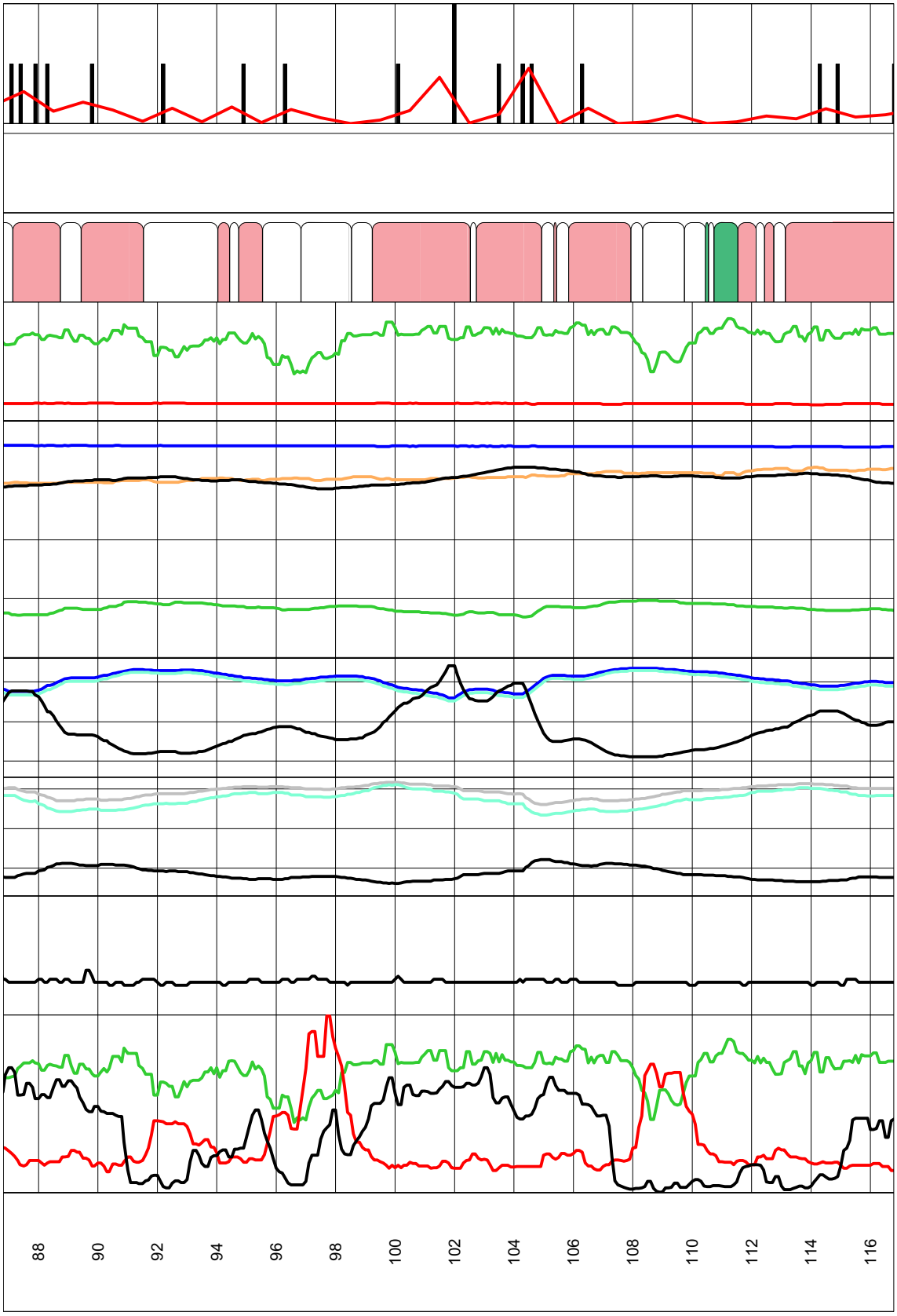
88
90
92
94
96
98
100
102
104
106
108
110
112
114
116

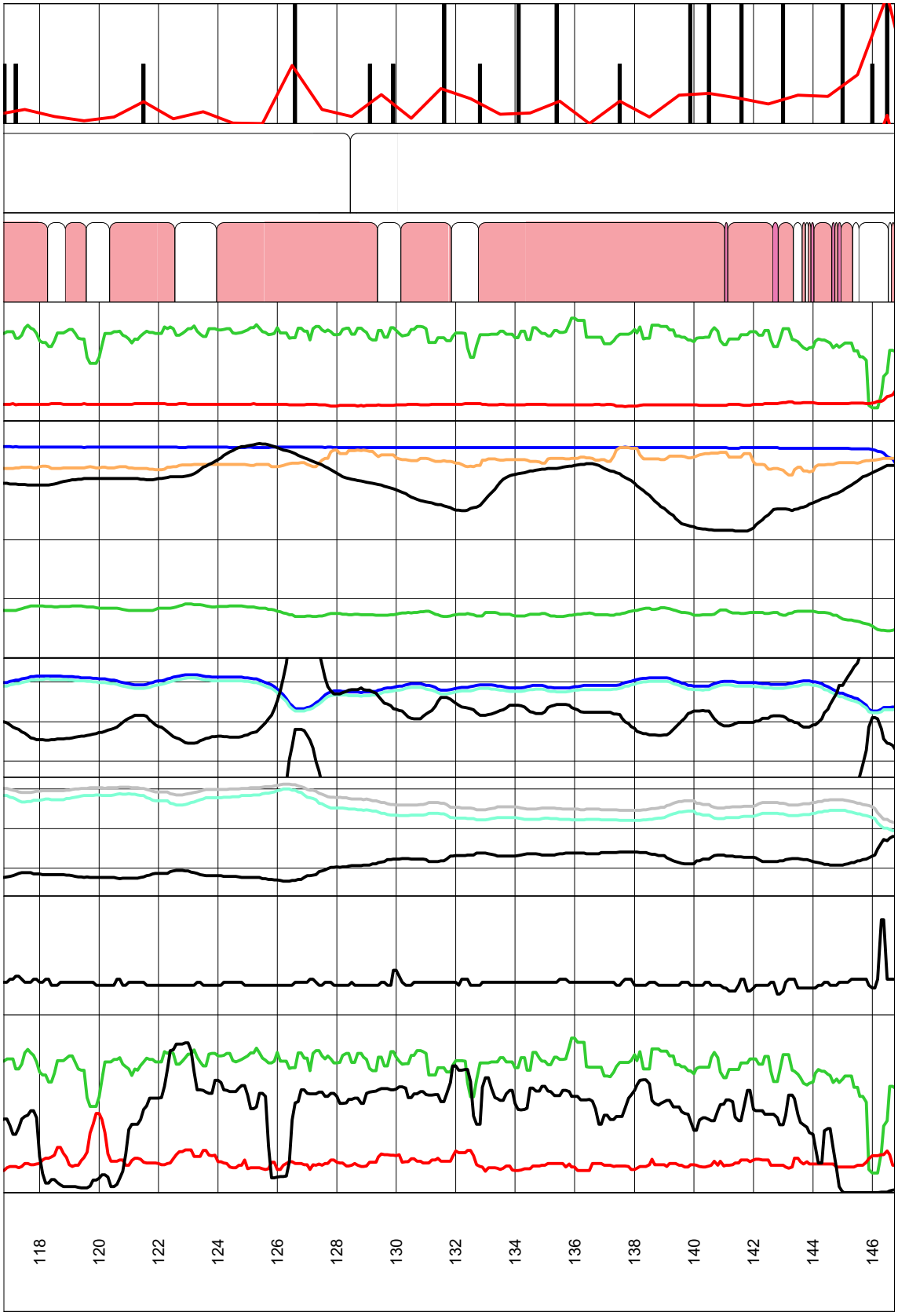
118
120
122
124
126
128
130
132
134
136
138
140
142
144
146

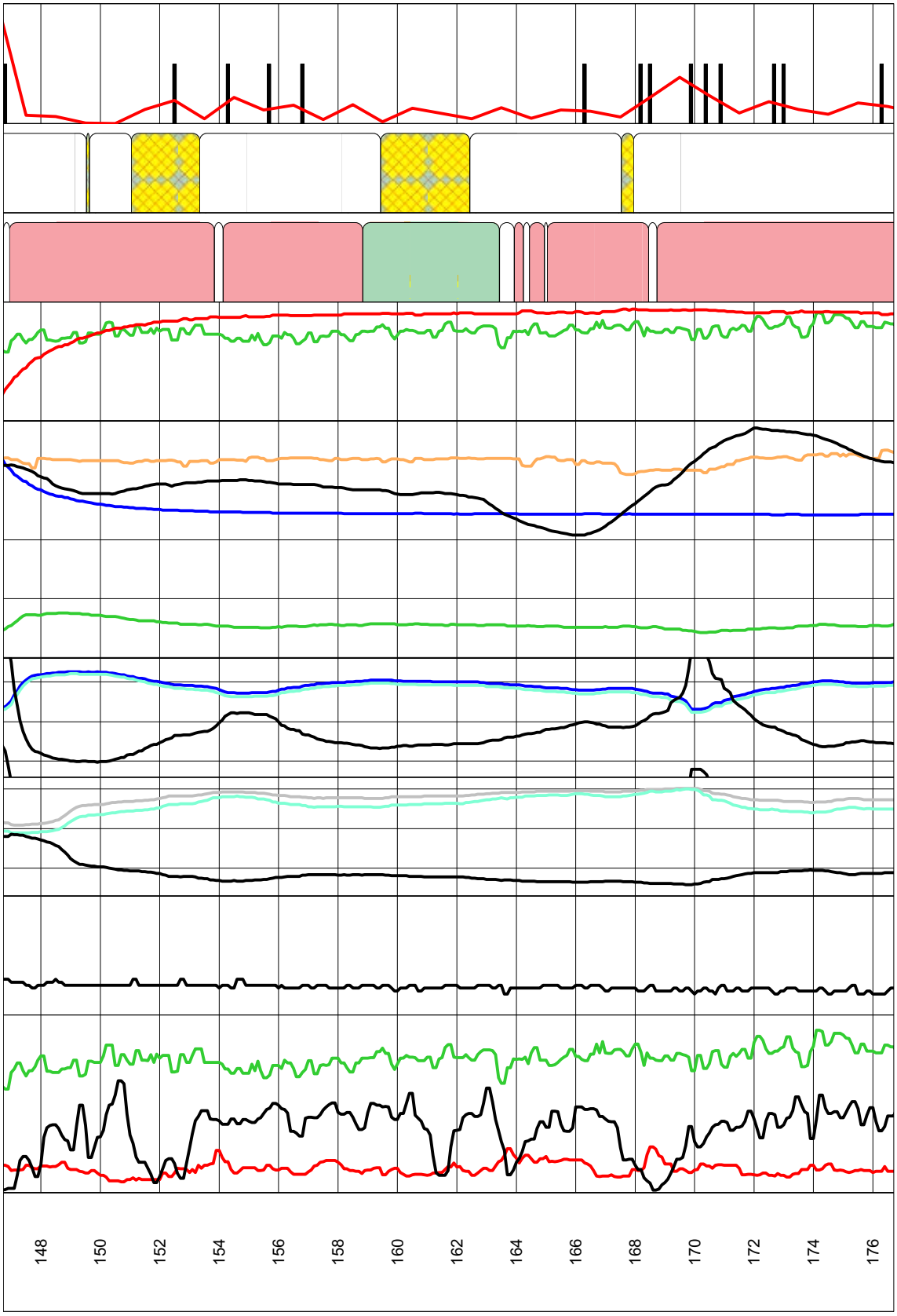
148
150
152
154
156
158
160
162
164
166
168
170
172
174
176

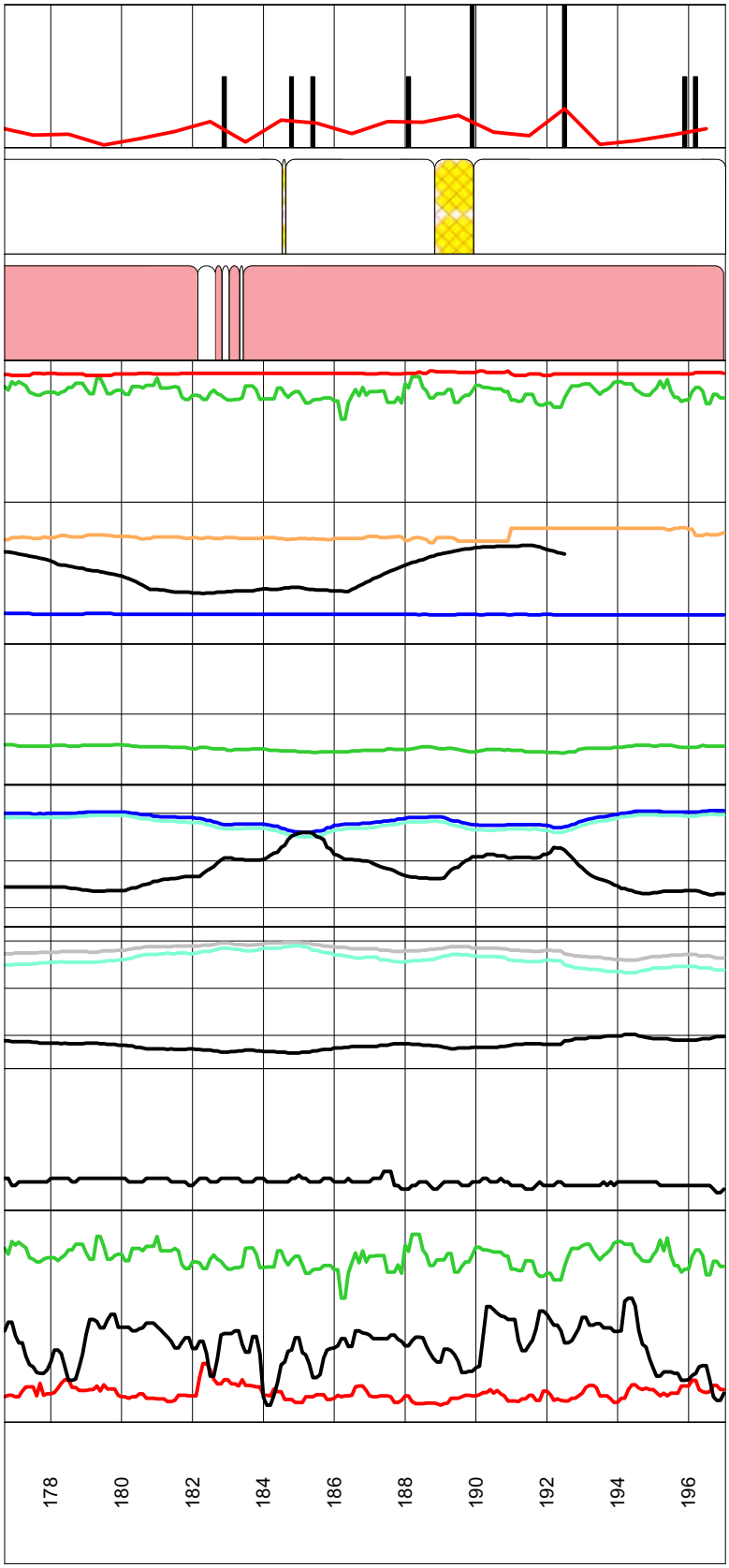
178
180
182
184
186
188
190
192
194
196

Appendix 7

Pseudogeology classification together with geophysical logging data for the borehole HSH03

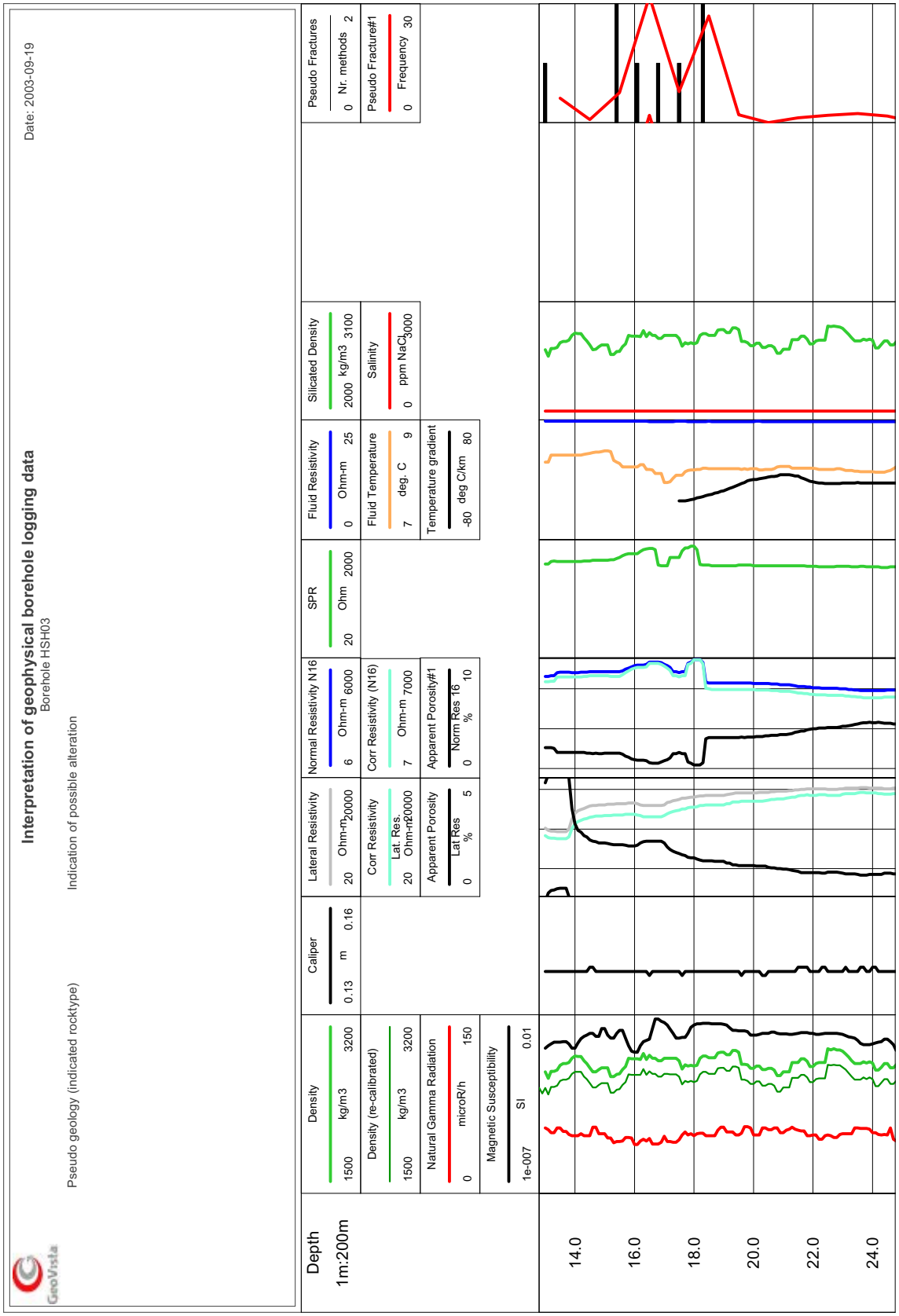

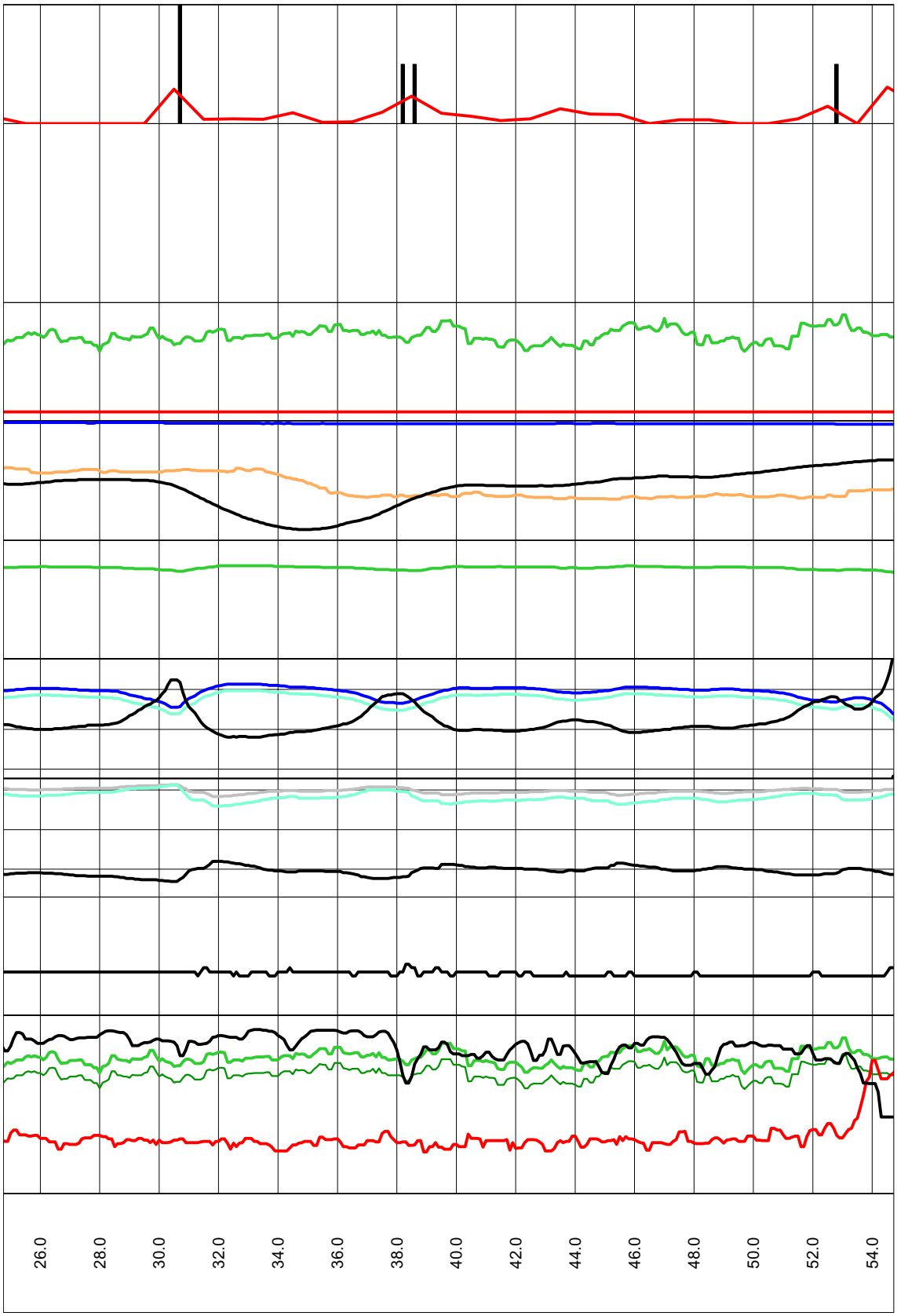
26.0
28.0
30.0
32.0
34.0
36.0
38.0
40.0
42.0
44.0
46.0
48.0
50.0
52.0
54.0

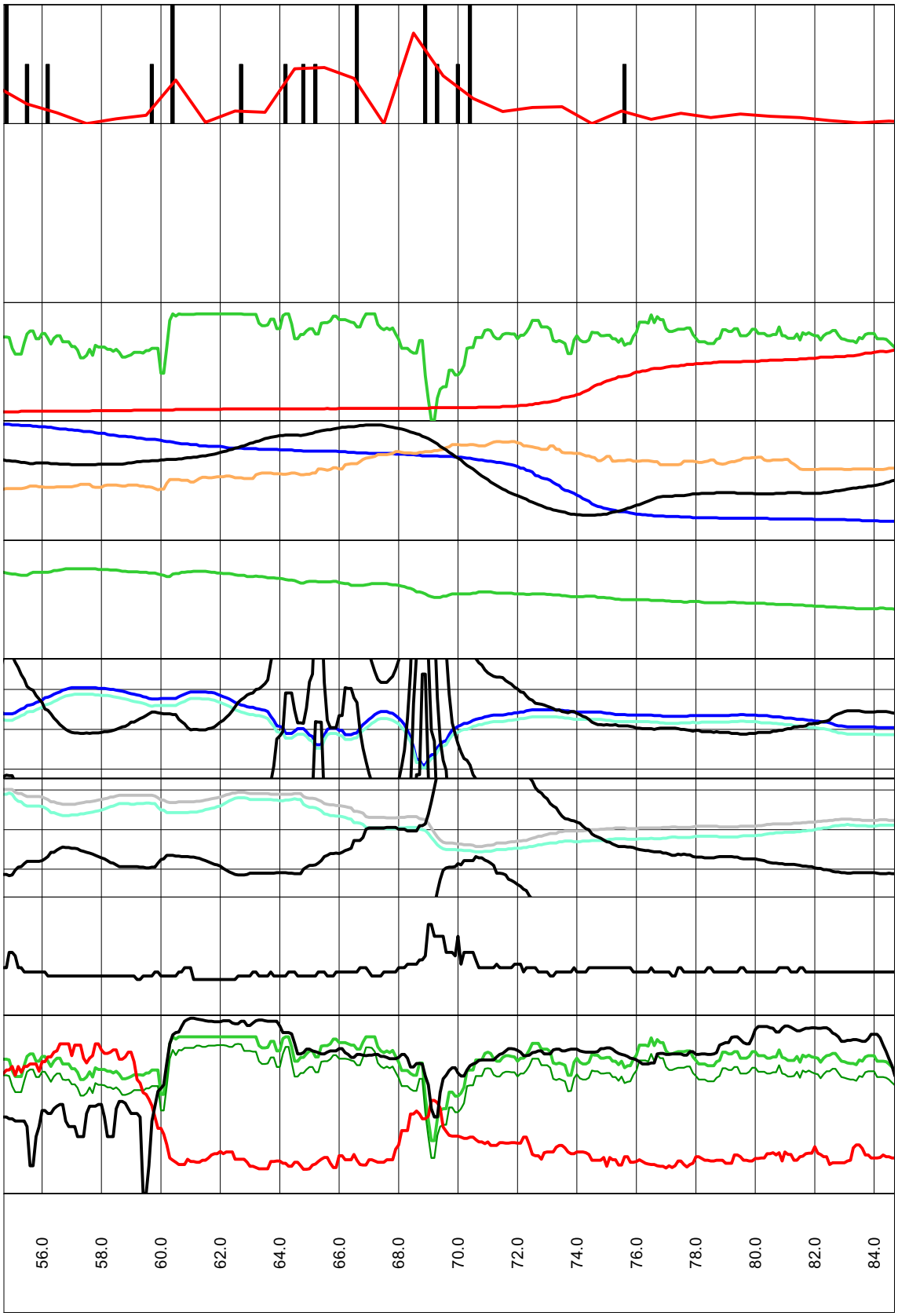
56.0
58.0
60.0
62.0
64.0
66.0
68.0
70.0
72.0
74.0
76.0
78.0
80.0
82.0
84.0

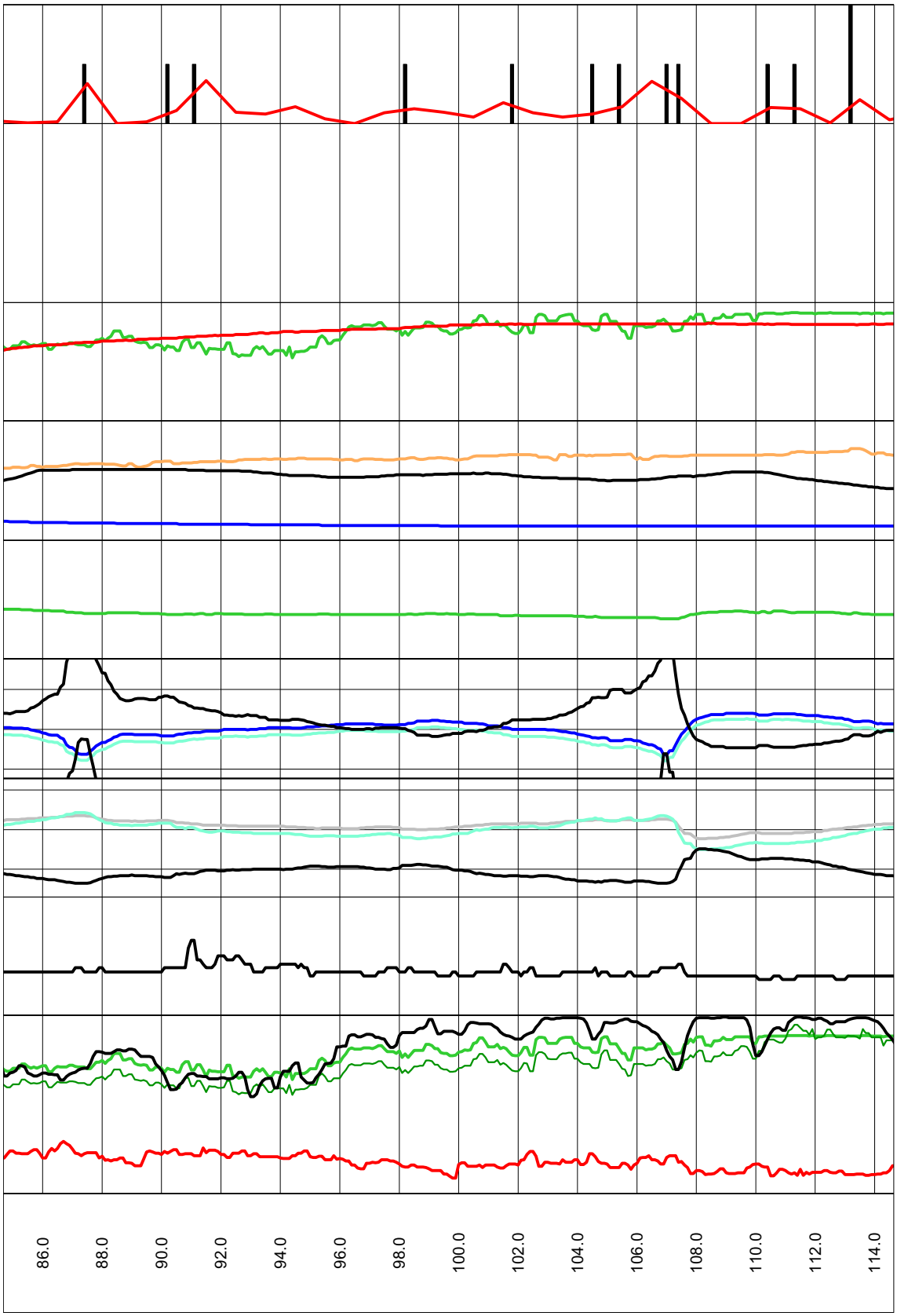
86.0
88.0
90.0
92.0
94.0
96.0
98.0
100.0
102.0
104.0
106.0
108.0
110.0
112.0
114.0

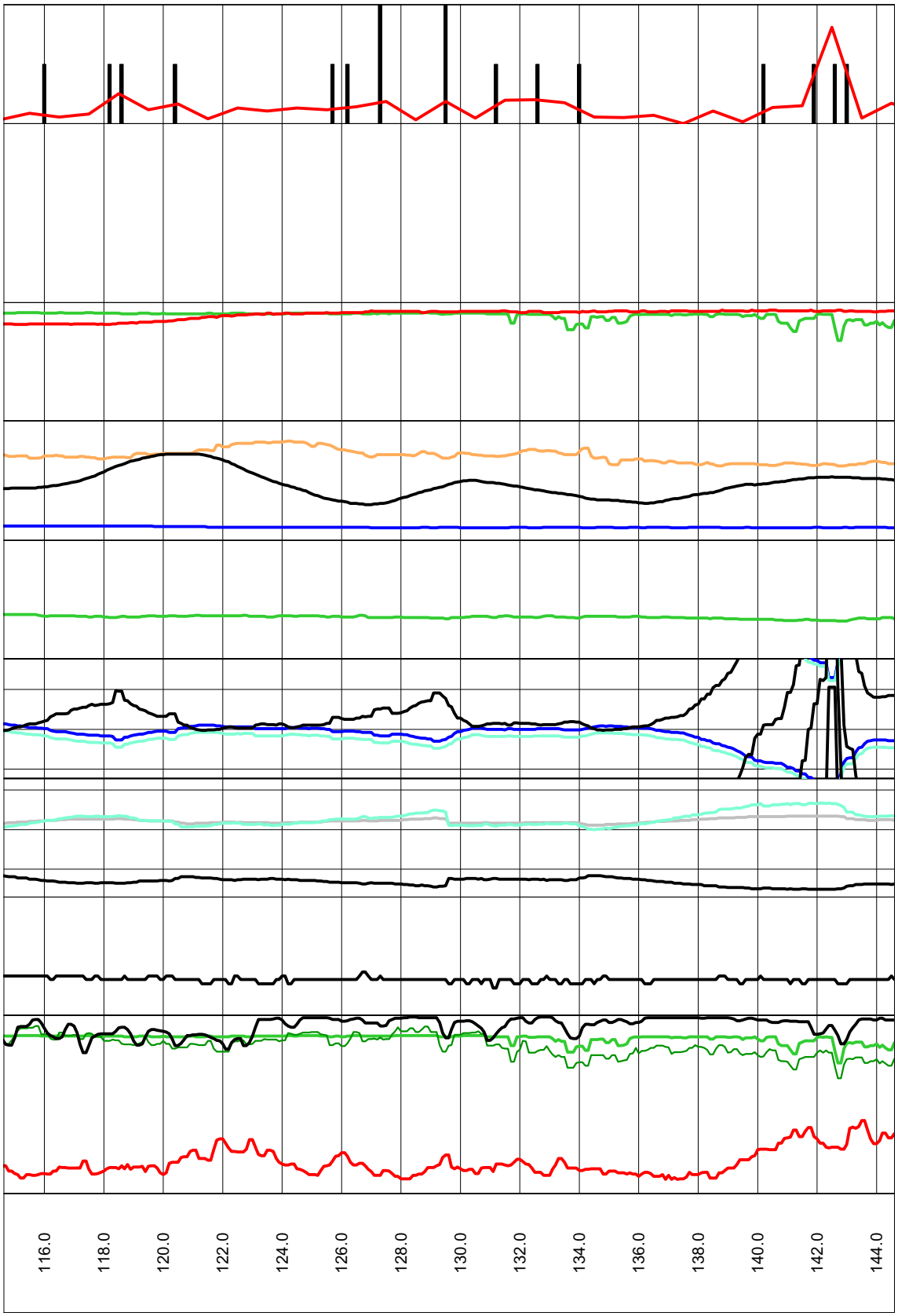
116.0
118.0
120.0
122.0
124.0
126.0
128.0
130.0
132.0
134.0
136.0
138.0
140.0
142.0
144.0

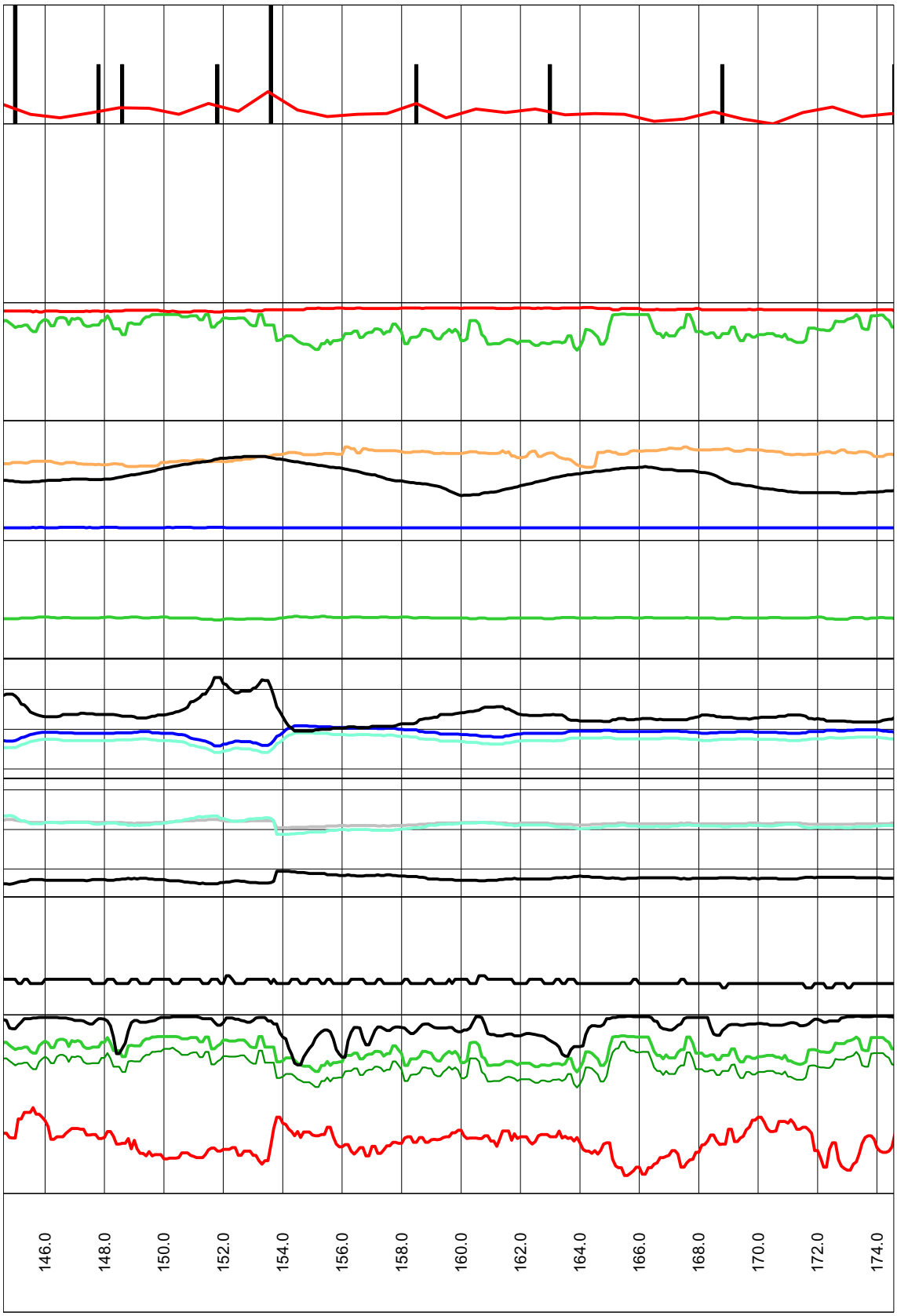
146.0
148.0
150.0
152.0
154.0
156.0
158.0
160.0
162.0
164.0
166.0
168.0
170.0
172.0
174.0

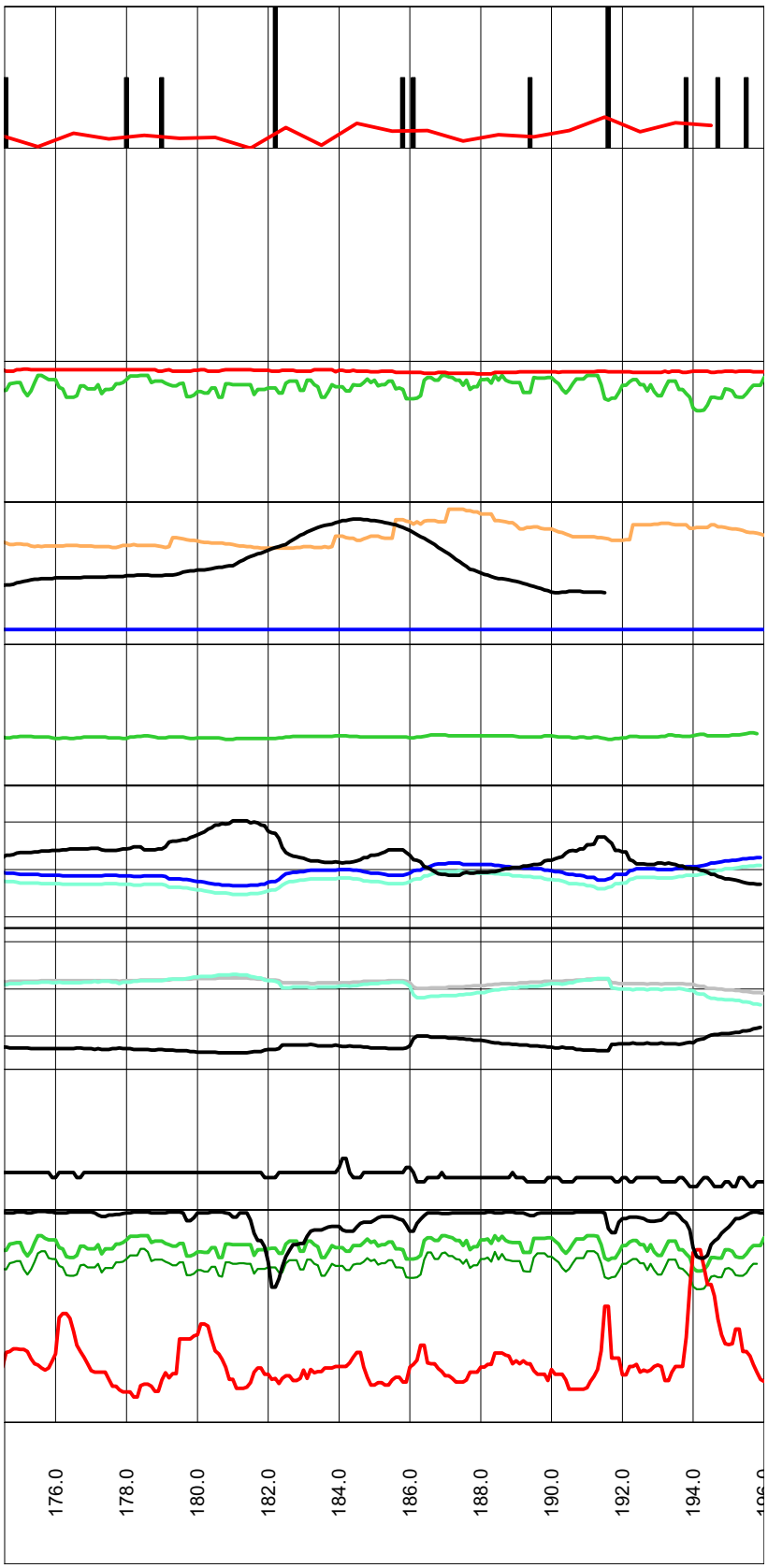
176.0
178.0
180.0
182.0
184.0
186.0
188.0
190.0
192.0
194.0